An Experimental Study on Cross-Flow Mixing in a Rod-Bundle Geometry using a Wire-Mesh

MSc Thesis

Delft University of Technology
Faculty of Applied Sciences
Departments of Physics of Nuclear Reactors and Multi-Scale Physics

Author:
Frederick Pieter Bulk
Studentnumber: 1404245
Thesis Registration Number: PNR-131-2012-010

Supervisors:
Dr. Eng. L.M. Portela
Dr. Ir. M. Rohde

Reviewers:
Prof. Dr. Ir. P. Kruit
Dr. M. Tummers

August 19, 2012

Abstract

The flow of water through a reactor core is of interest for various reasons associated with reactor safety and efficiency. In order to gain more insight into the behavior of this flow, this work aims to measure characteristics of the single-phase turbulent flow in this geometry. For this purpose, a wire-mesh measurement equipment was chosen. The wire-mesh is a conductivity-based measurement equipment that so far has mainly been used for measurements in gas-liquid flows.

Because this research focuses on single-phase flows, first, the capabilities of a wire-mesh in a single-phase flow were investigated using a simple pipe geometry. In this setup, the radial dispersion of a tracer injected in the center of the pipe was looked at. The calibration method of the signal was investigated, methods of improving the capabilities of the equipment were looked at and its reliability and accuracy were investigated. In particular, it was found that the use of added resistors to increase the measuring range of the equipment is problematic and, therefore, is not recommended. Values for the tracer concentration and dispersion as a function of Reynolds number and travel distance in the tube were investigated and compared to literature. The results are in a good agreement with the literature. Furthermore, the large-scaled turbulence structures were visualized and quantified with the help of the power spectra of the concentration fluctuations in the wire-mesh. The behavior and size of these structures was as expected, and consistent with the results found in literature.

Aside from the more general research on the measurement technique, in the second part of this work research was performed with the aim of investigating the possibilities and limitations of the wire-mesh technique for concentration measurements and mixing information in a rod-bundle geometry. For this purpose, a custom-designed wire-mesh was constructed and installed in the rod-bundle geometry. The wire-mesh was designed and constructed in-house, and specifically made for an existing rod-bundle geometry. Special care was taken in order to minimize the flow disturbance introduced by the measurement equipment. Some initial experiments were performed with this equipment. The measured dispersion shows a good signal without negative influence from any possible disturbances in the flow due to the measurement equipment or injection capillary. The reliability of the signals was looked at, and some first attempt were done in quantifying the size of the large scale coherent structures in the flow. This quantification shows a consistent behavior, with a reasonable agreement with the literature.

The experimental work was performed at the 'Kramers Laboratorium voor Fysische Technology' as a part of an on-going collaboration between the departments of Mutiscale Physics and Physics of Nuclear Reactors.

Contents

CHAPTER 1

Introduction

The turbulent flow through a rod-bundle geometry is an interesting case of applied fluid dynamics. These kind of flows can be found in several applications. For example, in a variety of heat-exchange systems between separated flow-loops. These rod-bundle flows have some interesting physical phenomena that are a direct result from the specific geometry of the flow. One interesting characteristic of these geometries, is the existence of different sub-channels in the different parts of the cross-section. This results in a varying velocity profile over the cross-section, resulting in interesting flow behavior. One of the applications where a rod-bundle geometry is often used is in the core of a nuclear reactor.

1.1 The Nuclear Reactor Core

Energy in general, and electricity in particular, is a vital resource of modern society. Therefore, research in more sustainable, more efficient, and safer ways of producing electricity is very important. Especially considering that the growing world population and wealth increases the need for more production of electricity. Many ways currently used for producing electricity have one thing in common: nearly all of the electricity that is produced in the world uses water, in one way or another, to transfer energy from one place to another and to converse it into usable electricity. Nuclear Power Plants (NPP) are in this regard no exception, the only uniqueness is the source of the initial energy. For example, in Pressurized Water Reactors (PWR) water is heated, and then transferred to a heat exchanger used for heating a secondary loop that powers the turbine, as can be seen in figure 1.1.

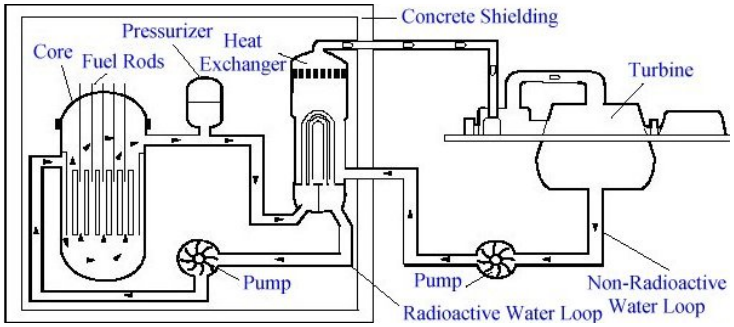

Figure 1.1: The schematics of a Pressurized Water Reactor.

Apart from the transport of heat, the water flowing in the core of these reactors serves another important purpose: moderate the neutrons produced in the nuclear fission. This is necessary, since neutrons with a low kinetic energy have a higher chance of being absorbed in the fissile material and thus have a higher chance of causing a fission themselves. The double purpose of the water in a NPP (moderating and transferring heat) can be used very effectively to create passively safe systems, meaning that the fission rate in a section of the core automatically slows down when the temperature in that section increases too much. Knowing this, it is clear that an efficient dispersion of heat throughout the core is vitally important for a NPP to operate not only efficiently but also safely and stably. A major role in this dispersion is played both by the turbulence and the flow structures that can arise as a result of the rod-bundle geometry.

1.2 Rod-Bundle Geometry

The geometry in a typical PWR or Boiling Water Reactor (BWR) can be best described as a rod-bundle geometry. The fissile material is contained in an array of long metal rods with water (and vapor in a BWR) flowing between them. Of course, this water not only transports heat in the flow direction (parallel to the rods), but also disperses heat from the rods into the cross-section. This lateral dispersion in the cross-section is where the focus of this thesis lies even though the study is not exclusively aimed in the cross-sectional dispersion. A part of this lateral dispersion of heat (treated in this work as a passive scalar) can be attributed to an interesting phenomenon: the occurrence of coherent vortices. In figure 1.2a a schematic of a rod-bundle geometry with the flow direction is shown. The vortices that arise in geometries like this are a result of the existence of a confined mixing-layer. The occurrence of these vortices can be explained by looking at figure 1.2b. Here, as an example, a channel is shown with a deep and a shallow part, this essentially means that the flow consists of two connected parallel streams with different velocities. Between both streams a shear-layer exists, which eventually results in a street of discrete vortices, because of a phenomenon called the Kelvin-Helmholtz instability (Winant and Browand, 1973).

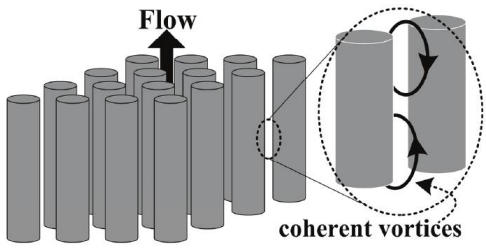

(a) Rod bundle with vortices on both sides of a gap.

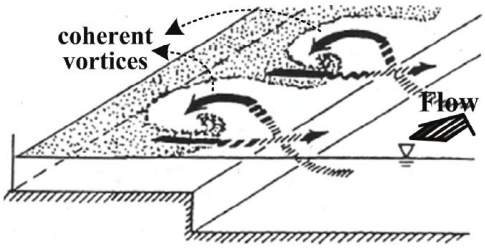

(b) Street of vortices as it arises in a shear flow.

Figure 1.2: The vortices in a typical rod-bundle flow (left) and as they arise in a channel with different heights (right) (Mahmood, 2011).

A flow in a rod-bundle geometry has some of the same characteristics shown in 1.2b for a channel flow. In a normal squared set-up of rods there are areas where the average wall-distance is larger (sub-channels) and areas where the mean wall-distance is smaller (gaps). The result is a street of coherent vortices on both sides of the gaps, which move along with the flow creating an oscillating local fluid velocity perpendicular to the flow. In nature, vortices like this can be found in different systems. Examples are shown in figure 1.3, where a street of vortices forming in the wake of two islands is visible in the clouds and a vortex street is seen in a river.

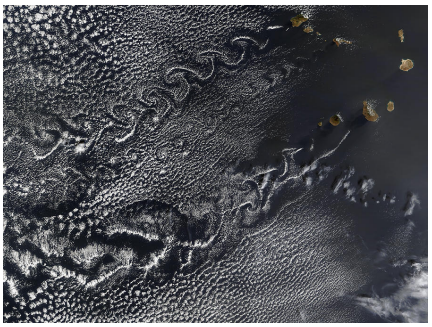

(a) Vortex street in the wake of an island.

(b) Vortex street in a river.

Figure 1.3: Two common examples of natural coherent structures in a fluid flow.

1.3 Previous Research

As pointed out, the mixing in a reactor core is very important for the operation of a nuclear power plant; as a part of this, the mixing between different sub-channels, wether or not caused by the coherent vortices, is of interest, as is clear from past research. Early research from Rogers and Todreas (1968) show that the mixing between different sub-channels in a rod-bundle geometry has been of interest since the early developments in nuclear power. Since then, many experiments were performed confirming the findings of Rowe et al. (1974) that macroscopic flow processes at the boundary of the gaps and sub-channels play a significant role in the lateral dispersion in a rod-bundle flow. Recently, many experiments and numerical work, were done in order to quantify the importance of coherent vortices in mixing. The previous work in this project, done by Mahmood (2011), focused on experiments (LDA and PIV measurements) and modeling (LES) in different gap/sub-channel geometries including a rod-bundle setup. Following the research from Mahmood (2011) and van Campen (2009), this work aims to add information about the mixing of a passive scalar in the same rod-bundle geometry used by them. Allthough a theoretical and numerical approach of this subject would also be interesting, this work is only an experimental enterprise, focused on the use of the wire-mesh technique to measure the concentration and mixing-characteristics of a passive scalar.

1.4 The Wire-Mesh

In order to get tracer dispersion data with high spatial and time-resolution a wire-mesh measurement instrument was chosen. A wire-mesh is a conductivity-based, slightly intrusive equipment developed by Prasser et al. (1998). It was originally developed for measuring the void fraction in gas-liquid flows and has since then been mostly used in multi-phase flow. Using it in single-phase flow requires injection of a conductive tracer, in order to acquire a measurable signal. The sensor itself consists of two perpendicular layers of wires that are slightly apart, through which the fluid flows. The wire-mesh can measure the conductivity of the fluid between each crossing of two wires independently. This way, in gas-liquid flows it can easily distinguish a conductive liquid and the non-conductive gas. Here, the conductivity measurements are used to determine the concentration of the tracer.

1.5 This Research

Since past use of the wire-mesh technique to measure concentration and mixing is very limited (in particular in a rod-bundle geometry), in this work it was chosen to do an in-depth research of the capabilities of the technique to perform such measurements. Also, ways of enhancing the capabilities of the technique were investigated, and the influence of various settings was looked at. This project has two main points of interest, hence, the thesis is also divided into two parts.

1.5.1 Part I

First, since the wire-mesh has been designed for gas-liquid flows and has been used mostly in this capacity, the application of it in a single-phase flow deserves some attention. Because of this, in the first part of this work a thorough investigation in the use of a wire-mesh in a single-phase flow was done, with the help of an already available wire-mesh, in a regular circular tube geometry. In chapter 2 the necessary theory on fluid dynamics, turbulence and tracer dispersion in pipe flow is discussed. In chapter 3, the idea behind the wire-mesh technique is discussed, as well as the necessary calibrations and the optimization of the device for its application in single-phase flow. Finally, in chapter 4 the results of the measurements in a fully-developed horizontal pipe are presented.

1.5.2 Part II

In part II, the actual construction and application of the wire-mesh equipment in the rod-bundle geometry is discussed, and the results of measurements in this setup are presented. In chapter 5, an overview of the theory of scalar transport in rod-bundle flow is given. In chapter 6, the wire-mesh is presented, followed by the results of the measurements in chapter 7. At the end, the conclusions of this research are discussed, together with some recommendations for future research.

Part I

The Wire-Mesh in Single-Phase Flow

CHAPTER 2

Dispersion in Turbulent Pipe Flow

The turbulent flow through a pipeline and its different phenomena associated with scalar transport is something that has been of interest for physicists for a very long time and the influence of turbulence on the dispersion of passive scalars has been the subject of many years of research. In this section the theoretical framework and existing measuring techniques are introduced and briefly explained.

2.1 Fluid Flow

The flow of a fluid can be described by a few basic formulas, one of them is the continuity equation. It describes that there is conservation of mass. If it is also assumed that the fluid is incompressible than the continuity equation is given by:

$$\nabla \cdot \vec{U} = 0 \tag{2.1}$$

where $\vec{U}$ is the velocity vector field. Another important set of equations to describe fluid flow are the Navier-Stokes equations. The Navier-Stokes equations are obtained from Newton's second law and relate the forces experienced in the fluid with an acceleration of the particles in the fluid. Adding the several terms responsible for the momentum in a flow (the local acceleration, the inflow and outflow of momentum, a pressure gradient, diffusion and the body-force term), results in the following equation:

$$\frac{\partial \vec{U}}{\partial t} + \vec{U} \cdot \nabla \vec{U} = -\frac{1}{\rho} \nabla P + \nu \nabla^2 \vec{U} + \vec{f} \tag{2.2}$$

With ρ the density of the fluid, P is the pressure, ν the kinematic viscosity, and f the body force which may contain, for example, gravitational forces.

2.2 Turbulence

As classical experiments, like Reynolds (1883) and Taylor (1954) show, experimental research into turbulent pipe flow and turbulent tracer dispersion played an important part in the broader research on turbulent flow. As a result of the research that has been done, turbulent pipe flow is well known. Therefore, it is a very suitable flow to test the capabilities of a wire-mesh in a single-phase flow environment.

2.2.1 Reynolds Number

In single-phase flow two different main regimes can be distinguished: laminar flow and turbulent flow. In laminar flow, the fluid can be seen as flowing in parallel layers that do not change over time. Particles move along with the flow in a very orderly fashion resulting in no mixing in the lateral directions on the flow. The other flow regime, turbulence, is actually more common in nature and in engineering. It is characterized by random, nonlinear changes in the magnitude and direction of momentum. This non-linearity results in high mixing in all directions and the occurrence of fluctuating structures, called eddies, in the flow. In the bottom left of figure 2.1 laminar flow is visible in the smoke of a cigarette,

further away from the cigarette the flow turns turbulent, due to an increase in velocity and characteristic length scale. This turbulence causes the smoke to diverge from the initial straight path into a chaotic swirl of smoke dispersing rapidly into the environment. In turbulent flows, the most important parameter is the Reynolds number, which is defined by:

$$Re = \frac{\mathcal{U}\mathcal{L}}{\nu}, \tag{2.3}$$

where $\mathcal{U}$ and $\mathcal{L}$ are the characteristic length and velocity scales of the flow respectively.

Figure 2.1: Laminar and turbulent flow regimes made visible with cigarette smoke.

2.2.2 Turbulence Structures

One of the characteristics of turbulent flow is the occurrence of unstable vortices. It is difficult to visualize how exactly these vortices behave but they can be seen as smaller or larger areas of the flow where the flow has a somewhat uniform behavior. These vortices are unstable and fall apart transferring their energy to smaller eddies, which after breaking-up do the same. The smallest scales that exist in the flow dissipate the energy through viscous diffusion. The characteristics of the structures vary over a large range. The largest structures have a size l_0, comparable with the flow scale $\mathcal{L}$, and a velocity u_0 comparable with $\mathcal{U}$ (Kundu and Cohen, 2000). The eddy turnover time τ_0 indicates the time that one eddy looses most of its energy and is given by the ratio between l_0 and u_0. The scales of the smallest eddies are given by the so called Kolmogorov scales, and in the order of millimeters or smaller:

$$\eta \equiv \left(\frac{\nu^3}{\epsilon}\right)^{\frac{1}{4}}, \qquad u_\eta \equiv (\epsilon\nu)^{\frac{1}{4}}, \qquad \tau_\eta \equiv \left(\frac{\nu}{\epsilon}\right)^{\frac{1}{2}}. \tag{2.4}$$

Here η, u_η and τ_η are the Kolmogorov length, velocity and time scales, and ϵ indicates the rate of dissipation of turbulence kinetic energy. The Kolmogorov length becomes smaller when the Reynolds number increases, so with higher turbulence the range of scales of the eddies increases.

2.3 Pipe Flow

When there is a turbulent flow through a pipe, many of the previous described characteristics of the flow depend on the pipe characteristics. In pipe flow ,the characteristic length scale $\mathcal{L}$ equals the pipe diameter D, and the characteristic velocity scale $\mathcal{U}$ is equal to the mean velocity of the flow in the pipe $\langle\vec{U}\rangle$. So equation 2.3 changes in:

$$Re = \frac{\langle\vec{U}\rangle D}{\nu} \tag{2.5}$$

where the flow is laminar with a Reynolds number lower then 2300 and fully turbulent above 4000 (Pope, 2000). It should be noted that allthough for many purposes, like finding the Reynolds number, calculating with the mean velocity is fine, this does not mean that the velocity for every point and time in the flow is equal to this value. In reality the relation between the velocity fluctuation $\vec{u}(\vec{x},t)$, the flow velocity $\vec{U}(\vec{x},t)$ and the mean velocity $\langle\vec{U}(\vec{x},t)\rangle$ can be described by using the Reynolds decomposition:

$$\vec{u}(\vec{x},t) \equiv \vec{U}(\vec{x},t) - \langle\vec{U}(\vec{x},t)\rangle. \tag{2.6}$$

It should be kept in mind that in turbulent pipe flow not only the velocity varies randomly, because of the turbulent nature of the flow, but also that there is a pipe wall having a significant impact on certain areas in the flow. The different zones in a wall-bounded flow can be seen in figure 2.2. Next to the wall there exists a thin layer, the so called viscous sub-layer. In this sub-layer, the Reynold stresses are small because of the dominance of the viscous forces. Further away from the wall there is a buffer layer, where both inertial and viscous forces affect the flow, and closer to the center of the flow only inertial forces are important. In essence a pipe flow has a boundary layer with a thickness δ that is equal to the radius of the tube R. The boundary layer can be split in an inner layer where the flow is mainly determined by the distance to the wall, and an outer layer where the geometry (the radius of the tube in the case of a pipe flow) is important.

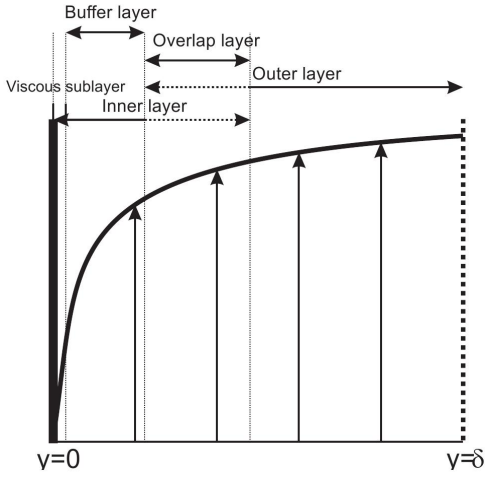

Figure 2.2: The Boundary layer of a wall bounded turbulent flow detailed (van Nimwegen, 2010)

2.4 Tracer Dispersion

In the experiments in this research a tracer is injected and its dispersion can be measured. When looking at the flow it is important that the results measured are a result of the behavior of the flow and give a realistic view of how the flow would behave if no tracer was injected. In order to be sure that the tracer behavior gives a representative view of the flow several flow characteristics can be estimated.

2.4.1 Taylor Dispersion

The dispersion of a tracer in turbulent flow has been researched in depth as far back as the 1920's by Taylor. One result of his research was the relation between the mean squared displacement $\langle y^2\rangle$ in the direction perpendicular to the flow and the mean squared velocity $\langle u^2\rangle$:

$$\langle y^2\rangle = 2\langle u^2\rangle \int_0^t \int_0^t R_L(\tau)\, d\tau\, dt, \tag{2.7}$$

where $R_L(\tau)$ is the Lagrangian velocity correlation coefficient, defined as

$$R_L(\tau) = \frac{\langle u(t)u(t-\tau)\rangle}{\langle u^2(t)\rangle}. \tag{2.8}$$

For small times τ, equation 2.7 can be simplified to:

$$\lim_{t\to 0}\langle y^2\rangle = \langle u^2\rangle t^2 \tag{2.9}$$

For times larger then t_1, which is the time it takes for the velocity fluctuations to become uncorrelated a Lagrangian integral time-scale can be defined, so that for times larger than t_1 the mean dispersion is given by

$$\lim_{t\to\infty}\langle y^2\rangle = 2\langle u^2\rangle T_L t \tag{2.10}$$

where the Lagrangian timescale T_L is defined as

$$T_L \equiv \int_0^\infty R_L(\tau)\, d\tau \tag{2.11}$$

In conclusion, it follows from Taylor's dispersion that for large t, when the correlation with the initial condition of each particle is completely gone, the dispersion follows a behavior similar to a 'random walk'. At small t, the behavior depends linearly on both the velocity and the time a particle is in the flow.

2.4.2 Radial and Streamwise Dispersion

In an circular tube with smooth walls the velocity profile of a turbulent flow has a large region where the velocity of the flow is nearly constant (Bird et al., 1962). Contrary to laminar flow where the velocity distribution follows a parabolic curve, as can be seen in figure 2.3. This means that when looking at tracer dispersion in the cross-sectional plane, in a large region in the core of the pipe the behavior of tracer particles is similar to the behavior in a turbulent field that is isotropic in two dimensions. As a result of the isotropic behavior in the cross-sectional direction the tracer dispersion follows the 'random walk' behavior with $\langle y^2\rangle \sim t$ at large t, as described in equation 2.10 (Pope, 2000).

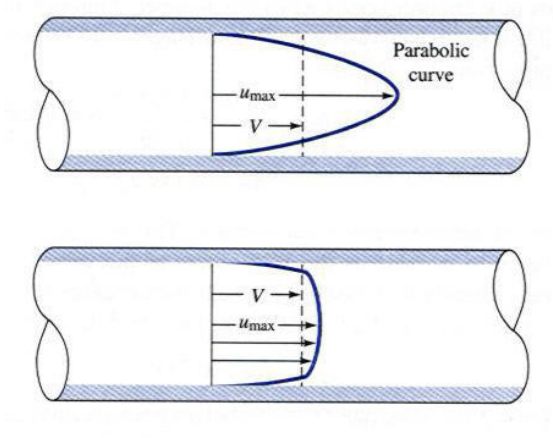

Figure 2.3: The velocity distribution of laminar (top) and turbulent (bottom) flow in a circular pipe.

Finally, it should be kept in mind that this approach only works in the outer layer region from the wall of the tube where the mean velocity can be assumed nearly constant. Closer to the wall, both the lower velocity, and thus the different turbulent characteristics there, and the wall, an impassable tracer barrier start playing a role, resulting in a distortion of the radial concentration distribution. In the core of the pipe, the turbulence structures causing velocity fluctuations in the radial direction cause tracers to disperse in a Gaussian fashion; this behavior is similar for the dispersion in the streamwise direction. Velocity fluctuations in the streamwise direction will cause any tracer to disperse with the same 'random walk' behavior resulting in Gaussian mean-concentration distribution both in the streamwise and the radial directions.

2.4.3 Schmidt Number

The dispersion of a tracer in turbulent flow can be caused by different mechanisms. Diffusivity caused by turbulence is described in the section above. Molecular diffusion is the other mixing process; it is caused by the the movement of individual molecules because of their thermal energy, which results in the tracer dispersing slowly. The ratio between these mixing processes is given by the Schmidt number:

$$Sc = \frac{\nu}{\Gamma} \tag{2.12}$$

where Γ is the molecular diffusivity. With the Schmidt number, the transport of concentration can be described by the convection-diffusion equation, which follows from the continuity equation 2.1:

$$\frac{\partial \phi}{\partial t} + \vec{U} \cdot \nabla \phi = \frac{\nu}{Sc} \nabla^2 \phi \tag{2.13}$$

where the passive scalar concentration is denoted by ϕ. The rate of change of a passive scalar can be seen as dependent on a convective term and a diffusive term. The ratio between the convective term and the diffusion term is given by the Péclet number:

$$Pe = \frac{\mathcal{U}\mathcal{L}}{\Gamma} \equiv ReSc \tag{2.14}$$

When the Péclet number is high, which will occur when the Schmidt number is high, it is clear that the diffusivity term in the equation plays a negligible role in the dispersion of a scalar. This means that nearly all of the tracer dispersion is caused by the fluid motion. Naturally, if one is interested in investigating the flow characteristics this is desirable.

2.4.4 Buoyancy

Besides the diffusivity, it is also important that the injected tracer can be seen as a passive scalar. Since an injected tracer can have a different density than the bulk medium it is important to compare the influence of buoyancy with the inertial forces. For this, the Grashof number divided by the Reynolds number squared can be used; in the case of a tracer in pipe flow with constant pressure and temperature this gives

$$\frac{Gr}{Re^2} = \frac{\beta g \left(\phi_b - \phi_{tr}\right) D}{\mathcal{U}^2} \tag{2.15}$$

where β is the cubic expansion coefficient of the salt in water given by

$$\beta = -\frac{1}{\rho}\left(\frac{\partial \rho}{\partial \phi}\right) \tag{2.16}$$

The concentration in the injected tracer and the concentration in the bulk medium are given by ϕ_{tr} and ϕ_b; g is the gravitational acceleration. For situations where $Gr/Re^2 \ll 1$ the inertial forces are much more important and the buoyancy plays a negligible role in the dispersion (Bird et al., 1962).

2.5 Measuring a Fluid Flow

2.5.1 Local Measurement Methods

In the earliest experiments on tracer dispersion, one used probes for measuring varying quantities of tracer concentration at a single point. These probes could be (i) conductivity probes, used with a salt water, tracer or (ii) temperature probes when the injected tracer is fluid with a different temperature, or a heat source is used. Also, sample extraction capillaries where used in many experiments, when the injected tracer was a dye or even radioactive material. The extracted sample could then be examined on tracer concentration externally, in a photometer for dye concentration, or in scintillation detectors for radio-active samples. Obvious downsides of these early techniques are that measurements are only done in one position per probe, and that time-resolutions where in most cases very low or that only time-averaged measurements where possible. Also, there is a small influence on the flow from the probe, which would influence additional measurements downstream from the probe.

2.5.2 Global Measurement Methods

A more modern method of measuring concentration values in a single-phase environment is (Planar) Laser-Induced Fluorescence. LIF uses a laser or laser-sheet in order to excite tracer particles injected in the flow in the plane of that sheet. Within a few nano or micro-seconds these particles get rid of their surplus energy by transmitting a photon. These photons can be measured with, for example a CCD camera perpendicular to the laser sheet, resulting in two-dimensional global measurement data of the tracer concentration. For example, Aanen (2002) used LIF in order to complement his Particle Image Velocimetry measurements with localized tracer concentration data. Vliet et al. (2004) managed to create a quasi-3D LIF measurement by sweeping the laser-sheet up and down, so that, effectively, the concentration in a three-dimensional region is measured. In LIF, a high spatial-resolution can be achieved, depending on the camera and photomultiplier used for measuring the emitted light. However, the time-resolution is limited; particularly in 3D-LIF, because of the need to sweep the sheet of laser up and down. In the research of Vliet, for example, the time-resolution was in the order of 10 ms. A disadvantage of this technique is the need for optical accessibility. In practice this means it is only viable in simple geometries like. e.g. a circular tube. In complex geometries, compensating for the different refractive indexes becomes very difficult.

2.5.3 The Wire-Mesh

In this research a global measurement method for measuring tracer concentration in a plane was desired. Because of the complex geometry of the rod-bundle setup, optical options where ruled out. The injection of radio-active tracers is difficult to organize with respect to costs and radiation-safety standards that have to be met. Therefore, the choice was made to use a wire-mesh measurement equipment. The wire-mesh is capable of measuring conductivity values at high frequency with good spatial-resolution over a plane. In essence, this equipment can be described as a global conductivity probe, which introduces only a small disturbance in the flow and combines a very high time-resolution with a good spatial-resolution.

CHAPTER 3

The Wire-Mesh

In order to gain insight in the mixing of heat in a rod-bundle geometry the choice was made to use a tracer with high conductivity (salt water) in order to mimic thermal energy. The dispersion and mixing of this tracer in the flow is measured with a wire-mesh equipment. The wire-mesh has mainly been used as a reliable way to distinguish gasses and liquids, with high spatial and time-resolution in the cross-section of a flow. The past results in multi-phase flows, however, do not give enough information about the actual capabilities and reliability of the equipment in a single-phase environment. Therefore, the capabilities of the sensor when applied in single-phase flow is something that is looked at, as well as the possibilities of improving these capabilities.

3.1 An Electrode Mesh

The wire-mesh measurement technique is basically an expanded version of the conductivity measurement probe used by Taylor (1954), in his pioneering work on tracer dispersion in pipe flow. The difference is that where Taylor could measure the conductivity in one point in the flow, the wire-mesh sensor can measure the conductivity in a plane, with a spatial-resolution of millimeters and a frequency of up to 5 kHz. The wire-mesh measurement sensor was developed by Prasser et al. (1998), based on an older U.S. patent from Johnson (1987). His goal was to develop a relatively cheap measurement method with high spatial and time-resolution, able to measure gas-liquid flow distribution over the cross-section of a flow. In fig 3.1, a schematic respresentation of a wire-mesh is given. Visible are the the two layers of wires, perpendicular to each other and to the flow direction, situated at a small distance from each other. By sending small electronic pulses one by one through each of the transmitter wires and measuring the received signal in every receiver wire separately, the conductivity of the fluid at every separate crossing between two wires is measured.

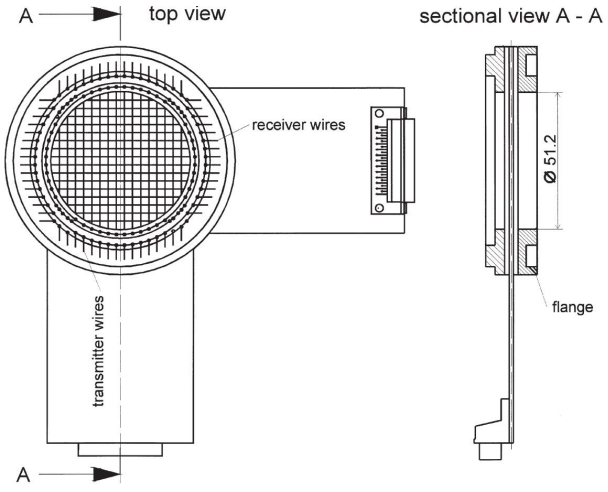

Figure 3.1: A schematic respresentation of a wire-mesh sensor by Prasser et al. (1998).

3.2 The Measurement Principle

The measurement principle of the wire-mesh sensor itself rests on a simple principle. It measures the conductivity of two wires which are separated by a small distance filled with the fluid that is to be measured. It manages to create a lot of measurement points in a plane by using a multitude of wires, which are controlled by some electronic equipment that also processes the acquired data.

3.2.1 The Sensor

The wire-mesh sensor that is used in this project is capable of measuring the conductivity of multiple points in a plane. Wire-mesh sensors based on capacity measurements are also available but will not be used in this research. In figure 3.2, a schematic of the wire-mesh system from the original paper by Prasser et al. is shown. It consists of four wires in one plane, through which electrical pulses are transmitted, and four wires located at a small distance below the top plane (2 mm in Prasser's case) perpendicular to the transmitter wires. The planes of the wires are perpendicular to the direction of the flow, so, when looking in the flow direction, every transmitter wire has one 'cross-point' with each receiver wire. Since the transmitter wires are transmitting a pulse one by one, the conductivity of the fluid flowing through one of the crossings in the mesh can be acquired by measuring the signal that is transmitted through the fluid from the transmitting wire to the receiving wire. In this example, this results in sixteen effective conductivity-measurement points in the measurement plane.

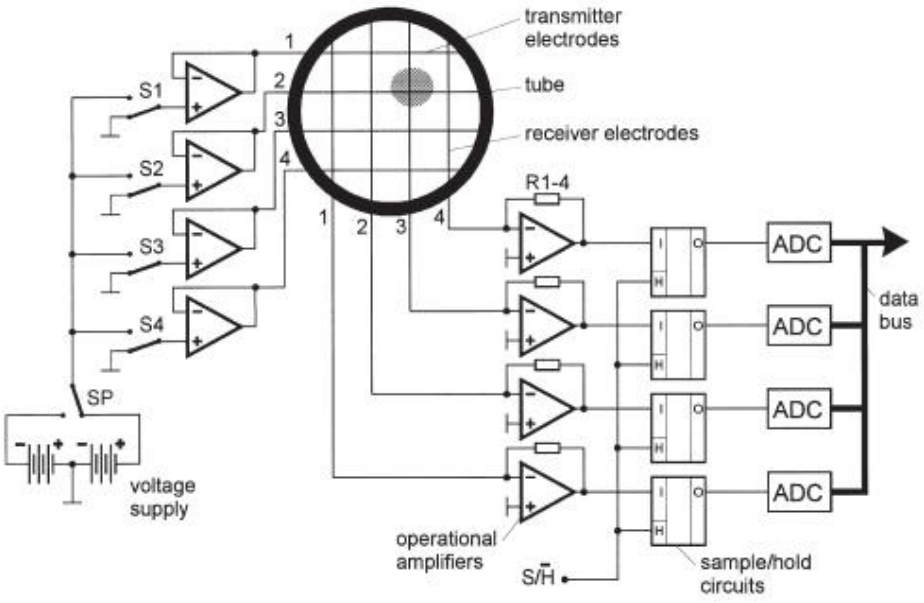

Figure 3.2: The wire-mesh sensor as it was designed by Prasser et al. (1998).

3.2.2 The Electronics

In order to prevent electrolysis the pulses that are transmitted are not DC, but consist of alternating positive and negative signals of equal size. Also, when a conductive fluid is present the received signal shows transient behavior because of the capacitance of the wires. In order to minimise this effect, the actual moment of measuring the received signal is after the transient behavior has died out, as can be seen in figure 3.3. Another problem with this setup, that Prasser et al. managed to solve with their

design, is the surpression of cross-talk. For a sharp resolution, it is vital that only the wire with a driven current is transmitting a signal. However, since the transmitter wires can be close to each other it is necessary to prevent the electrical field from the transmitting wire to generate a signal in neighboring wires. This cross-talk would result in a blurring of the signal, which is undesirable. In order to prevent this, the wire-mesh is constructed such that the wires have a significantly lower impedance than the fluid between them. This way, there is no driving potential difference between wires, so cross-talk is effectively surpressed (Prasser et al., 1998).

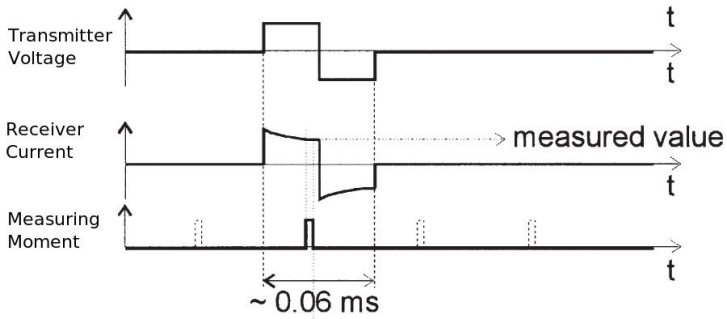

Figure 3.3: The transmitted and received signal, and the moment of measuring, from Prasser et al. (1998).

The electronics of the device is controlled by a specially designed program, which can be used to amplify the signal strength, the measurement frequency and the duration of one measurement. It can also give a live output of the measured signal and handles the transport of the temporary stored data to its final designated folder.

3.2.3 Electro-Magnetic Field

From the start of the development of the wire-mesh sensors the assumption was made that the volume of one measurement point could be defined as a square the size of one mesh with the actual crossing of the transmitter and receiver wires as its center (Richter et al., 2002). Unfortunately this seems to be a too simple assumption. Smeets (2009) found that bubbles situated outside a measurement volume have some measurable influence in this volume. By using the software package Simion 7.0, Smeets simulated the electric potential between a transmitter and perpendicular receiver wire, resulting in figure 3.4. From this finding Smeets proposes a new measurement volume for one measurement cross-section, which is not symmetrical in the receiver and transmitter 'directions'. Basically, this new proposed measurement volume is supposed to be diamond shaped and larger in the direction parallel to the receiver wires. The result is that in the transmitter direction the measurement sections somewhat overlap which adequately explains how bubbles can slightly affect the signal one or even two measurement points away.

The simulation that forms the basis of this approach is made with the assumption that there is a uniform medium between the two wires. It is not known how the equi-potential field looks like when there are regions with more or less conductivity present and how this would affect the measurement volume of one point. Besides, it is clear that alltough there is an influence of a bubble on neighboring measurement points, it is very hard to quantify this influence. No adequate solution that manages to accurately quantify and incorporate the model from Smeets has been found so far. Especially not for this research, where the shape of the equi-potential field depends not on the approximation of a non-conductive bubble, but on the more diverse concentration distribution of a tracer that will not have a sharp, cut-off boundary with non-tracer regions; instead it has a gradual and unpredictable distillation. Therefore, like in many other wire-mesh experiments in the literature, it was chosen in this research to use the more simple approach of assuming that the wire-mesh measures in a point representing the squared measurement volumes.

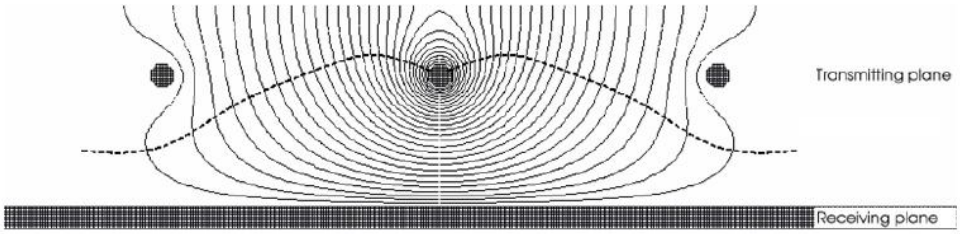

(a) Equi-potential field in the plane of the receiver wires.

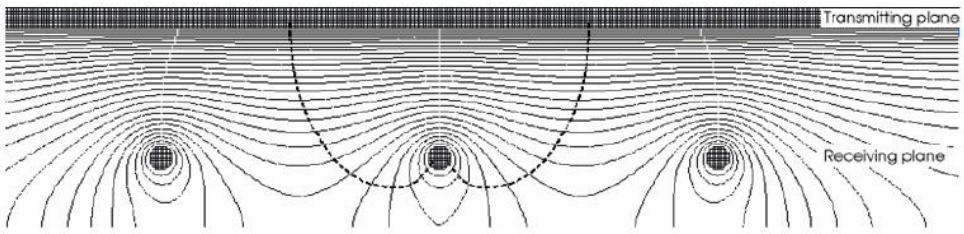

(b) Equi-potential field in the plane of the transmitter wires.

Figure 3.4: The simulated equi-potential fields in two planes caused by the wire-mesh signal, where the dashed lines represent the boundary of the measurement section as proposed by Smeets (2009).

3.3 Applications

The wire-mesh has been implemented in the past in various experiments with a variety of different characteristics. In this research, the challenge lies in getting a grip on the reliability of the equipment for single-phase concentration measurements.

3.3.1 Multi-Phase Flows

Since its invention, the wire-mesh has been used both at Delft University and in other places in various experiments and geometries for different purposes. Examples of wire-mesh-based research in Delft are Manera (2003), Belt (2007), Smeets (2009) and Descamps (2007), who performed measurements with a wire-mesh for different purposes. Manera looked at the flashing induced instabilities in the gas-liquid flow when starting a BWR, Belt used a novel custom-designed wire-mesh for measuring the film-thickness at the walls in annular flow, and Descamps measured the bubble sizes in a gas-driven driven vertical flow.

Outside Delft, the the wire-mesh technology has been used in a similar range of applications, with Prasser et al. (2005) comparing the capabilities of a wire-mesh with fast X-ray tomography, Pietruske and Prasser (2005) using the apparatus for measurements in high flow and pressure multi-phase flow, and Silva et al. (2007) developing a wire-mesh that uses the capacitance of a fluid instead of its conductivity.

In figure 3.5 an example of a wiremesh used in a two-phase flow by Prasser et al. (2005) is shown. The signal output of the wire-mesh is not dependent on the fluid properties at the crossing of two wires but actually it depends on the mean properties at of the fluid in a small volume between the two wires. Because of this, the output can vary depending on how big a piece of this volume is covered by a bubble. This makes it possible to use the wire-mesh for the reconstruction of bubble sizes and shapes, as well as the measuring of void fractions, as done by Prasser et al. (2005).

Figure 3.5: The measurement of a gas bubble with a wire-mesh in a two-phase flow Prasser et al. (2005).

3.3.2 Single-Phase Measurements

What all these examples of the use of wire-meshes have in common is that they are used in the kind of flows for which the wire-mesh originally was designed: gas-liquid flows. In this research, however, the interest lies in single-phase flows. In essence, the use of the wire-mesh this way is not much different from the experiments from Taylor. A conductive tracer is injected and at a certain distance downstream the fluid conductivity is measured. The difference is that where Taylor had only one measurement point, the wire-mesh is capable of measuring up to 1024 points instantaneously.

In the literature two other projects where found where a wire-mesh was used in single-phase flow. Walker et al. (2009) use three wire-meshes for measuring the way liquids from two legs in a T-junction are mixed in the third outflowing leg. Ylönen et al. (2011) performed the only other research that was found which uses a tracer injected with a small capillary in order to look at dispersion in single-phase flow. Ylönen et al. performed these measurements in a rod-bundle geometry that is comparable to the rod-bundle setup that is used in this project (described in part 2 of this thesis). In the works of both Walker et al. (2009) and Ylönen et al. (2011) the emphasis lies on the physics of the phenomenom observed. Central to this thesis is the technique and its possibilities and limitations when measuring mean tracer concentrations and identifying turbulence structures in single-phase flow. For this purpose, the reliability and accuracy of the equipment was investigated and several benchmarks were performed using experimental results from established techniques.

3.4 Capabilities and Limitations of the Wire-Mesh

3.4.1 Capabilities of the Wire-Mesh

As Prasser et al. (2005) show, the wire-mesh proves to be a reliable alternative for X-ray tomography in acquiring the void fraction in a gas-liquid pipe flow as can be seen in figure 3.6. The equipment is capable of a high spatial-resolution, in the order of millimeters, and a frequency of up to 5 kHz. This high spatial and time-resolution allows the wire-mesh to even distinguish small bubbles which cannot be measured with X-ray tomography, since they move too fast through the measurement plane to be detected (Prasser et al., 2005).

Also, the wire-mesh does not need optical access in order to measure. This gives it an advantage compared to optical global experimental techniques, like Laser Induce Fluorescence, which are not able to measure if non-transparent fluids are involved or the tube cannot be made of transparent material. A disadvantage of the wire-mesh is that it is a slightly intrusive measurement technique. This will result in a small influence in the flow downstreams of the detector; This may cause problems when using it in online measurements in an operational system. In an experimental facility, however, only a small influence in the measurement results is mentioned by Prasser et al. (2005): a small distortion of Taylor bubbles and a small pressure drop over the flow.

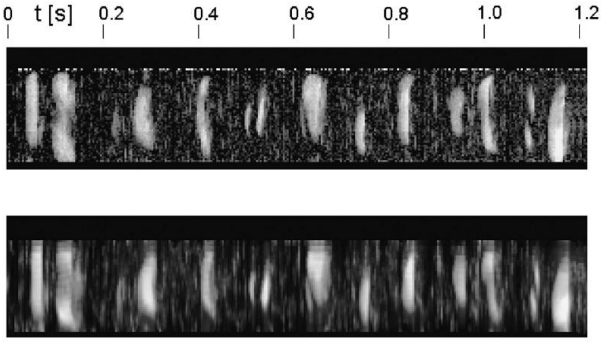

Figure 3.6: Comparison of the void fraction measured with a X-ray tomograph (top) and wire-mesh (bottom), by Prasser et al. (2005).

3.4.2 Limitations of the Wire-Mesh

As explained in 3.2.3, the output of the sensor in one point of the cross-section is not only dependent on what the conductivity is at that point but is also influenced by the conductivity around that point. In figure 3.7, the wire-mesh output and the actual bubble that it is measuring are shown. It is clear that especially in the plane of the receiver wires (horizontal) the influence of the bubble is noticeable outside the area where the bubble actually is. In gas-liquid flow, some of this excess signal may be removed in post-processing by using a threshold for the signal output, but it is clear that the spreading of the electrical field will remain a source of inaccuracy. Other sources of the error in measuring with the wire-mesh are not caused by physical effects, but rather by limitations in the equipment. Signal noise can be observed in some parts of the measurement section, and besides that, the relation between signal output and conductivity is not everywhere as constant as it should be (see also sections 3.5 and 4.2).

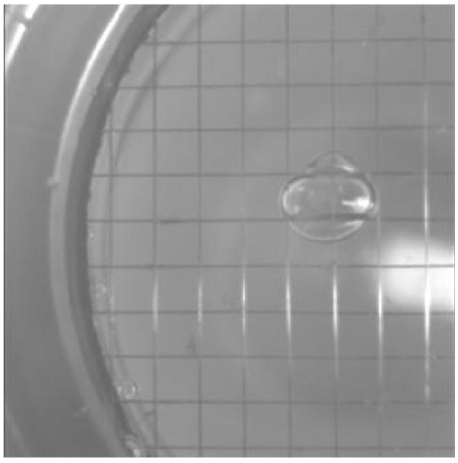

(a) A gas bubble photographed when moving through the a wire-mesh.

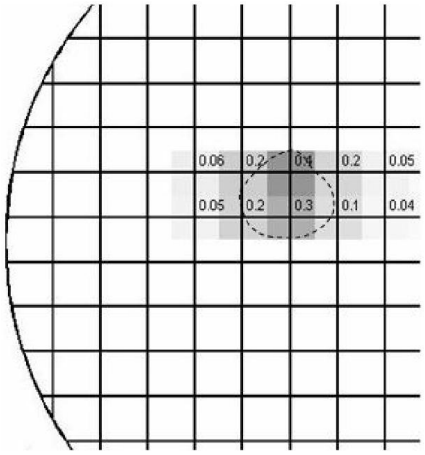

(b) The wire-mesh output from the bubble.

Figure 3.7: A comparison between a gas bubble (left) and the wire-mesh output from this bubble (right) (Smeets, 2009).

3.5 Calibration Procedure

As stated before, the wire-mesh measures the conductivity between two separated wires. As in any experimental method this signal is not perfect: small irregularities may occur during the construction, or the electronic equipment may cause some wires to give a lower signal than others. In order to compensate for this Prasser et al. (2005) assume a linear relation between conductivity and the void fraction $\varepsilon_{k,i,j}$ at each time-frame and wire-crossing:

$$\varepsilon_{k,i,j} = 1 - \frac{I_{k,i,j} - I_{gas,i,j}}{I_{liquid,i,j} - I_{gas,i,j}} \tag{3.1}$$

where $I_{\text{k,i,j}}$ is the measured signal at point i, j in frame k, $I_{\text{liquid,i,j}}$ is the average signal strength measured in point i, j in a reference measurement where the tube only contains liquid, and $I_{\text{gas,i,j}}$ is the average measured signal with only gas. Except for a few recent exceptions, the wire-mesh equipment has been used in two-phase flows only.

In this research only one liquid is flowing through the mesh. In order to obtain a signal that is actually providing useful information, a tracer (salt water) is injected at certain distance upstream of the wire-mesh. The wire-mesh can then provide information about the concentration of the tracer in its various measurement points, and thus tell something about the dispersion of this tracer in the flow. Since at low concentrations the relation between salt concentration and conductivity is linear, in principle an equation similar to 3.1 could be used. Unfortunately measuring with a pure tracer is not possible due to limitations of the equipment; therefore, Ylönen et al. (2011) use a reference measurement where the wire-mesh is covered with a higher conductivity liquid then the 'background' medium but below the maximum conductivity that can be measured. After that, these values are compensated with the difference in conductivity between the tracer and this reference liquid. Using this approach the tracer concentration is given by:

$$\phi_{k,i,j} = \frac{I_{k,i,j} - I_{bulk,i,j}}{\frac{\sigma_{trace}}{\sigma_{ref}} I_{ref,i,j} - I_{bulk,i,j}}, \tag{3.2}$$

where $\phi_{\text{k,i,j}}$ is the measured tracer concentration value at point (i, j) for each frame k, $I_{\text{k,i,j}}$ is the intensity of the output signal for the measurement itself, $I_{\text{ref,i,j}}$ is the intensity of a reference measurement in a high conductivity, homogenous solution, averaged over time, and $I_{\text{bulk,i,j}}$ is the intensity of the output signal of the bulk liquid, the 'background signal', measured right before injection of the tracer; σ_{trace} and σ_{ref} are the conductivities of the injected tracer and reference liquid, respectively, which where measured with a separate conductivity sensor. The result of this calibration procedure is a dimensionless value for the tracer concentration in every measurement point, for every time-frame.

3.5.1 Calibration Obstacles

Anyone who ever tried measuring the conductivity of a liquid with a simple setup of two copper wires and a multi-meter can agree that there is not a simple relation between the signal output of such a simple setup and the conductivity. Leakage of the signal in the liquid (if conductive), electrolysis and the shape of electrical field lines in the liquid all result in difficulties when acquiring the conductivity while measuring the current. In the wire-mesh equipment this kind of problems are compensated by the electronic circuitry and by the use of a driving voltage without a DC component. Further calibration during the post-processing, using reference measurements, provides even more reliable data.

A main problem of the equipment and calibration procedure is that it assumes a linear relation between signal output and the conductivity of the liquid. The manufacturer of the equipment only guarantees this linearity up to one $\mathrm{mS/cm}$, which is a value that is quite small, considering the background conductivity of the bulk liquid in the loop and the conductivity of the tracer that is injected. In this research, steps are taken to look into possibilities to increase the measurable range, to verify the linear relation

between signal output and conductivity, and to acquire information about the reliability of the output of the wire-mesh in general. In section 4.2, the results of this are further discussed and evaluated.

CHAPTER 4

Measurements in Single-Phase Pipe Flow

In order to investigate the capabilities of a wire-mesh sensor in single-phase, turbulent flow, measurements where performed in a horizontal tube. A tracer is used in order to measure and visualize different properties of turbulent flow. First, the measurement set-up for single-phase wire-mesh experiments is discussed. After the overview of the equipment, the outcome of the calibrations described in section 3.5.1 is treated. The chapter is finished with the results from the measurements and their implications..

4.1 Experimental Set-up

The set-up used in part I of this research is a set-up that has previously been used for other experiments including measurements in multi-phase flow using a wire-mesh. Because of this a set-up large enough for a fully developed single-phase flow, equipped with a wire-mesh, was available.

4.1.1 Flow-Loop

The flow that is used in the horizontal tube is a gravity-driven flow that was originally used in measuring slug-flow and for doing research in new methods for multi-phase flow measurement, where a wire-mesh was used for controlling the results (figure 4.1).

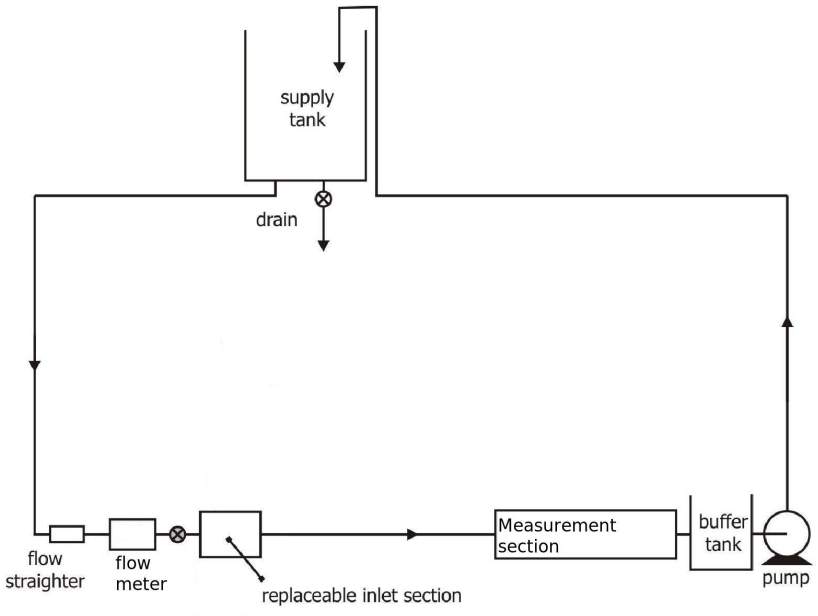

Figure 4.1: The flow-loop used used for the measurements in the horizontal tube.

As mentioned, the flow is gravity-driven; this is achieved by collecting the water in a buffer tank and using a pump controlled by an ultrasound level-sensor to pump it into the supply tank, which is situated 4 meters above the measurement section. The flowrate can be measured with an electromagnetic flowmeter and set with a manually controlled valve (figure 4.2). The internal diameter of the pipe is 9.9 cm and it has about 300 diameters of undisturbed development length from the valve to the measurement section.

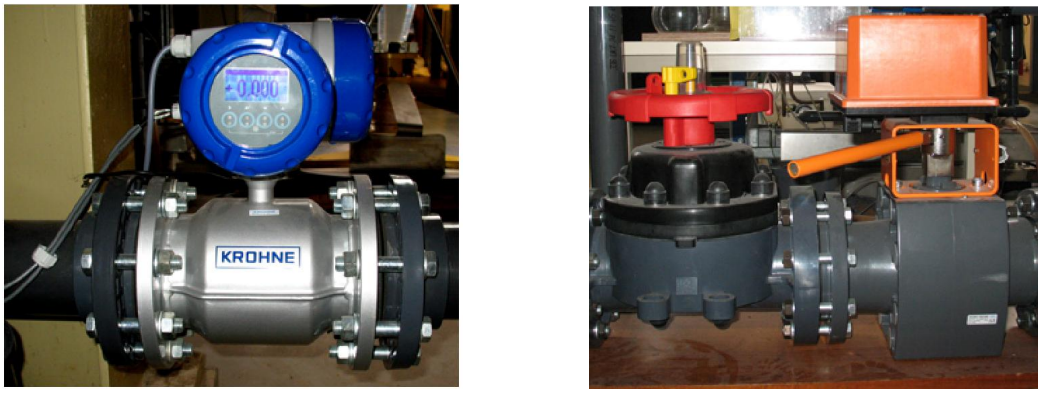

(a) Krohne Optiflux 2300 C flowmeter. **(b)** George Fisher EA 41 valve.

Figure 4.2: The electromagnetic flowmeter (left) and the manually controlled electronic valve (right).

4.1.2 Measurement Section

A wire-mesh was installed in the flow-loop, with several tracer injection points located upstream of it. The wire-mesh used in this set-up consist of two layers of 32 wires each, covering the cross-section of the tube with about 800 measurement points, with a spatial-resolution of 3 mm. The distance between the layer of transmitter, and the layer of receiver wires is 1.5 mm. The wires are 0.125 mm in diameter and thus have only a small influence on the behavior of the large scale structures in the turbulent flow. The used wire-mesh is shown in figure 4.3a. The tracer is injected with a custom-made capillary. The capillary has an outer diameter of 1.2 mm and an inner diameter of 0.9 mm. In order to minimise the disturbance of flow promoted by the part of the capillary that is perpendicular to the flow, the part of the capillary parallel to the flow is 13 cm long (figure 4.3b).

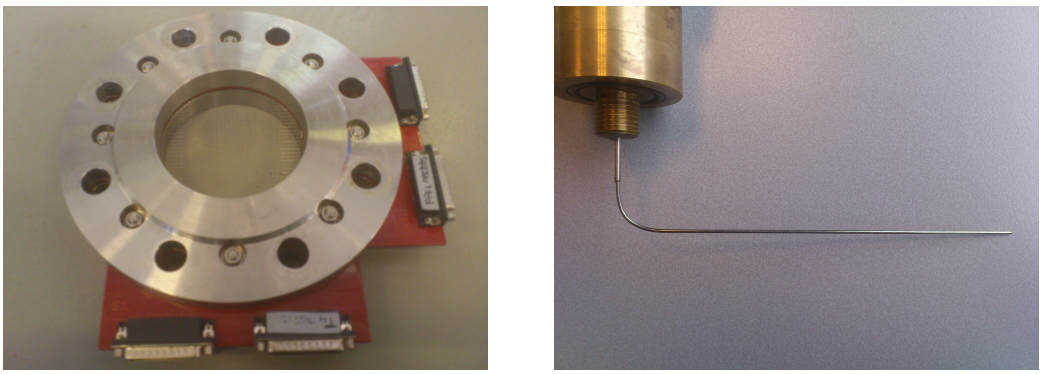

(a) Wire-mesh **(b)** Injection capillary

Figure 4.3: The wire-mesh (left) and the capillary used to inject tracer in the horizontal pipe (right).

The capillary can be installed at six different points upstream from the wire-mesh. The actual distances between the exit point of the injector, expressed in pipe diameters, are shown in table 4.1.

Table 4.1: The different injection positions upstream from the wire-mesh position normalized with the pipe diameter D=9.9cm.

Injection Point	Distance from Wire-mesh
A	0.4D
B	2.0D
C	3.5D
D	5.1D
E	6.6D
F	9.7D

In figure 4.4, the injection of a tracer, as it was done in experiments, is shown. In this case, as a tracer was used Potassium Permanganate ($KMnO_4$) dissolved in water in order to give a visualization of the turbulent dispersion of the tracer. In the experiments in the rest of this research sodium chlorite ($NaCl$) dissolved in water is used as a tracer. The use of dye as a way of visually checking the tracer dispersion showed that the injection capillary that was initially used, which had a much shorter length parallel to the flow had a significant influence on the tracer dispersion. By checking with dye, it was found that using a length of 13 cm for the part of the L-shaped injector parallel to the flow instead of the initial 15 mm, removed the tendency of the tracer to disperse in the upwards direction. In figure 4.4 the result of this is shown, the tracer disperses both up and down. Dye injection was also used to visually check the behavior of tracer in the turbulent flow. This visualization gave a rough estimate of the dipsersion process and how it evolves in the downstream direction, providing insight while post-processing the wire-mesh data. At the right side of figure 4.4, the end of the capillary is still visible. At the top of the tube closed alternative injection points are visible, on which the injection capillary can also be attached. The wire-mesh is not visible in the picture, but is situated further downstream.

Figure 4.4: A picture of the dispersing purple dye that was injected into the turbulent pipe-flow.

4.1.3 Further Setup Properties

The tracer that is injected consists of water taken out of the flow-loop to which salt is added with a concentration of 50 grams per liter. This and further information about the measurement set-up can be found in table 4.2. The Reynolds, Schmidt and Grashof numbers are obtained from the formulas introduced in chapter depends 2, where for the Grashof number the properties of the injected tracer were used. The tracer conductivity depends not only on the salt concentration but also on the temperature, resulting in slightly varying values for the conductivity.

Table 4.2: Different flow and set-up properties summarized.

Concentration of the injected tracer	50 g/L
Conductivity of the injected tracer	65 mS/cm
Tube diameter	9.86 cm
Tube length	30 m
Reynolds number	0 - 70000
Schmidt number	6700
Grashof number with the properties of the injected tracer	$3.2 \cdot 10^8$

4.2 Calibration

During the application of the wire-mesh in single-phase flow various solutions for expanding the capabilities of the equipment and solving some of the existing problems came up. Of course, modifying the equipment in order to apply these solutions must not have a negative influence on the reliability of the signal. In order to confirm this, several tests were performed, as well as the general calibrations necessary for using the equipment.

4.2.1 Increasing the Measurement Range

One of the problems in applying the wire-mesh in this research is the limited conductivity range of the fluid in which the wire-mesh is applicable. The wire-mesh originally has only been guaranteed by the manufacturer to have a reliable signal for conductivities in the range 0-1000 $\mu\mathrm{S/cm}$. In these experiments the bulk medium has, depending on the temperature and other factors, already a 'background' conductivity in the range 450-650 $\mu\mathrm{S/cm}$. To put this in perspective, the injected tracer has a conductivity in the order of 50 $\mathrm{mS/cm}$. Therefore, the effective measurement range left by the background conductivity and the upper limit of the equipment is only 1% of the total conductivity of the tracer. As can be seen in figure 4.4, the fluctuations of the tracer concentration can be so large in the turbulent flow that it is difficult to make sure that the conductivity remains within the measurable range. Due to this, an also to reduce the risk of essentially short-circuiting and damaging the equipment when measuring a conductivity that is too high, it was chosen to try adding resistors to the receiving wires. Since the signal produced by the equipment in the transmitter wires is voltage-driven, the total voltage in the circuit stays the same. Therefore, increasing the total resistance by adding resistors results in a lower current in the measurement section of the electronics. In theory, this should decrease the signal and possibly increase the measurement range the equipment can withstand before the circuitry burns.

In figure 4.5, the output of the wire-mesh in two different homogenous liquids is shown, with and without any modification. The maximum conductivity that was measured was 2010 $\mu\mathrm{S/cm}$. Above this value the output of the wire-mesh collapsed and the electronic equipment started to heat-up noticeably when no resistors were added; so, this was deemed to be the maximum measurable conductivity. Figure 4.5 shows that the wire-mesh gives a reasonable signal. However, there are areas where the signal is less strong, which could be due to wear of the sensor or in the electronic device. When resistors are added, the homogeneity of the output does not become better or worse. However, it is clear that the the output is significantly lower everywhere in the mesh, and thus can potentially increase the range of measurable conductivities. The output is displayed as a percentage of the maximum current that the equipment can withstand before the signal colapses.

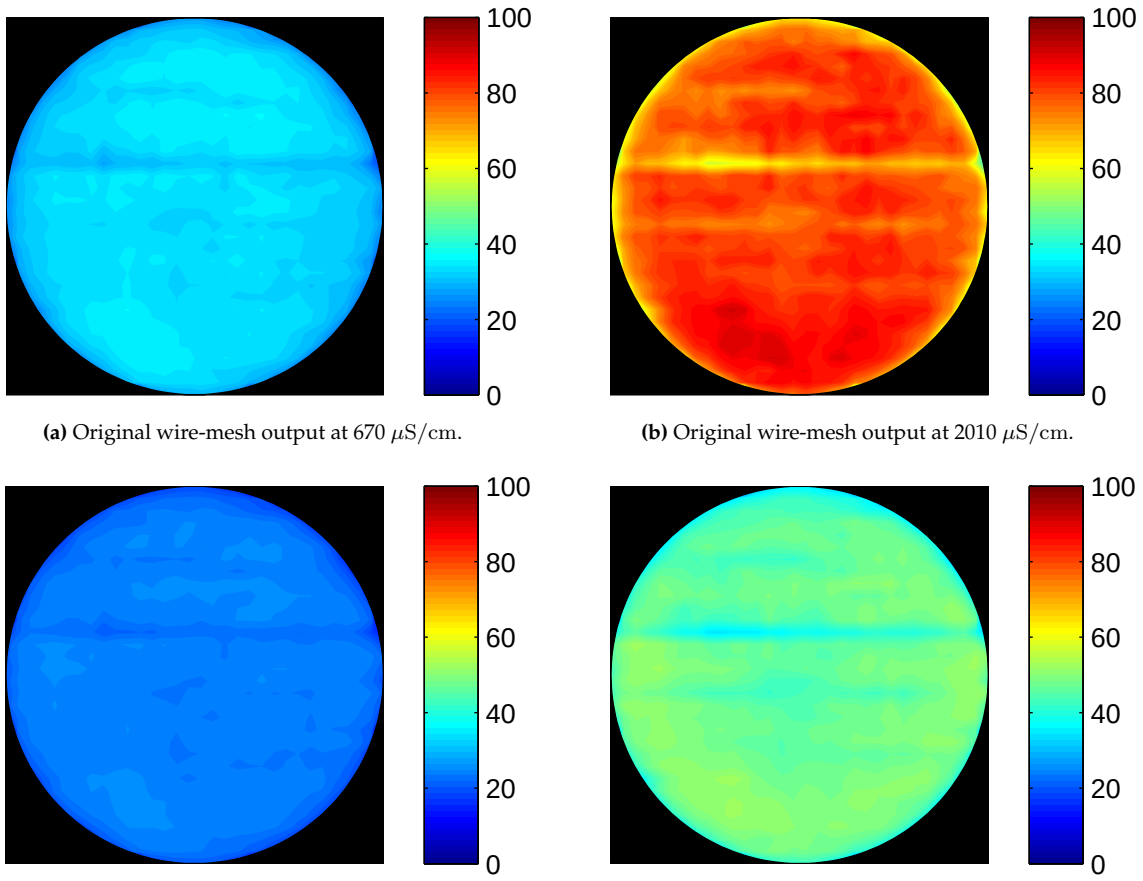

(a) Original wire-mesh output at 670 μS/cm.

(b) Original wire-mesh output at 2010 μS/cm.

(c) Modified wire-mesh output at 670 μS/cm.

(d) Modified wire-mesh output at 2010 μS/cm.

Figure 4.5: Wire-mesh output in percentage of the maximum allowable signal output for liquids with different conductivities, measured without (a,b) and with (c,d) as additional resistance.

4.2.2 Linearity of the Signal Output

Before increasing the measurement range with added resistors, the linearity of the signal output has to be investigated. The application of the wire-mesh for single-phase flow with a high conductivity tracer requires some calibration, as was described in section 3.5. The principle of this calibration relies on a linear dependency of the output of each measurement point on the conductivity of the liquid. The relation between signal output and conductivity does not need to be the same for all measurement points, as long as it is linear at each point. In order to investigate the linearity of the signal, and its behavior in general, a measurement set was performed. The wire-mesh was used in homogenous solutions of different conductivities, both with and without additional resistors applied to the equipment. To illustrate the results of this measurement set, in figure 4.6 is shown the output in percentage of the maximum allowable output, as a function of the conductivity in mS/cm for five different points in the wire-mesh. From figure 4.6 the same conclusion can be drawn as from figure 4.5, that the added resistors result in a smaller sensor output than without the resistors. Unfortunately, it is also clear that the linear relation between conductivity and sensor output, which holds fairly well without resistors even up to 2010 μS/cm, cannot be applied when the equipment is modified. Because of these results, the choice was made to do the measurements without added resistors, in order to get the most reliable results.

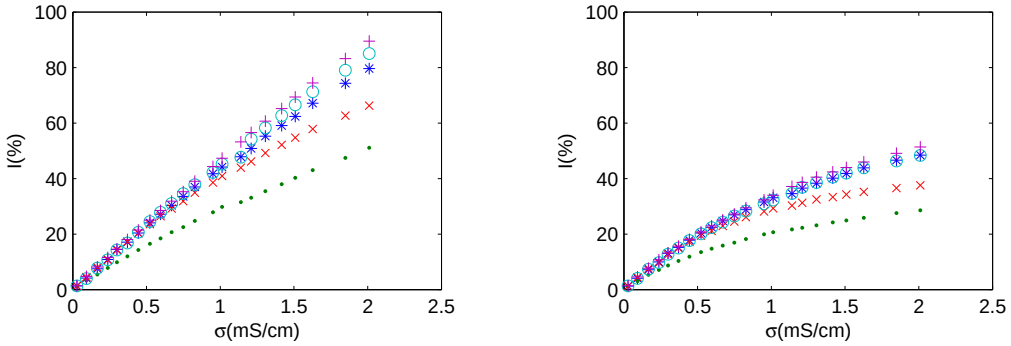

(a) Output without resistors.

(b) Output with added resistors.

Figure 4.6: Wire-mesh output in percentage of the maximum allowable output without (left) and with (right) added resistors, at five different measurement points, as a function of the conductivity, in mS/cm.

4.2.3 Calibration Accuracy

The calibration method described in section 3.5 is necessary to translate the raw wire-mesh output in an accurate representation of the tracer concentration. The results of these calibrations are visible in figure 4.7: the calibrated wire-mesh output of the same two homogeneous solutions as in figure 4.5, expressed in μS/cm. The values over the wire-mesh still show fluctuations; however, whereas the uncalibrated signal has variations in the output of up to 40%, the calibrated signal gives an output that deviates less then 10% from the measured solution.

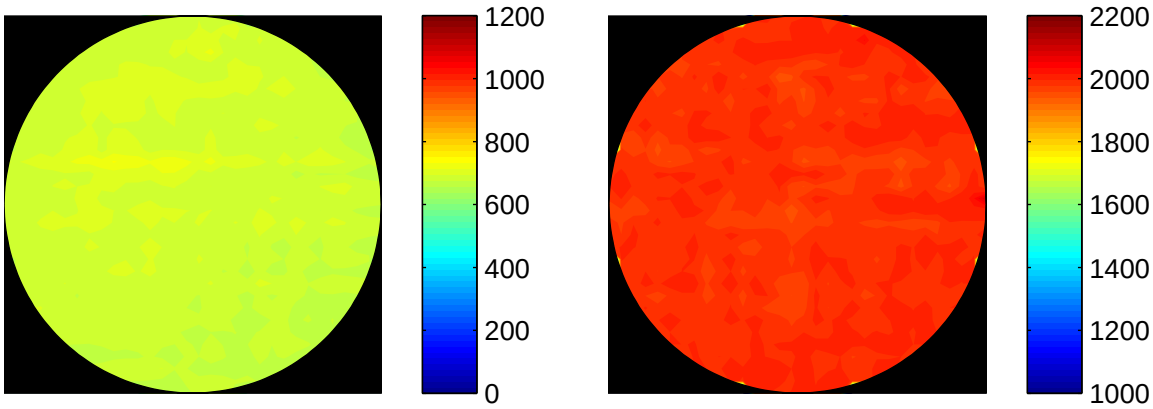

(a) Calibrated output at 670 μS/cm.

(b) Calibrated output at 2010 μS/cm.

Figure 4.7: Wire-mesh output at two different conductivities after calibration of the signal.

During these calibrations, it was also noted that the sensor output at higher frequencies had a tendency to become inconsistent, especially when measuring in solutions with higher conductivities. Also, at higher frequencies the signal output during a measurement series in a constant liquid varied more heavily over the course of the measurement series then when measuring at lower frequencies. An explanation for this might be that operated at its highest frequencies the equipment starts to heat faster, since the measured pulses follow each other faster than at lower frequencies. Especially at higher conductivities, where the measured current is also higher this could start playing a role. Since the behavior at 2500 Hz, or lower did not show the same irregularities, it was chosen to perform the measurements at 2500 Hz, or lower.

4.2.4 Calibration Results

In conclusion, the calibration of the equipment allows to perform conductivity measurements in a homogeneous solution within 5% of the actual conductivity. Variations over the cross-section of the sensor stay within 10% of each other whereas before calibration these values could vary up to 40% from each other. Unfortunately, the increase of the measurement range through the addition of resistors does not give the desired result, since the relation between conductivity and sensor output looses its linearity. Therefore, it makes the calibration procedure less effective, resulting in less accurate measurements. Due to this, for measurements described in the continuation of this chapter no added resistors were used. Unless stated otherwise, the measurements are performed at 2500 Hz. Special care was taken in order to make sure that the measured signal resulting from the injected tracer stayed in the optimal measurement range, with maximum values below 2000 $\mu\mathrm{S/cm}$ but high enough to result in a clear signal.

4.3 Radial Dispersion

In the previous section of this chapter the calibration method and the benefits and downsides from calibration and from adding resistors to increase the measurement range were discussed. In this section, the calibrated wire-mesh is used to look at a tracer injected in turbulent flow and its dispersion. The high time-resolution of the wire-mesh allows for a very realistic visualization and analysis of the movement of the tracer through a plane. With the set-up that was described in section 4.1, it is possible to inject a liquid tracer continuously in the flow. A continuous injection of the tracer at different positions and in flows with different Reynolds numbers gives an excellent way to use the wire-mesh equipment. Due to the high spatial and time-resolution, the radial dispersion of a tracer in turbulent flow can be measured nearly instantaneously for the entire cross-section of the tube.

In figure 4.8, the cross-section of the flow is visible in four different time-frames, separated each on 2 ms from each other. The results from figure 4.8 were measured with 2.5 kHz, but, in order to visualize the evolution of the tracer plume through the wire-mesh more clearly only one in five frames are shown. The tracer was injected in the center of the pipe at a distance of 5.1D upstream of the wire-mesh. The values shown are relative to the injected concentration, so, the highest measured concentration is at least diluted 200 times between the injector and sensor. To further visualize the evolution of the tracer plume, in figure 4.9 the tracer concentration in the wire-mesh is shown for 2500 frames corresponding to one second. The measurements were performed in a flow with Re=45000, with the tracer injected in the center of the pipe at 6.6D upstream of the wire-mesh and is measured with 2.5 kHz. Here, the x-y plane is the plane of the wire-mesh and the consecutive frames are stacked in the z direction. Hence, this is not a visualization in three spatial dimensions but the visualization of the time evolution of the signal from the wire-mesh plane. The x-y plane shows the wire-mesh output at frame 2500, the other planes show the horizontal and vertical centerlines in the cross-section with the time evolution of the signal, allowing the visualization of the movement of the tracer plume through the wire-mesh.

4.3.1 Dispersion Statistics

If the force exercised by the buoyancy is small compared to the forces associated with the chaotic turbulent behavior of the flow, Then the dispersion of the tracer in the cross-section should be axisymmetric. As described in setion 2.4.4, the relative influence of the buoyancy can be estimated by dividing the Grashof number by the Reynolds number squared. For measurements in this part of the thesis, this ratio varies between approximately 1 for Re=17800 and 0.09 for Re=60000. This means that for the measurements at the lower velocities the buoyancy plays a noticeable role. This was also seen in the measurements at lower velocities where the tracer disperses more strongly towards the bottom.

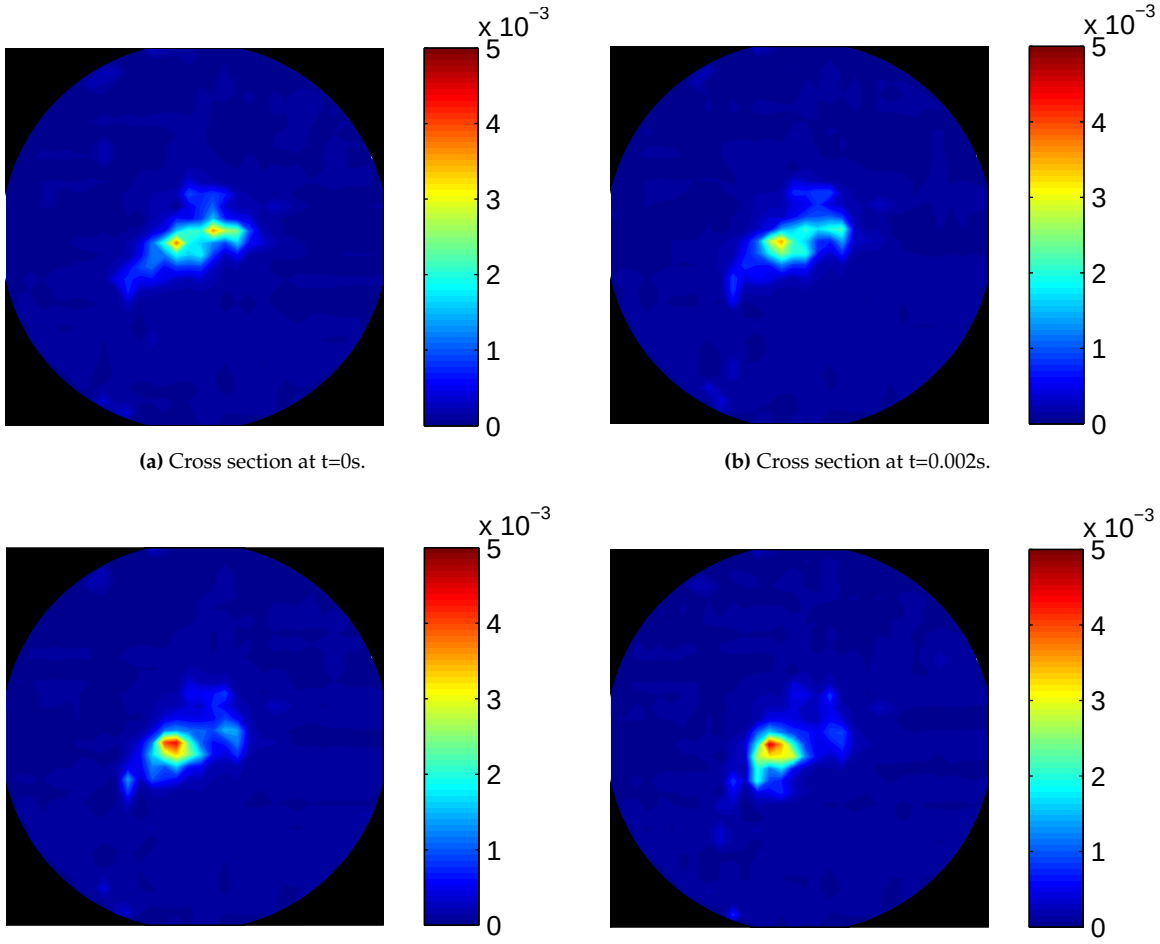

(a) Cross section at t=0s.

(b) Cross section at t=0.002s.

(c) Cross section at t=0.004s.

(d) Cross section at t=0.006s.

Figure 4.8: Tracer concentration normalized by the concentration of the injection over the cross-section of the tube, at four different moments, with the tracer injected in the center of the pipe at 5.1D upstream from the sensor, in a turbulent flow with Re=45000.

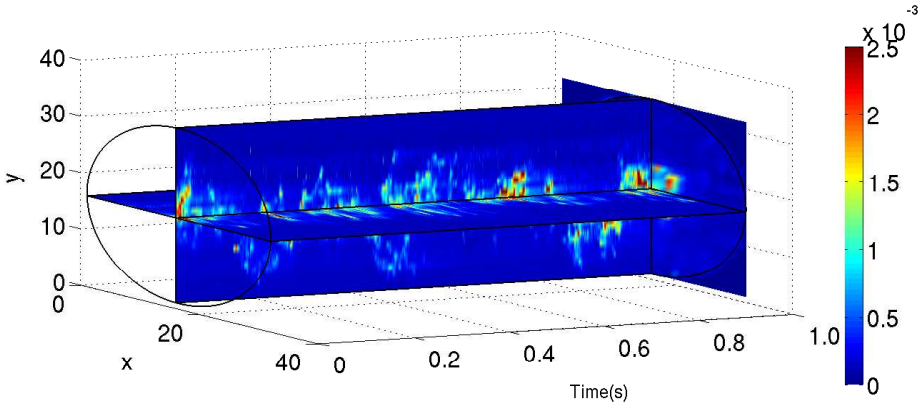

Figure 4.9: Evolution of the tracer plume in time, visualized in three planes. The contours represent the concentration, normalized by the concentration at the injection.

The gravity-induced displacement of the tracer towards the bottom of the pipe was compensated in the post-processing by determining the time-averaged position of the maximum concentration, which was considered as the "effective injection point". The comparison between the measurements at low and high velocities showed that this post-processing compensation of the small gravity-induced displacement did not produce any noticeable strange behavior. Hence, it appears that in these experiments the main effect of the buoyancy is to simply induce a small average displacement of the tracer towards the bottom.

The gravity-induced displacement of the tracer can be seen in 4.10, which shows the time-averaged tracer concentration, with the tracer injected at the center of the pipe at four different positions upstream of the wire-mesh, for a flow at Re=30000. Clearly, there is a small shift in the position of the maximum concentration towards the bottom of the pipe. This shift increases as the distance between the wire-mesh and the injection point increases (i.e., as the tracer spends a longer time inside the flow). This indicates that the buoyancy induces a small average tracer velocity towards the bottom of the tube.

The equipment seems to have generated only a little background noise. However, the bottom figure in the right, in figure 4.10, shows clearly some signal "noise". This "noise" does not show up in the

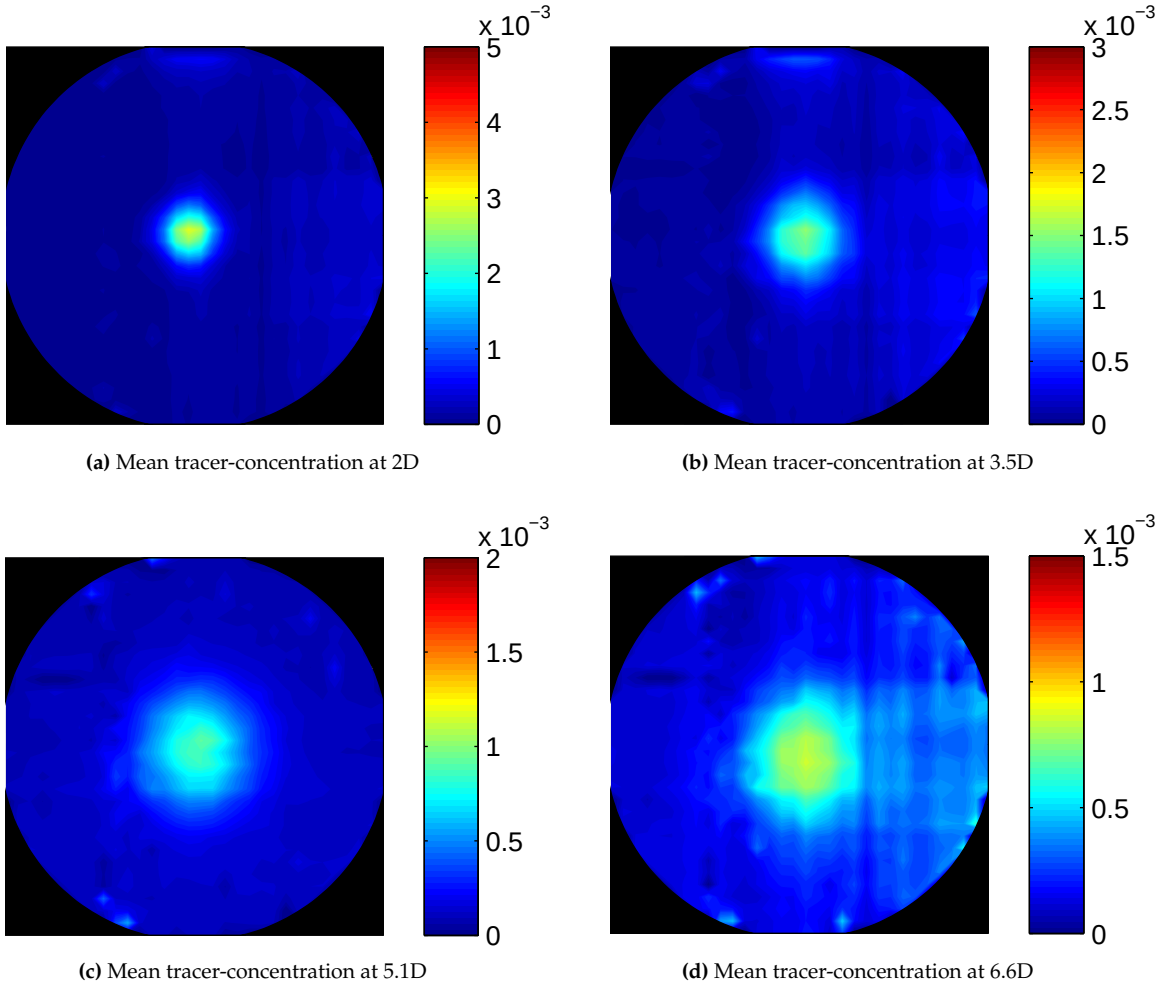

(a) Mean tracer-concentration at 2D

(b) Mean tracer-concentration at 3.5D

(c) Mean tracer-concentration at 5.1D

(d) Mean tracer-concentration at 6.6D

Figure 4.10: Mean tracer-concentration in the cross-section of the pipe. The tracer is injected at the center of the pipe at four different positions upstream of the wire-mesh. The contours represent the concentration, normalized by the conncentration at the injection..

individual measurements of one time-frame seen in figure 4.8. Since it is a recurring small error, it shows up when averaging the signal over a large amount of time-frames, and is most pronounced when the tracer has dispersed a lot. In figure 4.10, this signal "noise" adds up to half of the mean signal measured in the center of the tube.

In figures 4.11 and 4.12, the mean concentration is shown as a function of the radial distance of the tube for a set of measurements with a flow at Re=45000. Figures 4.11 and 4.12 confirm the earlier observation: increasing the injection distance from the wire-mesh results in a higher dispersion of the tracer. The measurement data were fitted with the help of Matlab, and the measurement points close to the wall where excluded. The reason for this is that the radial injection position is not perfectly centred. Because of this, the centreline position used to get R/R_0 in figures 4.11 and 4.12 has been manually adjusted. The maximum adjustment was $\Delta R/R_0 = 0.09$ and was found using a least-square fit. A second reason for excluding points close to the wall is the lack of axisymmetry due to buoyancy effects as discussed previously. Due to the adjustments that were made to correct for (i) the actual position of the injection points and (ii) the gravity-induced displacement of the tracer, some measurement points with a corrected value of the radial position R/R_0>0.9 fall outside of the tube. For this reason only measurements points where R/R_0<0.9 were used. Also, since the left side of the wiremesh delivers a signal with much less "noise" as can clearly be seen from figure 4.10, only the left half of the measurement points were used for figures 4.11 and 4.12. For the fitting was used a normal distribution of the form:

$$\phi = c1 \cdot e^{\frac{-(Y-\langle Y \rangle)^2}{2\langle Y^2 \rangle}} + c2 \tag{4.1}$$

where Y is the distance to the centreline of the tube normalized with the radius of the tube, $\langle Y \rangle$ is the mean of the distribution and $\langle Y^2 \rangle$ the variance of the distribution. $c1$ and $c2$ are constants: the value of $c2$ depends on the tracer concentration near the wall (outside the region containing most of the tracer) and the concentration at the center is given by $c1$+$c2$. In figure 4.11 the concentration is normalized by the concentration at the injection point, whereas in figure 4.12 the concentration is normalized by the concentration at R/R_0=0, ϕ_0.

The Gaussian shape of the tracer concentration as a function of radial distance closely follows the theory of Taylor (1954), where the dispersion of a tracer particle follows a 'random walk' principle. As described in section 2.4, the dispersion of a tracer particle is caused by it being subjected turbulence structures of different sizes and strengths. This causes the particles to move "randomly" resulting in a normal distribution in the radial direction.

It is interesting to note the offset of the concentration close to the wall of the tube that indicates that outside of the 'main dispersion area' in the center of the tube the concentration spreads equally throughout the tube. Part of the offset is most probably a result from signal "noise" caused by the electronic equipment that results in a fairly steady background signal when averaged over all frames. The remaining part of the offset is a result of the tracer spreading throughout the entire cross-section of the tube, especially for locations far away from the source. This results in an offset at the edge of the cross-section that gets larger the further away the measurement is performed. The concentration tends to a constant level at the edge of the cross-section because the wall of the tube is impassable for the tracer, so, that there is a maximum dispersion distance.

According to Taylor and Middleman (1974), taking the variance $\langle Y^2 \rangle$ from the Gaussian fittings in figure 4.11 as equal to the mean squared displacement $\langle y^2 \rangle$ in equation 2.9, should result in a linear relation between the variance of the dispersion and the time squared. In figure the 4.13 the relation between the variance and t^2 is shown. The time t is obtained from the injection distance using the mean velocity of the flow. The result is a linear relationship, as predicted from of Taylor's dispersion theory.

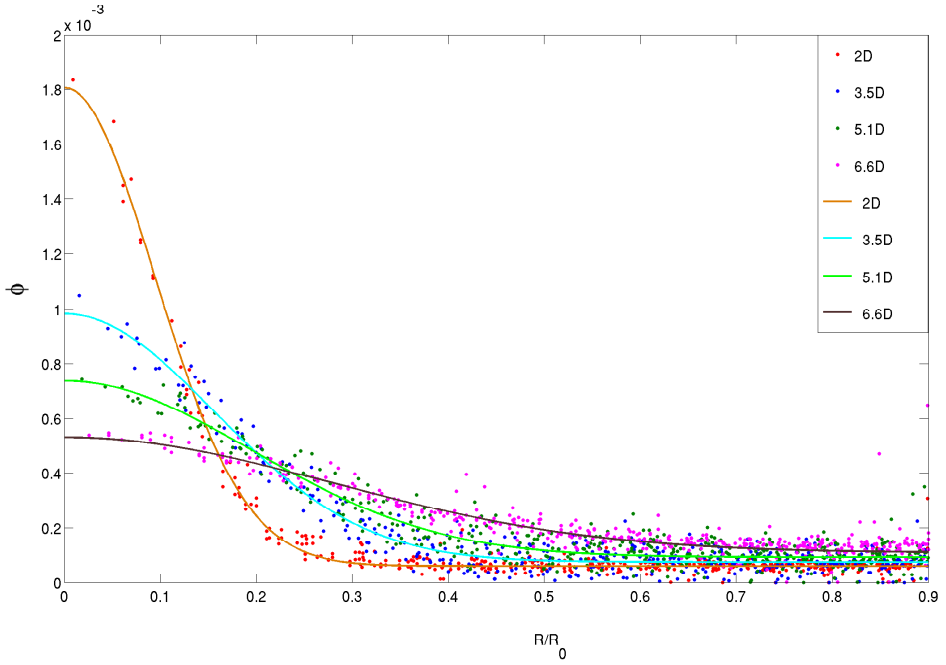

Figure 4.11: Mean tracer-concentration, as a function of the radial distance for injection points at the center of the pipe, located at four different positions upstream of the wire-mesh, with Re=45000. The concentration is normalized by the concentration at the injection.

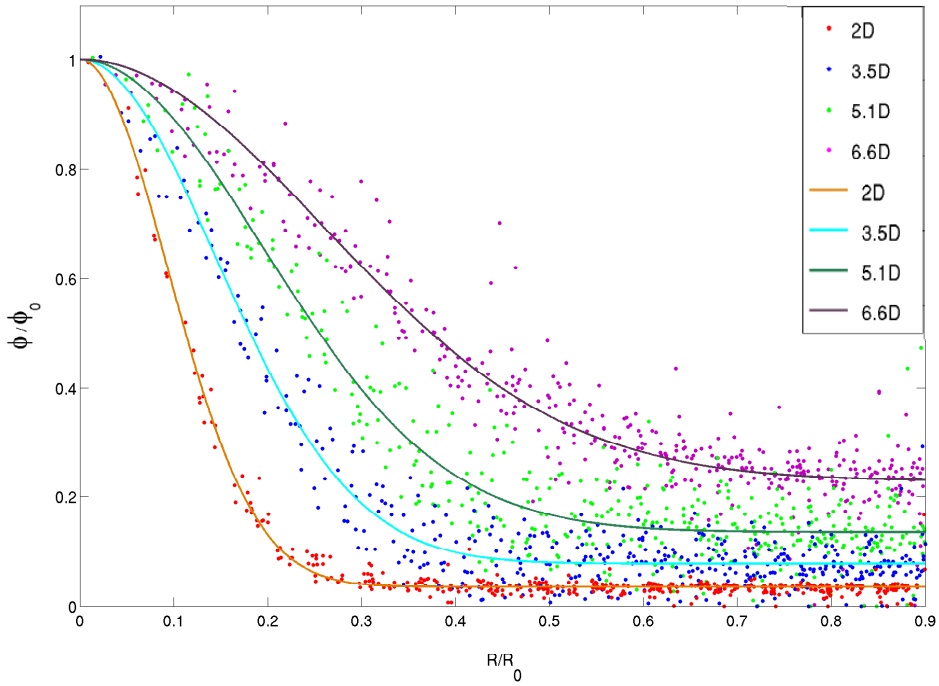

Figure 4.12: Same results as in 4.11, but with the concentration normalized by the concentration at R/R_0=0, ϕ_0.

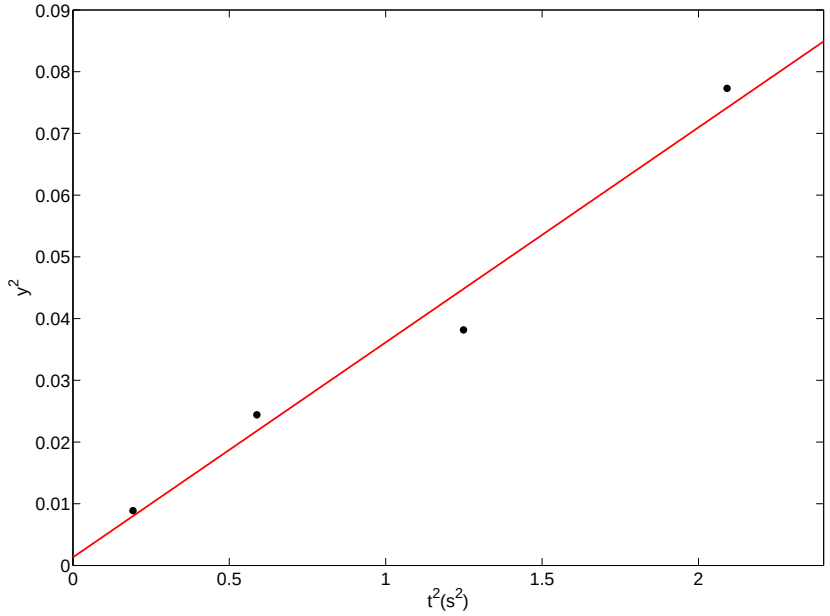

Figure 4.13: Variance of the the tracer dispersion in the radial direction, obtained from the fitted experimental results, as a function of t^2.

In figures 4.14 and 4.15, a comparison is made between the mean dispersion, for Reynolds numbers 17800, 30000, 45000 and 60000, for one centerline injection point at 3.5D upstream of the wire-mesh. Clearly visible in figure 4.14 is that the for higher Reynolds numbers the concentration is lower. This is because the measurements where done with a constant amount of tracer injection, so, when the fluid is flowing faster, the amount of tracer per liter flowing through the wire-mesh is lower, even though the same amount of tracer per second is flowing through the wire-mesh. However, when normalizing the concentration by the concentration at the center of the cross-section, as shown in figure 4.15, it is clear that the radial dispersion of the tracer is not significantly affected by the Reynolds number.

From figure 4.13 it follows that there exists a linear relationship between the variance of the tracer dispersion and the square of the time between the injection and the measuring cross-section. According to equation 2.9, the mean dispersion depends linearly on both the mean squared fluctuating velocity, $\langle u^2 \rangle$, and the square of the time, t^2. The explanation why an increased turbulence does not result in an increased dispersion is therefore clear.

If the fluctuating velocity, $\vec{u}$, is proportional to the mean velocity in the pipe, $\langle \vec{U} \rangle$, and if the time before the tracer reaches the wire-mesh is inversely proportional to $\langle \vec{U} \rangle$, then the radial dispersion is independent of the Reynolds number. For the turbulent flows at the relatively high Reynolds numbers considered here, very close to the wall, the velocity is approximately uniform and $\vec{u}/\langle \vec{U} \rangle$ is only very weakly dependent on the Reynolds number. Therefore, the radial dispersion should not be significantly affected by the Reynolds number, as, indeed, can be seen in figure 4.15.

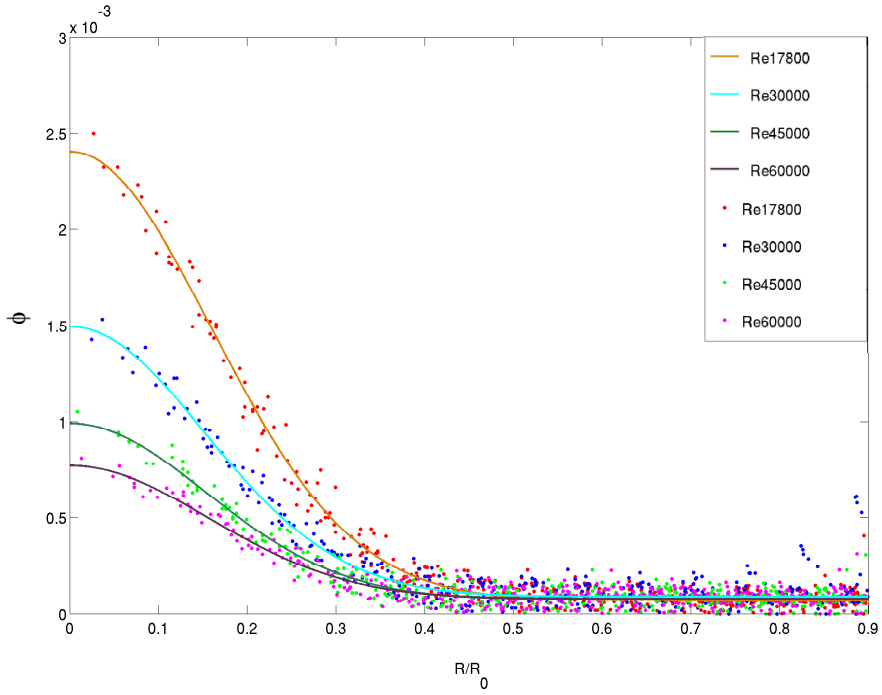

Figure 4.14: Mean tracer-concentration as a function of the position for four different Reynolds numbers for a centerline injection point at 3.5D

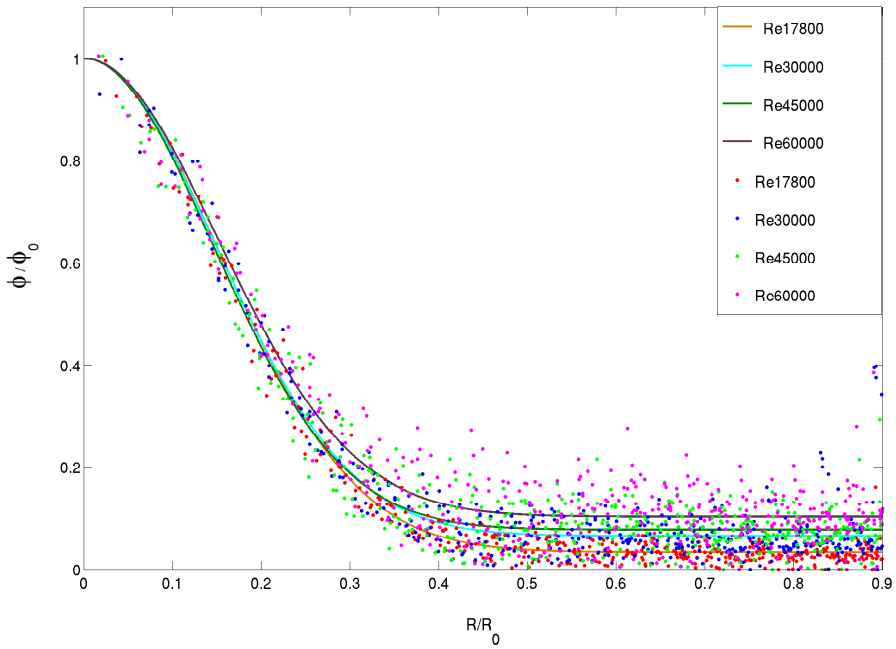

Figure 4.15: Same result as in figure 4.14, but with the concentration normalized by the concentration at R/R_0=0, ϕ_0.

4.4 Validation of the Results

In order to investigate the reliability of the wire-mesh in tracer dispersion experiments in pipe-flow, the previous results were compared to literature results. In figure 4.16, the dispersion with a Reynolds number of 45000 and a centerline injection distance of 2D is compared with two experiments performed with different measurement techniques.

The first data set used for comparsion is from Taylor and Middleman (1974), who injected a dye tracer in the same way as in this research. They extracted this dye at several radial positions, with the same kind of capillary used for the injection. The liquid extracted was examined to get the concentration at that point. The second data set used for comparison is from Altinsoy and Tuğrul (1999), who used the same method of Taylor and Middleman, except in their case a radio-active tracer was used. In these researches the tracer dispersion data was fitted with a Gaussian curve, without the constant $c2$ that was used in equation 4.1. As explained before, the constant $c2$ was necessary to compensate for the offset in the signal close to the wall. From figure 4.16 it is clear that there exists a good agreement between this study and the findings of Taylor and Middleman (1974) and Altinsoy and Tuğrul (1999).

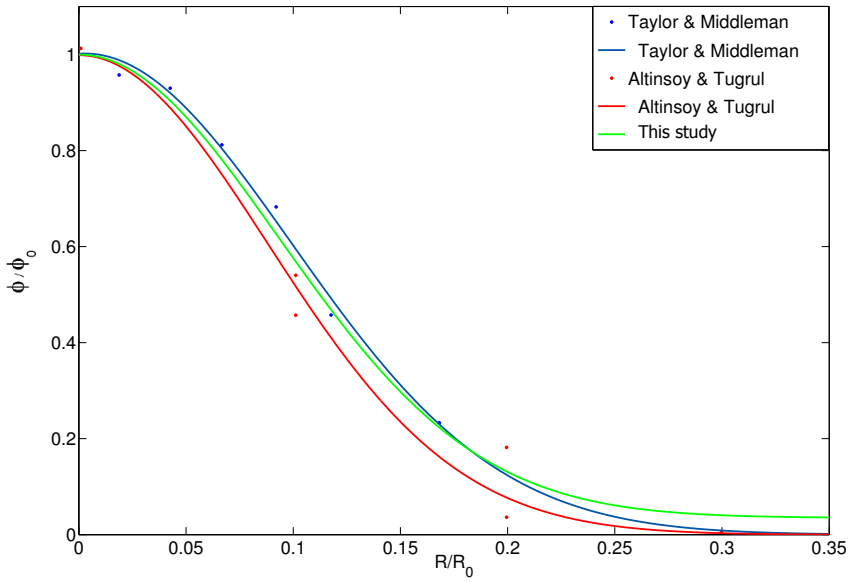

Figure 4.16: The tracer dispersion with Re=45000 and injection at 2D compared with Taylor and Middleman and Altinsoy and Tuğrul.

Aanen (2002) and Brethouwer (2001) performed research on the scalar transport in turbulent pipe-flow. Aanen did experimental work using a combination of Particle Image Velocimetry and Laser Induced Fluorescence, while Brethouwer performed Direct Numerical Simulation. Their measurements and simulations were performed in a 50 mm tube at a Reynolds number of 5300 which is considerable smaller then the Reynolds numbers in this research. However, a few usefull comparisons can be made. Aanen and Brethouwer both found an inversely proportional relationship between the concentration at the center of the pipe and the axial distance from the injection point.

In figure 4.17a the fitting curve from the experiments of Aanen is plotted together with the measurements from this research. From figure 4.17a, it can be seen that the decrease in the centerline concentration follows exactly the same trend ($\sim 1/z$) as found by Aanen. It is clear that the concentration values found in this research are lower then in the research from Aanen, which can be attributed to the difference in Reynolds number and differences in the flow rate of the injected tracer. The different height, of the curves for the different Reynolds numbers are again explained by the difference in injected tracer per volume of fluid flowing through the wire-mesh.

In figure 4.17b, is shown the radial dispersion normalized by the diameter as a function of the axial injection distance, together with the simulation results from Brethouwer. It is clear that in this research the Reynolds number in this research has no detectable influence on the radial dispersion of the tracer. The evolution of the radial dispersion with z/D shows the same trend as in the results from Brethouwer. The difference is in a shift in the value of σ/D, which is most likely caused by an initial offset caused by the injection method. Brethouwer used simulations with a true point-source whereas the results from this research are experimental; therefore, reproducing a perfect point-source was not possible. The independency of the dispersion on the Reynolds number confirms the conclusions from earlier figures where no detectable influence of the Reynolds number on the radial dispersion could be seen.

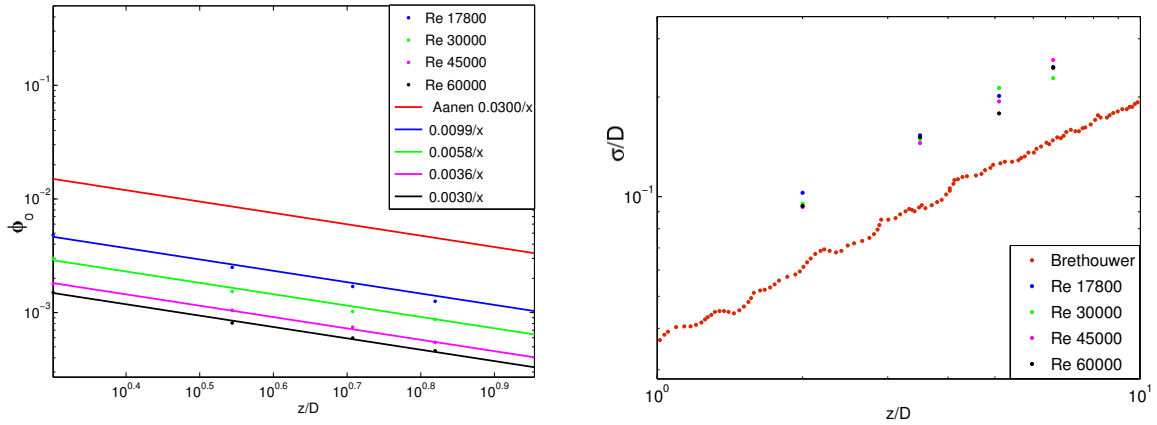

(a) Streamwise evolution of the centreline concentration.

(b) Streamwise evolution of the tracer dispersion in the radial direction.

Figure 4.17: (a) Centerline concentration values compared with experimental data from Aanen (2002); (b) standard deviation of the concentration compared with simulation values from Brethouwer (2001).

4.5 Turbulence Structures

In sections 2.2.2 and 2.3 the existence of structures in a turbulent flow was discussed. These structures can have a large spectrum of characteristics, with the length-scale ranging from the geometry scales of the flow all the way down to the Kolmogorov scales. Since identifying structures in the flow is an important part of this thesis, in this section the wire-mesh is used for looking at these structures. The wire-mesh is only able to measure scalars and therefore will not be able to measure velocity fluctuations. The high time-resolution of the wire-mesh makes it capable of measuring very fast scalar-fluctuations. This capability of measuring very fast scalar-fluctuations, in essence, results also in a high spatial-resolution in the direction of the mean flow.

Figure 4.18 shows the tracer concentration in the center of the tube for two different Reynolds numbers. It is clear that a higher Reynolds number results in faster fluctuations in the tracer concentration flowing through the wire-mesh. These faster fluctuations are easily registered since the measurement frequency was 2500 Hz. The difference in the value of the concentration results from the fact that the injection rate of the tracer is equal in both situations, so, the total amount of tracer per liter water flowing through the mesh is different in both cases.

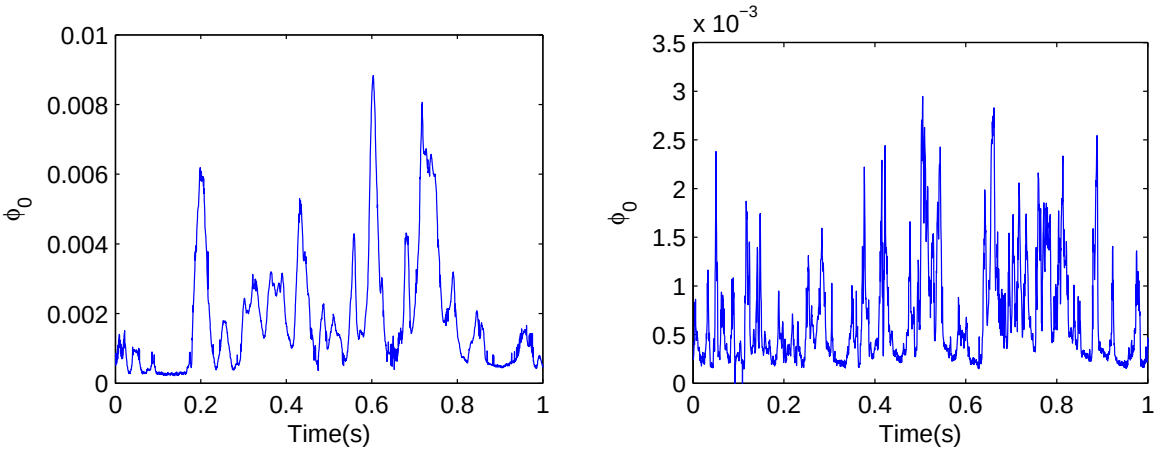

(a) Tracer concentration for 1 second at Re=17800.

(b) Tracer concentration for 1 second at Re=60000.

Figure 4.18: Measured concentration in the center of the tube for 1 second for two different Reynolds numbers, with the tracer injected at the centerline of the pipe at 5.1D upstream of the wire-mesh

At least a significant part of the difference in frequency of the tracer fluctuations in figure 4.18 must be caused by the fluid flowing faster through the sensor. Besides this, some of the difference in the frequency may be also caused by a possible difference in the size of the turbulence structures at different Reynolds numbers. In order to see if this is a reason for the difference in the frequency of the fluctuations, it is necessary to compensate for the different velocities of the fluid. This can be done by assuming that the turbulent fluctuations are caused by a 'frozen' field flowing through the sensor with the mean velocity of the flow. This approach is called *Taylor's hypothesis* and it is simply done by multiplying the time with the mean velocity of the flow. It must be noted that this approach can only be used when looking at the larger structures for which the movement is governed mostly by the mean velocity of the flow. the application of Taylor's hypothesis to the signals from figure 4.18 is shown in figure 4.19. From this approach, it follows clearly that the differences between the figures in figure 4.18 were mostly caused by the velocity of the fluid, and not by any other turbulence effects, since both signals shown in figure 4.19 are very much alike.

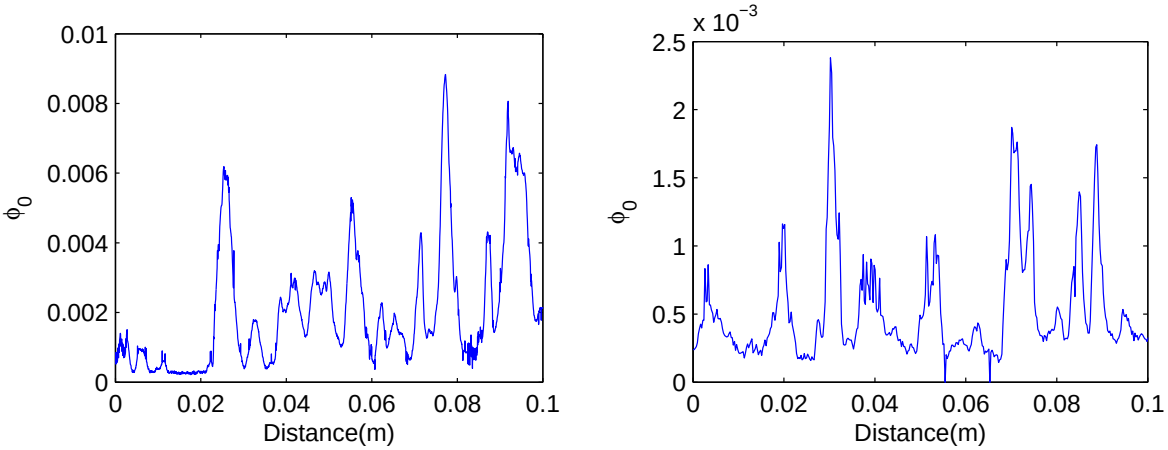

(a) Tracer concentration for 0.1 meter at Re=17800.

(b) Tracer concentration for 0.1 meter at Re=60000.

Figure 4.19: Measured concentration in the center of the tube for 0.1 meter for two different Reynolds numbers, with the tracer injected at the centerline of the pipe at 5.1D upstream of the wire-mesh.

4.5.1 Turbulence Power Spectra

The fluctuations in tracer concentration can be used to produce a power spectrum of the turbulence in the flow. In figure 4.20, the power spectra for the two different time-signals from figure 4.18 are shown. The power spectrum is plotted as a function of the spatial wave-number instead of the frequency with the purpose of better comparing both signals; again this is done using the bulk velocity. It is clear that no distinguishable peaks are visible in the power spectra which would indicate some kind of disturbance in the turbulence. This indicates that the tracer injection method, indeed, has no noticeable influence on the turbulence structures at the measuring-point. The lack of distinguishable peaks make, the signals difficult to compare. To help with the comparison three vertical lines at ν=40, 400 and 2000 m^{-1} are plotted. The vertical lines roughly indicate areas where the slope of the power spectrum shows different behavior in figure 4.20a. Before the first line the power-spectrum is roughly horizontal, after the first line a transition region to the relatively straight slope between line two and three can be seen. After line three clearly there is no measureable signal anymore. The three vertical lines are kept at the same positions thoughout figures 4.20 and 4.21, for better comparison between them.

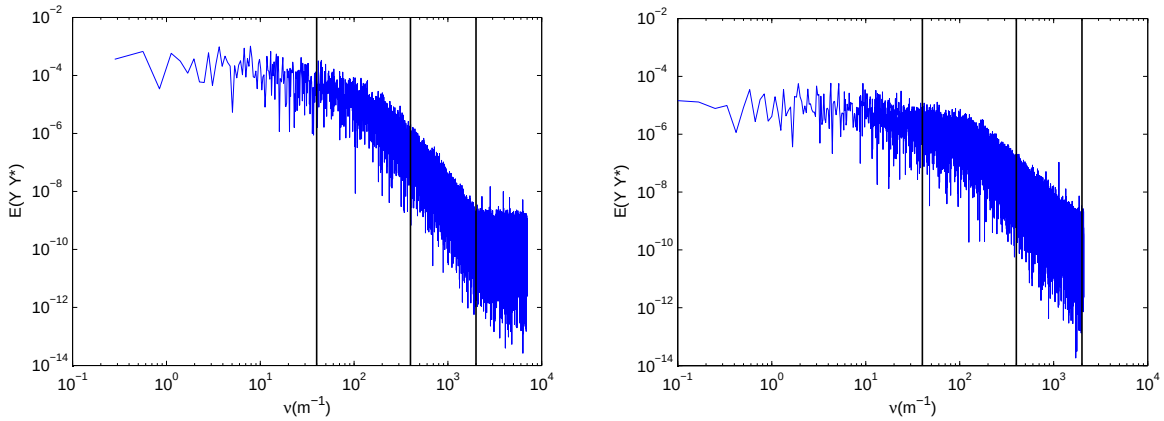

(a) Power spectrum at Re=17800.

(b) Power spectrum at Re=60000.

Figure 4.20: Power spectrum of the concentration in the center of the tube, for two different Reynolds numbers, with tracer injected at the centerline at 5.1D upstream of the wire-mesh.

In order to get a more clear understanding of the frequencies that contain most of the "energy" in the signal a well-known method is multiplying the power spectrum with the wave-number ν of the signal (Jiménez, 1998). In figure 4.21 this so called pre-multiplied power spectrum is plotted as a function of the wave-number. The wave-number is related to the frequency f and the wave-length λ by:

$$\nu = \frac{1}{\lambda} = \frac{f}{U_{bulk}} \tag{4.2}$$

where it is assumed that the "waves" or fluctuations in the tracer concentration move along with the bulk velocity, U_{bulk}, of the flow. Normally, a pre-multiplied spectrum yields the amount of kinetic energy that is contained in a logarithmic band of eddy sizes around the wave-number. In this research, no information on the velocity fluctuations can be obtained from the wire-mesh. Nevertheless, the pre-multiplied spectrum of the concentration fluctuations gives an indication of the magnitude of the scales.

Figure 4.21 gives a clear indication of the range of scales that are most important in the fluctuations of the concentration in the flow and are being measured in with the wire-mesh equipment. At the high wave-numbers in both figures 4.21a and 4.21b, it is visible that at wave-numbers higher then approximately 400m^{-1} no significant contribution is made towards the concentration fluctuations. This wave-number corresponds to a turbulence scale of a few millimeters. Since the scales in a turbulent flow range all the

way down to the Kolmogorov scale, it is unlikely that there is so little contribution to the pre-multiplied spectra. A better reason for the strong decay of the spectra around this wave-length can be found in the equipment. As explained in chapter 3, the wire-mesh uses a layer of transmitting wires and a layer of receiver wires in order to measure the conductivity in the layer between these wires. In the wire-mesh used here the distance between these layers is 1.5mm. It is clear that fluctuations caused by turbulence scales of this size and smaller cannot be measured with this equipment.

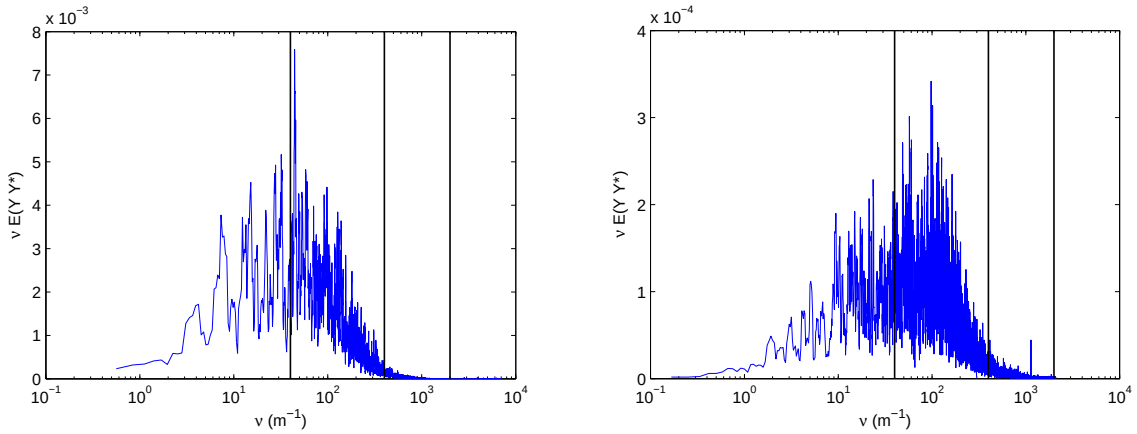

(a) Pre-multiplied powerspectrum at Re=17800.

(b) Pre-multiplied powerspectrum at Re=60000.

Figure 4.21: Pre-multiplied powerspectrum of the turbulence in the center of the tube for two different Reynolds numbers with the tracer injected at the centerline of the pipe at 5.1D upstream of the wire-mesh.

At the lower end of the pre-multiplied spectra there is a more gradual decay. From these figures can be observed a decay up to a wave-number of 1m^{-1}, indicating the existence of a few turbulence structures with a length in the flow direction of up to 1 meter. The spectra are filtered with a moving average filter to remove part of the noise. Also plotted, are the same vertical lines as in figure 4.20, for better clarification of the connection between the figures. There is not much difference in the position of high peaks between both pre-multiplied spectra. This indicates that the Reynolds number does not have much influence on the size of the longer structures, as expected, since the size of the longer turbulence structures is mostly determined by the geometry. Note that for both Reynolds numbers most of the "energy" content of the pre-multiplied spectrum is contained roughly between 0.1m and 0.01m, i.e., roughly between 1D and 0.1D.

4.5.2 Signal Correlation

The normalized auto-correlation of a time signal gives an indication of how much the signal corresponds to itself when it is shifted in time. For the timesignals of the tracer concentration from figure 4.18 the normalized auto-correlation function is defined by:

$$r(\tau) \equiv \frac{\langle \phi(t)\phi(t+\tau) \rangle}{\langle \phi^2 \rangle} \tag{4.3}$$

where $\phi(t)$ is the concentration as a function of the time, τ is the time shift and $r(\tau)$ is the normalized auto-correlation as a function of the time-shift. Like in its application in analysing the spectra in section 4.5, Taylor's hypothesis can again be used in order to get information about length scales instead of time scales. In figure 4.22, the auto-correlations show a clear peak at a shift of zero for obvious reasons. The interesting part is visible when zoomed in. The width of the peak gives information about the streamwise length of the turbulence structures. The maximum width of the peak is approximately 8 cm. As was seen in the power-spectra most of the "energy content" of the concentration signal was contained

between 10 cm and 1 cm, with structures larger than 10cm having only a very small contribution to it. This indicates a good agreement between the spectra and the auto-correlation results.

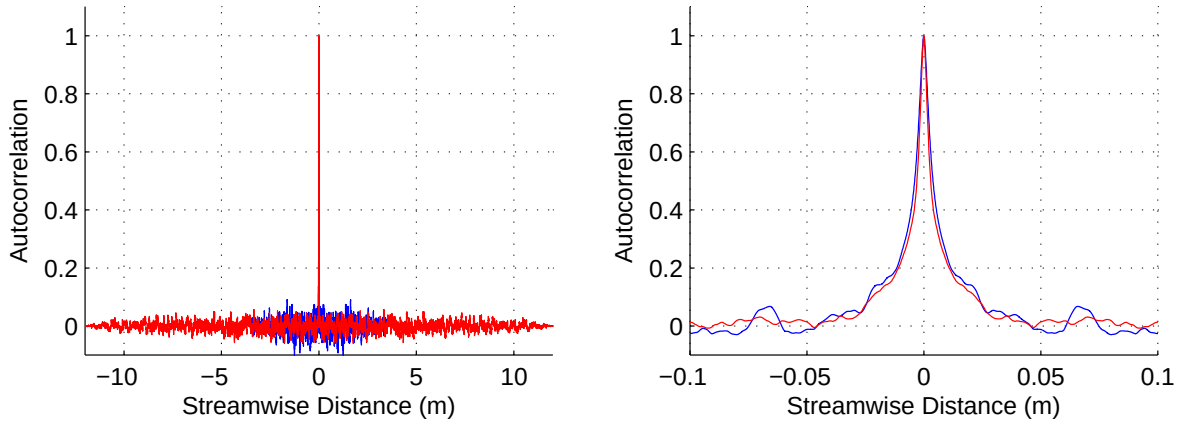

(a) Auto-correlation for Re 17800 (blue) and Re 60000 (red).

(b) Zoomed-in auto-correlation for Re 17800 (blue) and Re 60000 (red).

Figure 4.22: Auto-correlations for both time signals from figure 4.18, as a function of a shift in the streamwise direction

Besides looking at the fluctuations in time and gaining insight in the streamwise scales of the turbulence by using the mean velocity, it is also interesting to look at the magnitude of the scales in the direction perpendicular to the flow. For this purpose the cross-correlation coefficient can be used. A cross-correlation is a widely used measure of how much two signals relate to each other. The cross-correlation coefficient between the signal at two different positions (A and B) in the cross-section is given by:

$$R_{AB} = \frac{\langle(\phi'_A(t))(\phi'_B(t+\Delta t))\rangle}{(\phi'_A(t))_{rms}(\phi'_B(t+\Delta t))_{rms}} \tag{4.4}$$

where R_{AB} is the cross-correlation between point A and B and $\phi'_A(t)$ and $\phi'_B(t+\Delta t)$ are the concentration values minus the average concentration for point A and B. In figure 4.23 is shown the cross-correlation between the time signal in the center of the pipe and the time signal in the other points of the cross-section, for two different Reynolds numbers. No noticeable differences can be seen between the two Reynolds numbers. This is consistent with the earlier results for the streamwise structure size and indicates that the earlier assumptions about the homogeneity of the flow in the central region of the tube where correct. It can be observed that more than three measurement points away no significant correlation exists between the two points. Since the measurement points are 3 mm apart, it can be concluded that no structures larger than D/10 are observed. Again, this indicates that the Reynolds number does not have much influence on the size of the longer turbulence structures, as expected. Also, it indicates that the maximum cross-sectional length of the turbulence structures is of the order of D/10, which is consistent with the literature. Note that, as expected, the cross-section length of the large turbulence structures is smaller than the streamwise length.

It should be noted that because of the effect mentioned in section 3.2.3 the measured correlation between two neighboring points may be slightly larger than the actual correlation. Especially in the direction of the receiver wires, which is the vertical direction in this case. If this influence would be important, this effect should be noticeable in the results. Since no significant influence can be detected, it can be concluded that the approximation of square measurement areas around every wire crossing is accurate enough.

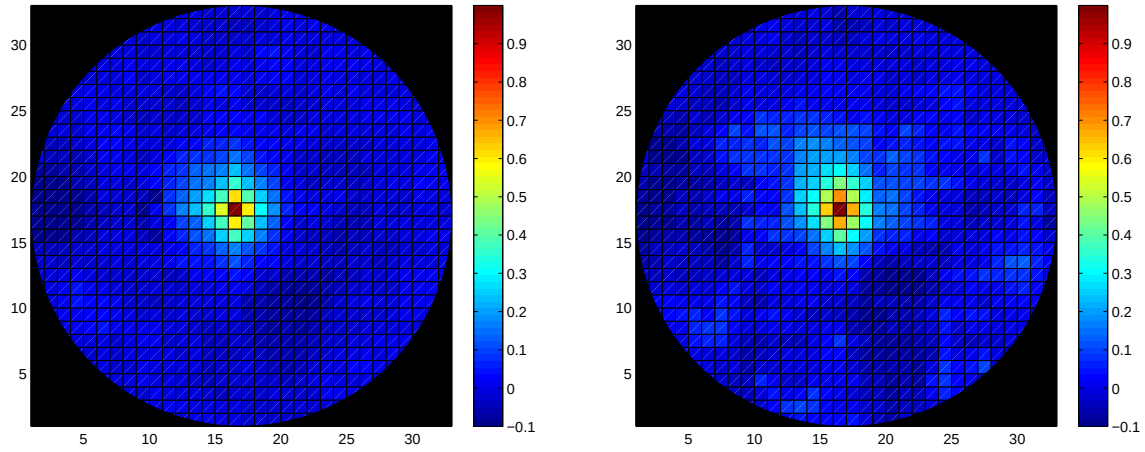

(a) Cross-correlation at Re=17800.

(b) Cross-correlation at Re=60000.

Figure 4.23: Cross-correlation between the signal in the center of the pipe (row 17, column 16) and the signal of all the other points, for two different Reynolds numbers with the tracer injected at the centerline at 5.1D upstream of the wire-mesh.

Another thing that can be seen in figure 4.23 is that there are some areas where there is a small negative correlation. This is most likely a result from limitations in the electronic circuit, which in some places is probably over-compensating a little bit for cross-talk between neighboring transmitter wires. In figure 4.24, is shown the cross-correlation between a point near the wall and all the other points in the cross-section. It can be seen that the correlating area is slightly bigger and more irregular then in the center as a result of the effect of the wall of the tube. The correlation length is longer in the circumferential direction, whereas in the radial direction it is roughly the same as in the center of the pipe. This anisotropy is a consequence of the wall, which tends to compress the structures in the wall-normal direction and to stretch them in the spanwise direction. Again, as expected, no significant differences are observed between the two Reynolds numbers.

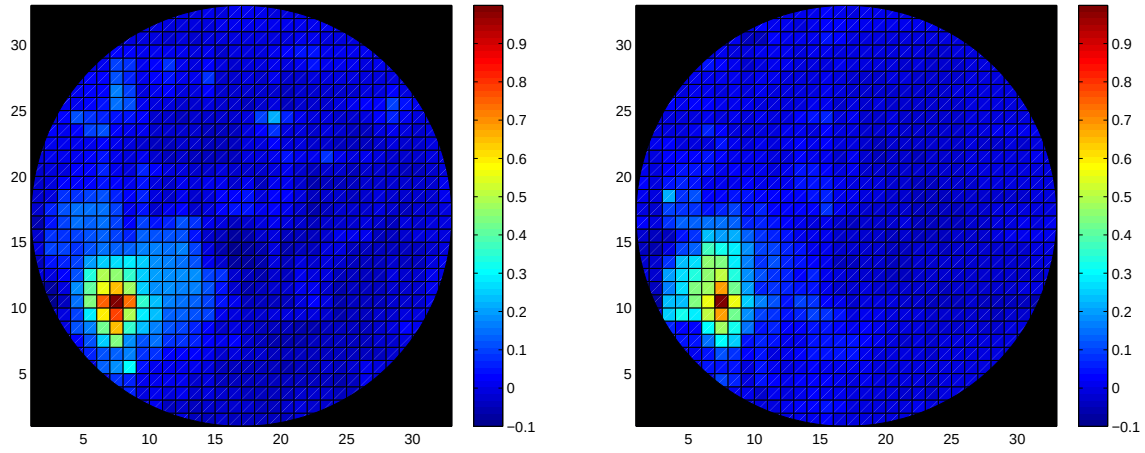

(a) Cross-correlation at Re=17800.

(b) Cross-correlation at Re=60000.

Figure 4.24: Cross-correlation between the signal in row 10, column 7) and the signal of all the other points, for two different Reynolds numbers with the tracer injected at the centerline at 5.1D upstream of the wire-mesh.

4.5.3 Concentration Visualization

By plotting the tracer concentration in a three-dimensional figure, a visual representation is given of the way tracer flows through the wire-mesh. Again Taylor's hypothesis was used, using the bulk velocity to transforms the time into streamwise distance. In figure 4.25, the tracer concentration is shown for a distance of 1 meter; the signal is the same as the one used in figure 4.18. The threshold values used for the visualization where chosen with the help of the time series for producing the most interesting plots. In figure 4.26, the same figures are zoomed in. As expected, no distinguishable differences exist between the data for the two Reynolds numbers. In both figures recurring regions of higher concentration with a spacing between them of about 5 cm can be observed. Overall, the qualitative picture given by figures 4.25 and 4.26 is consistent with the previous results.

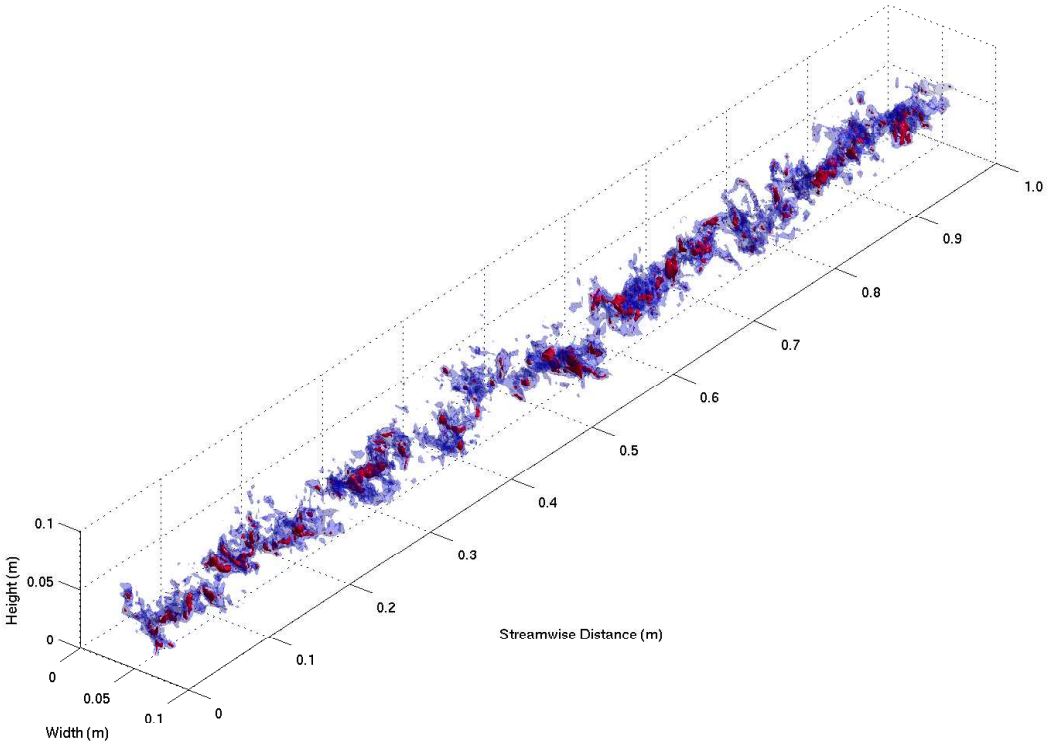

(a) Three-dimensional visualization of the tracer, with Re=17800, for concentration thresholds 0.0015 (blue) and 0.0033(red).

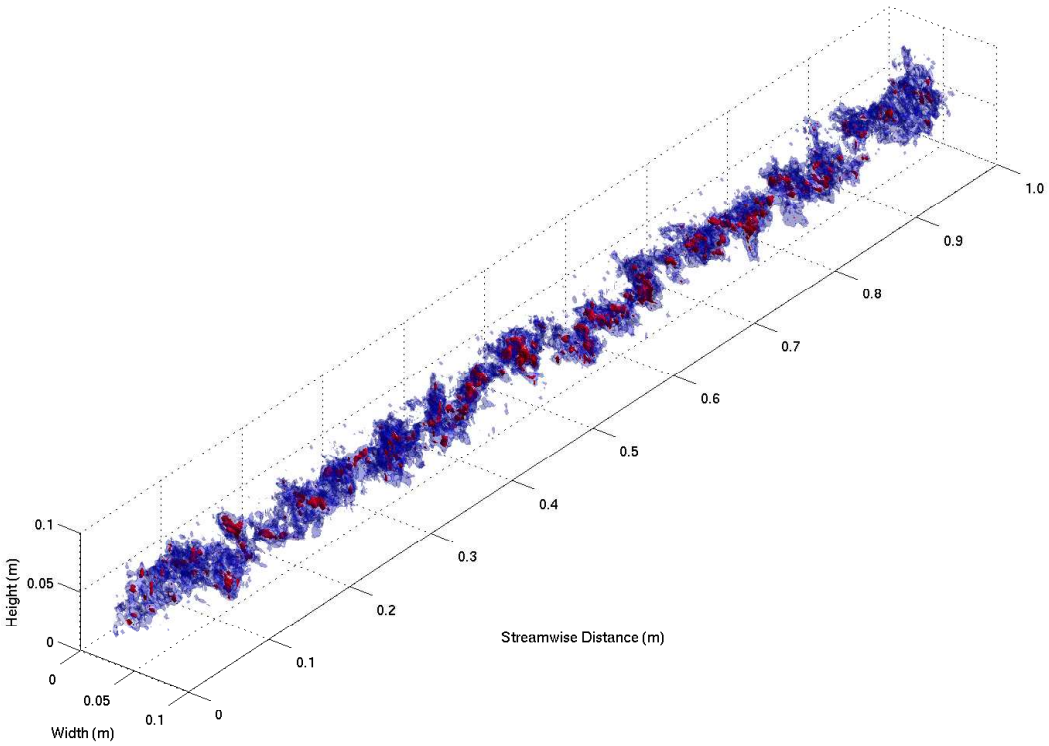

(b) Three-dimensional visualization of the tracer, with Re=60000, for concentration thresholds 0.0005 (blue) and 0.0011(red).

Figure 4.25: Tracer visualizations , as it passes through the wire-mesh, using Taylor's hypothesis to transform the time into streamwise distance.

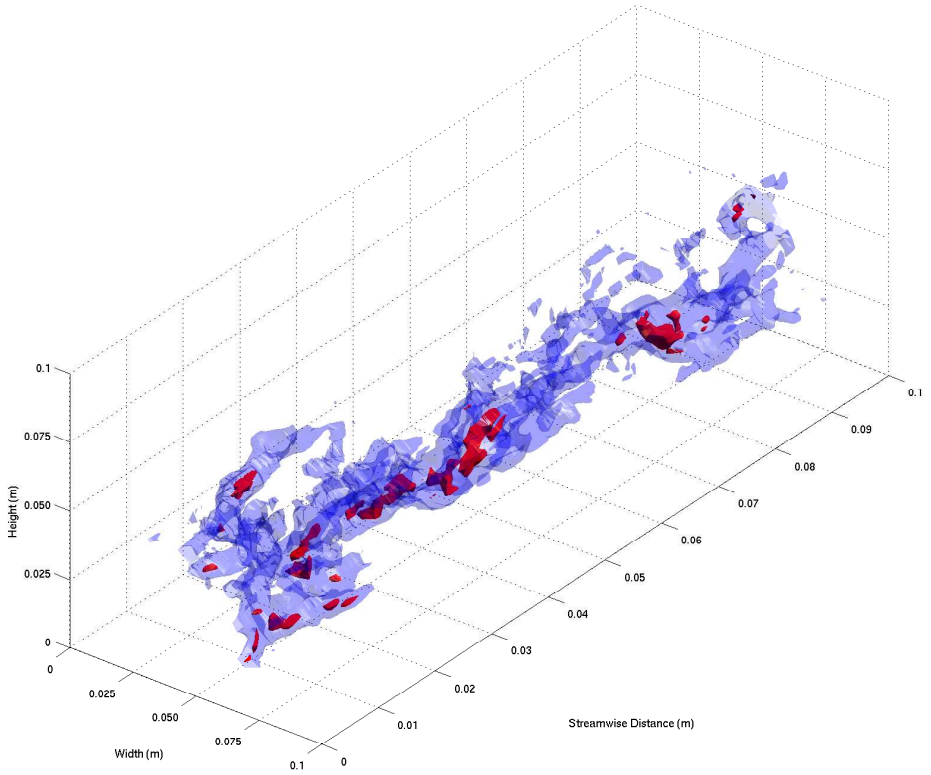

(a) Three-dimensional visualization of the tracer, with Re=17800, for concentration thresholds 0.0015 (blue) and 0.0033(red).

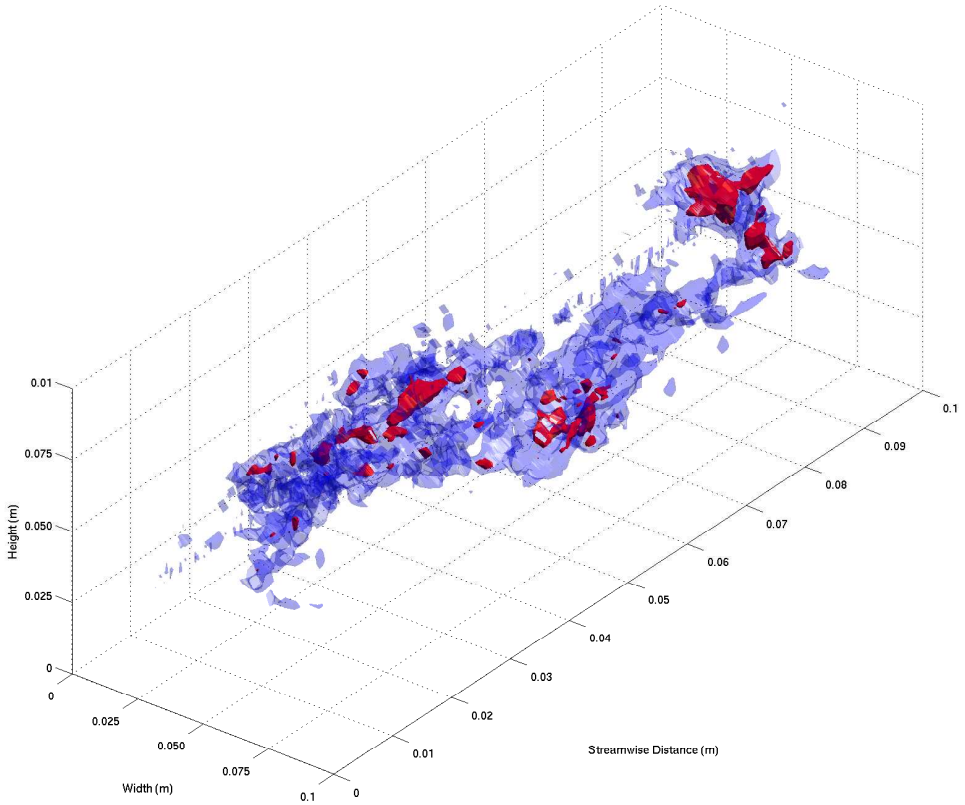

(b) Three-dimensional visualization of the tracer, with Re=60000, for concentration thresholds 0.0005 (blue) and 0.0011(red).

Figure 4.26: Tracer visualizations , as it passes through the wire-mesh, using Taylor's hypothesis to transform the time into streamwise distance.

Part II

The Rod Bundle Geometry

CHAPTER 5

Cross-Flow Mixing in a Rod-Bundle Geometry

The central point of part two of this thesis is the measuring of cross-flow mixing and coherent structures in a rod-bundle geometry. The measurements performed in this part use the same experimental rod-bundle set-up as the work of Mahmood (2011) and van Campen (2009). The added value of this research, is the acquisition of scalar mixing information, in addition to the localized velocity data they acquired with Laser Doppler Anemometry. Mixing of a scalar tracer, injected as a point source, gives an indication of the magnitude of mixing between different sub-channels, as well as information on the flow in the cross-section. This in the cross-section, as explained in the introduction, is vital for a good spread of heat through the core; therefore, is is vital for the safety, and efficiency of a nuclear reactor.

5.1 Secondary Flow

Secondary flow describes the flow in the direction perpendicular to the primary flow. So, in the case of a pipe flow in the z-direction, the secondary flow describes the flow in the x-y plane. The secondary flow is directly caused by anisotropy of the Reynolds stresses. The Reynolds stresses can be described as a tensor that follows from averaging the Navier-Stokes equation (equation 2.2), and is a result of turbulence fluctuations in the flow. When these turbulence fluctuations are anisotropic they can induce a flow in the cross-section. In a developed flow, anisotropic turbulence fluctuations exist in straight pipes when the cross-section is not axi-symmetric (for example, the square duct in figure 5.1a). Therefore, a rod-bundle geometry has a secondary flow, i.e. a mean velocity field in the cross-section. This mean velocity field promotes mixing and causes a net scalar transport in the cross-section. In figure 5.1b the secondary flow between four parallel rods is plotted.

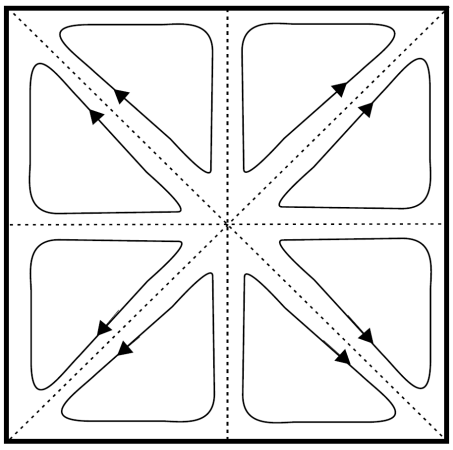

(a) Secondary flow in a square duct (Belt, 2007).

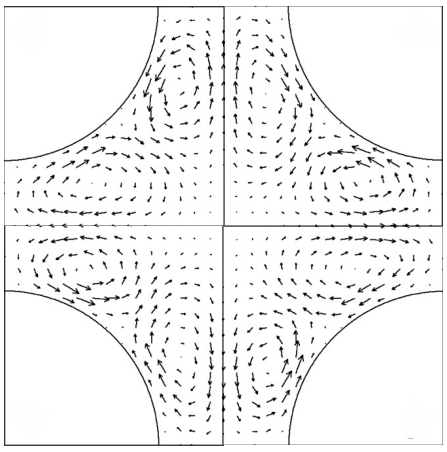

(b) Secondary flow between four parallel rods, (Ikeno and Kajishima, 2010).

Figure 5.1: Secondary flow plotted in (a) a square duct and (b) in a rod-bundle geometry.

5.2 Coherent Vortices

Aside from the secondary flow and molecular diffusion, there is a third mechanism in the flow in a rod-bundle geometry that causes a net transport in the cross-section. Among others, research from Mahmood (2011), and Ikeno and Kajishima (2010), showed the existence of large-scale coherent structures at the boundary between the gap and the sub-channel regions, moving along with the mean flow. These structures exist not only in turbulent flow but also show up in the laminar and transitionary flow regimes, where they are associated with the Kelvin-Helmholz instability.

5.2.1 Kelvin-Helmholtz Instability

The Kelvin-Helmholtz instability occurs at the boundary of two flow layers that run parallel, but have different characteristics. These different characteristics can be the density of the fluid or the mean velocity. Neither an abrupt transition between the two layers, nor turbulence are necessary. A gradual transition over a finite distance in laminar flow can also result in a Kelvin-Helmholtz instability. In figure 5.2; is shown the velocity profile in two parallel streams with a shear layer between them, as observed when moving with the mean velocity of the flow. In this figure, small disturbances, were added to the flow causing the edge of the layers to become less smooth.

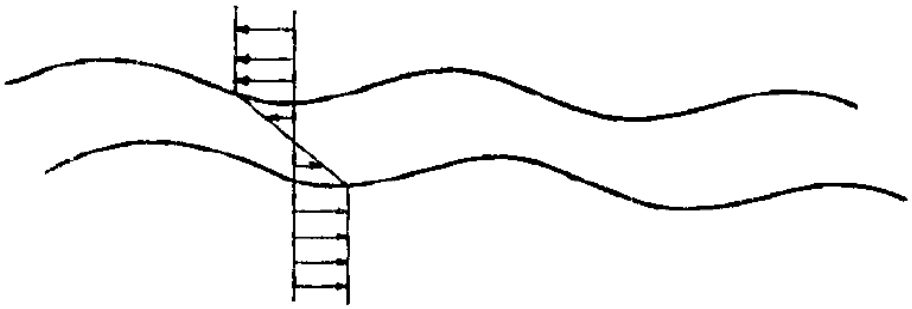

Figure 5.2: Mean velocity profile in two different flow layers with a small disturbance, as seen by an observer moving along with the bulk velocity.

The instability is caused by the destabilizing effect of the shear between both layers. Because of the disturbances the 'top' and 'bottom' of the peaks and valleys of the shear-layer are influenced more strongly by the higher relative velocities that exist further away from the center of the shear layer. This causes the disturbances to grow, as can be seen in figure 5.3. Finally the disturbances 'roll over' because of the velocity difference, creating vortices (Kundu and Cohen, 2000). The vortices are quite stable, and travel in the mean flow direction, along the boundary between both layers.

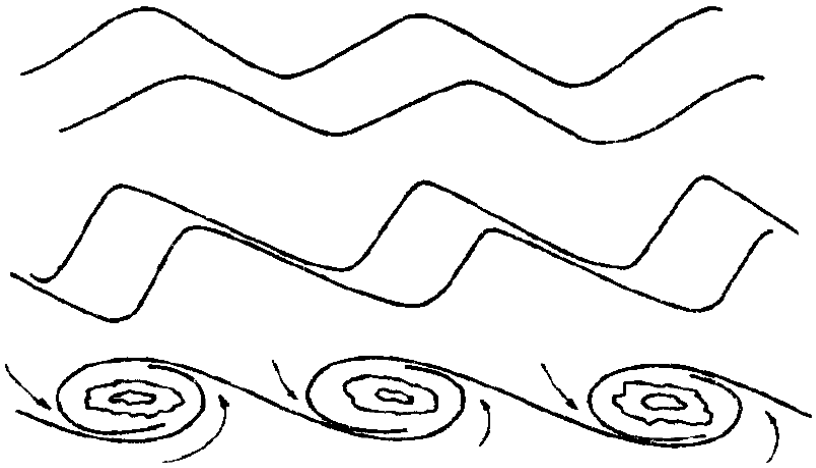

Figure 5.3: Evolution of a vortex street, as the result of a small initial disturbance in the shear-layer.

5.2.2 Coherent Structures in the Rod-Bundle Geometry

When looking at the flow velocity in a rod-bundle geometry, two different types of flow regions can be distinguished: (i) the gaps, where the velocity of the fluid, on average, is a bit lower then the mean velocity of the entire tube, and (ii) the sub-channel areas, where the velocity is a bit higher. This velocity difference is caused by the closer proximity of the wall in the gaps, when compared to the distance to the walls in the sub-channel. In the cross-section shown in figure 5.4, this is clearly visible.

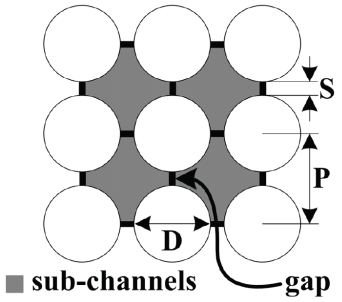

Figure 5.4: Sub-channels and gaps in a rod-bundle geometry.

Because of this velocity difference, the shear layer described in the last section occurs in a developed rod-bundle flow. This results in a Kelvin-Helmholtz instability originating the same type of vortex street on both sides of a gap. In a rod-bundle geometry, these vortices can have a significant effect on the mixing between sub-channels. The difference with respect to the previously described situation of two layers is that in a rod-bundle every gap has on both sides a sub-channel with higher velocity. For a stationary observer, the vortices on one side of the gap result in a an oscillating velocity perpendicular to the mean flow. Because of this oscillating velocity the vortices on the one side of the gap influence the vortices on the other side. This results in vortex streets on both sides of a gap, flowing along the stream, in reverse-phase from each other

5.3 Previous Work

It is important to emphasize that these vortices are not a turbulence phenomenon, but rather a result of the destabilizing effect of the shear-layer. Because of this, these coherent structures exist also in the laminar and transitional flow, as shown by Mahmood (2011). In his research, Mahmood proposed the model shown in figure 5.5. This simplified model assumes that each structure consists of two Continuously Stirred Tanks (CST). Because of the vorticity of the structure, CST's on both sides of the gap exchange a passive tracer, as can be seen in figure 5.5. Besides this model, Mahmood worked on measuring the sizes of individual structures for different Reynolds numbers, as well as the contribution of the coherent structures to the mixing in a rod-bundle geometry. In order to expand on, and verify his research, dat on localized mixing of a passive scalar is desired.

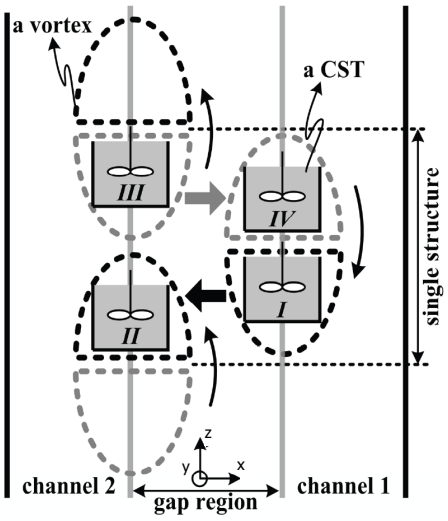

Figure 5.5: Model proposed by Mahmood for the interaction between vortices on both sides of a gap in a rod-bundle geometry (Mahmood, 2011).

CHAPTER 6

Rod-Bundle Set-Up

A main reason why this research was started, was the acquisition of localized mixing data in a rod-bundle geometry. For this purpose, a dedicated wire-mesh measurement section was designed and constructed by DEMO, the in-house mechanical and electronic development service from Delft University of Technology. This measurement section fits in the rod-bundle set-up used in a previous research with LDA.

6.1 Rod-Bundle Flow-Loop

The set-up where the measurement section is installed consists of six, 1 meter long, Polyvinyl chloride (PVC) sections. Running through these sections are four hollow PVC tubes of 25 mm diameter. At the walls of the tube, solid half and quarter-tubes are glued, in order to mimic a larger geometry, and reduce differences between the center sub-channel and the ones at the side. In figure 6.1, one of these sections is shown. Also, in figure 6.1 is shown one of the metal spacers that are used in the set-up for keeping the PVC tubes in place. These spacers are installed at the top of each PVC section; therefore, in principle they could have an influence on the flow. However, in the preliminary research by (Mahmood, 2011), they where used without any measurable consequences for the relevant flow characteristics.

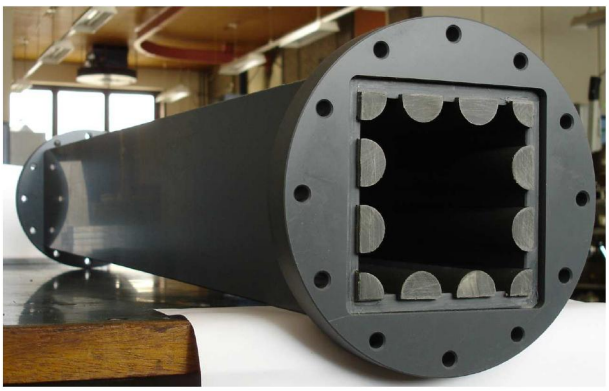

(a) One section of the rod-bundle tube lying down (van Campen, 2009).

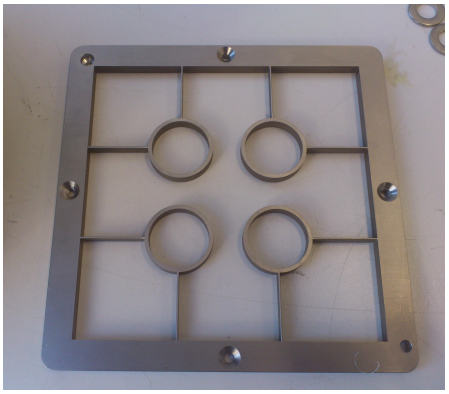

(b) A metal spacer used for keeping the rods in place.

Figure 6.1: One of the sections of the set-up (left), and a spacer (right).

The flow in the rod-bundle loop is driven by gravity, in order to generate a constant pressure drop, and a constant velocity profile without the need for an accurate pumping system. In the current set-up, a submerged pump at ground level is used to fill a vessel above the tube inlet, until it overflows. This way, a constant pressure is provided, resulting in a stable flow that can be adjusted by controlling the valves at the tube exit, in the bottom end of the tube. Upstream from the measurement section of the tube, five PVC sections are installed one PVC-section is installed downstream. Together with the upstream length of the measurement section, this gives the flow a development length of approximately $135D_h$. Downstream from the measurement section the rod-bundle geometry continues undisturbed for

one meter, $25D_h$, so no outflow disturbances should be present. The rods themselves are also filled with stagnant water along their entire length, in order to decrease the weight difference with the water around them, making them heavier, and reducing movement of the tubes caused by turbulence. The flow-loop is shown in figure 6.2.

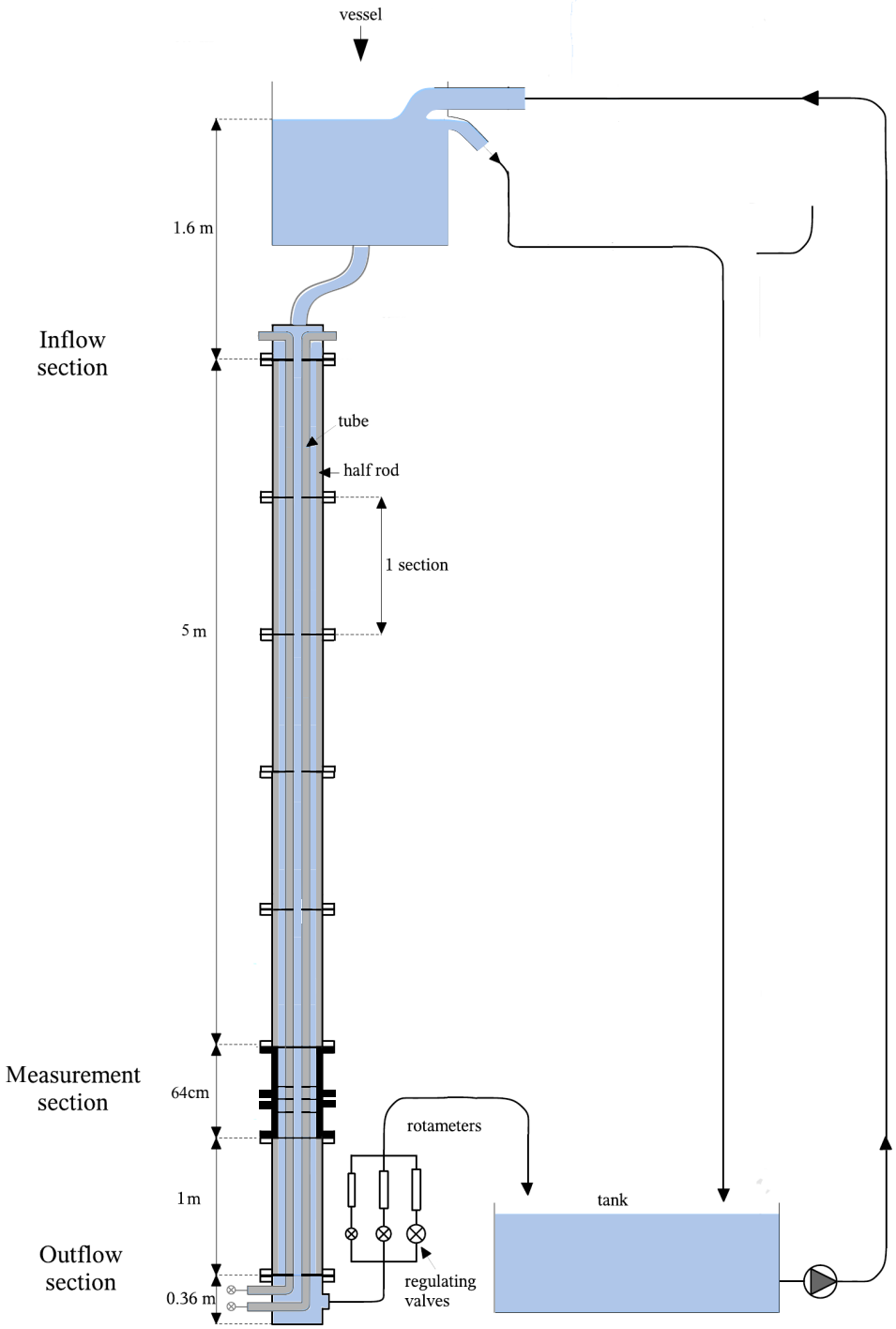

Figure 6.2: Schematic respresentation of the rod-bundle flow-loop.

6.2 Cross-Section

The flow-loop with the rod-bundle geometry was originally designed for LDA measurements. Considering the constraints caused by this technique with respect to the distance between the measurement probe, and the volume that was to be measured, the cross-section of the tube consists of nine sub-channels, arrayed as can be seen in figure 6.3. By using this array, the center sub-channel is surrounded by the other sub-channels, and has only limited effect from the wall. The eight outer sub-channels all have one, or two walls, instead of gaps to another sub-channel. Therefore, the main part of the measurements are performed in the center channel. An important characteristic of a rod-bundle geometry, is the pitch to diameter ratio P/D, which was decided to be 1.4 in the preliminary research, for a good comparison with data from Ikeno and Kajishima (2010). The radius of each of the tubes, including the half- and quarter-tubes placed along the walls, is 25 mm, so that as a result of the P/D ratio the other dimensions are as they are given in figure 6.3.

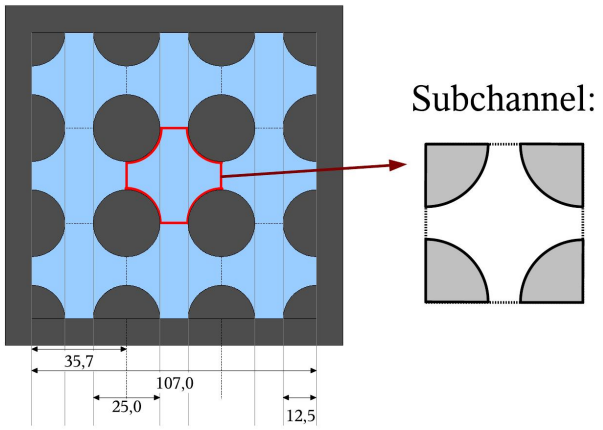

Figure 6.3: Cross-section of the rod-bundle flow-loop, dimensions are in mm; blue is the flow area and the PVC walls and rods are in black (van Campen, 2009).

With these dimensions, the hydraulic diameter of the sub-channel, which replaces the normal diameter when calculating flow characteristics in tubes with a non-circular cross-section, can be calculated using:

$$D_h = \frac{4A}{Q} \tag{6.1}$$

where A is the surface of the cross-section through which the fluid flows and Q is the wetted perimeter. When using this equation it follows that: $D_h = 40.0 \cdot 10^{-3}$m for this set-up, when looking at the central sub-channel.

6.3 Measurement Section

The previous experiments in this set-up where done with LDA equipment. This required Fluorinated Ethylene Propylene (FEP), in order to have a matching refractive index with water. Since this FEP is notoriously weak (van Campen, 2009), it was deemed necessary to remove this section from the equipment, and create a completely new section, in order to include the two wire-meshes.

6.3.1 Geometry

It should be noted that the PVC sections and rods do not follow the desired dimensions perfectly. This has to do with PVC being a flexible material, and with choices made when the sections where originally

build. The solid half- and quarter-rods glued against the side of the tube have a slightly larger diameter (25.6 mm) than desired and are countersunk somewhat into the plates at the side, in order not to protrude too far inside. The result of this is a less than perfect rod-bundle geometry close to the walls. Also, the spacers that enclose the rods (figure 6.1b) are relatively thick (2 mm). In order to reduce the influence of these irregularities in the flow, the measurement section that was build is a bit longer than necessary for the sensors. This way, the tube-section closest to the sensors was designed and built from scratch. The walls of this new part of the set-up are milled out of one piece, instead of glued together from different parts and the rods are from stiff aluminum instead of PVC. This results in a much more accurate rod-bundle geometry that starts $12.5D_h$ upstream from the top wire-mesh and ends $2.5D_h$ below the bottom sensor.

In figure 6.4, the schematic of the measurement section is shown. The horizontal cross-section is the same as shown in figure 6.3. The vertical cross-section from figure 6.4 shows the rods (light grey), the wall of the tube (red stripes), the flow area (light blue) and the positions of the spacers (dark grey). The dimensions are given in milimeter, so the distance between the two wire-meshes corresponds to one hydraulic diameter. The tubes in this section are made out of aluminum and PVC, the 5 spacers out of stainless steel and the walls of the tube are milled out of PVC.

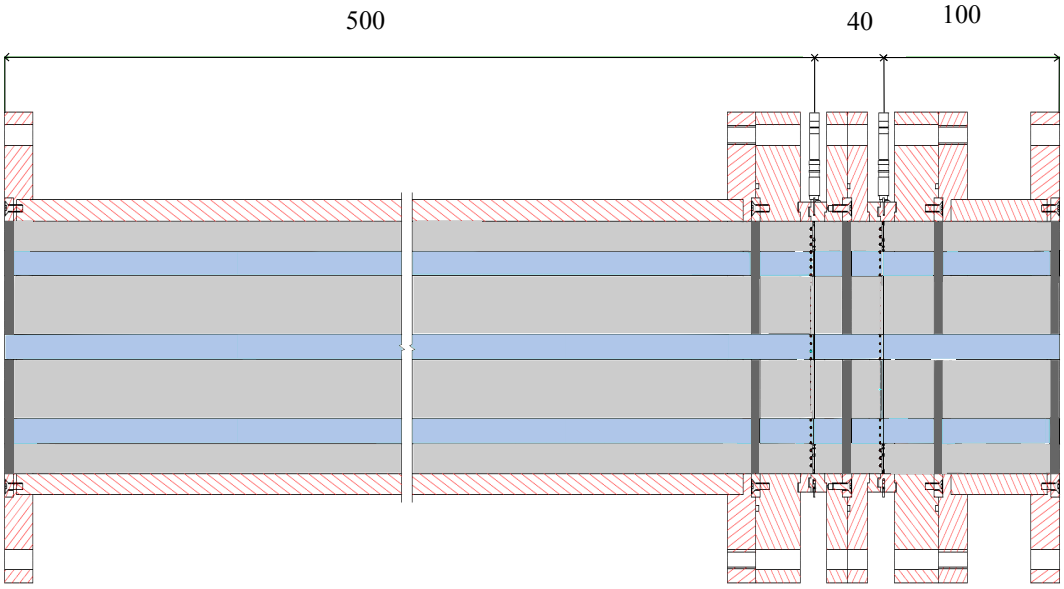

Figure 6.4: The schematics of the measurement section, dimensions are in mm.

6.3.2 Spacers

At the designing phase of this project the main points of concern were the irregularities in the set-up, and their disturbances in the flow. One way of decreasing their influence, as explained before was making the measurement section longer upstream from the wire-mesh. This increases the distance between the wire-meshes and the transition between the older rod-bundle section, and the newer. Another cause of flow disturbances are the spacers used throughout the flow-loop for keeping the rods in place.

The spacers outside of the measurement section were used previously by Mahmood, without measureable influence on the structures. In this research, however, there are also spacers situated very close to the measurement sensors themselves. These spacers are necessary to strengthen the set-up, and keep the rods firmly in place. This is needed because the rods in the measurement section are connected directly to the 5 meter-long, PVC-rods above them. In order to minimize the influence of the spacers,

the set-up was designed such that the spacers are actually countersunken into the rods and only create disturbances at the outside of the tubes. In figure 6.5a, this is shown in a part of the measurement section. Also visible are the four small holes in each pipe used for attaching the next section of the pipes, and the larger central hole which makes sure that water can flow through the entirety of the rods. A spacer is also used for smoothing the transition of the PVC-rods from above with the aluminum rods in the measurement section. In figure 6.5b, this transition is shown. It is clear that both the PVC and the aluminum rods fall into the spacer, so any irregularities fall inside of the spacer, which is somewhat higher than the other spacers for this purpose.

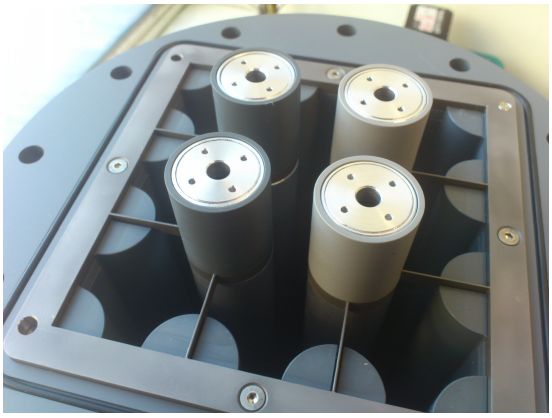

(a) One of the spacers countersunk in the rods.

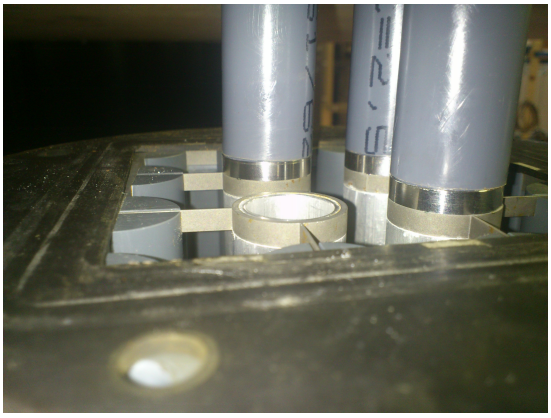

(b) Connection between the PVC and aluminum rods.

Figure 6.5: Pictures of the actual spacers countersunk in the rods and used for connecting the rods in the flow measurement sections.

6.3.3 Tracer Injection

Similarly to the research in the first part of this work, the tracer necessary for measuring a signal is injected in the flow with an L-shaped injector at several different distances upstream of the wire-meshes. For construction reasons, it was chosen to limit the injection to four points in the newly constructed measurement section. The injection points where chosen such that the capillary-exit can be situated at distances of $1D_h$, $4D_h$, $7D_h$ and $10D_h$ away from the top wire-mesh, with D_h being the hydraulic diameter, equal to 40 mm. In figure 6.6a the capillary is shown positioned in the lowest injection point in the rod-bundle; its horizontal position can vary between postions A to B, as shown in figure 6.6b. The tracer can therefore be injected in the central sub-channel, in a gap, and in an outer sub-channel.

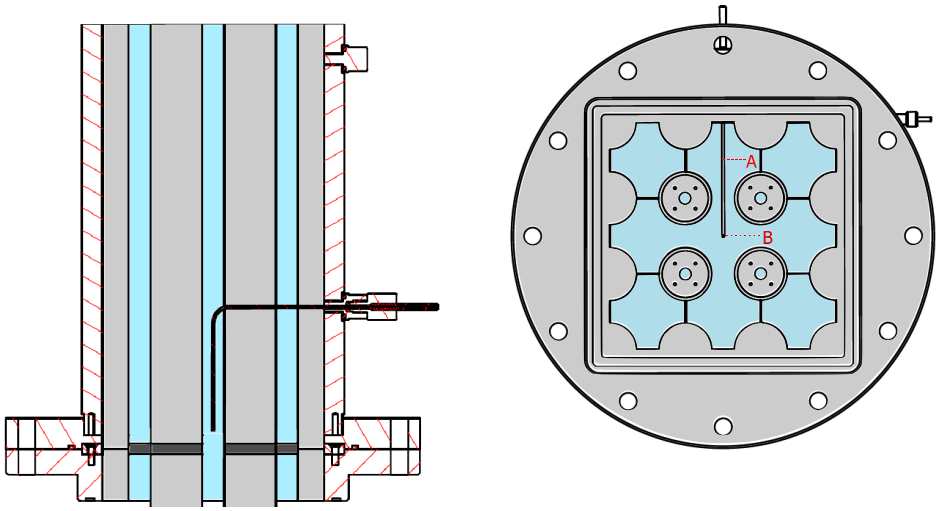

(a) Vertical cross-section **(b)** Horizontal cross-section.

Figure 6.6: Positioning of the injection capillaries, shown in the horizontal and vertical cross-sections.

6.4 Sensors

Central to this research are the two wire-mesh sensors designed and built specifically for the purpose of measuring in the rod-bundle geometry described above. The idea was to create two sensors with a spatial resolution as high as possible, and that could be used with the available electronic equipment which is capable of a high time-resolution. Because of the small streamwise distance between both sensors, they can be used for correlating their signals, to get localized velocity information, in addition to local tracer concentration and mixing data. The biggest challenge of the construction was to find a way to let the wires go through the four central rods without subjecting the wires to mechanical forces strong enough to break them. At the same time, the wires have to be strung tight enough to avoid flow-induced vibrations. Also, the holes in the rods through which the wires go have to be small, in order for the flow to be as undisturbed as possible. It was chosen to use two wire-meshes of 32 by 32 wires, evenly distributed over the channel. In figure 6.7 is shown the lay-out of one of the wire-meshes. The large amount of crossings, and thus the large amount of measurement points per sub-channel is clearly visible; Even in the gap regions, multiple measurement points are available for analysing the tracer concentration. As shown in figure 6.7, the mesh was constructed in two separate frames, for the two layers of perpendicular wires. This way, it was possible to create small PVC discs, with small milled channels, in which the wires could rest (figure 6.8). The end result is a set of two wire-mesh sensors, each covering the flow area of the rod-bundle with approximately 600 measurement points. The wire thickness is 0.2 mm and the distance between the two layers of one wire-mesh sensor is 1.5 mm. This way, the distance between both wire-mesh sensors is 200 times the diameter of the wires; therefore, the flow disturbance of the upstream wire-mesh sensor has only a small influence in the signal of the downstream wire-mesh sensor.

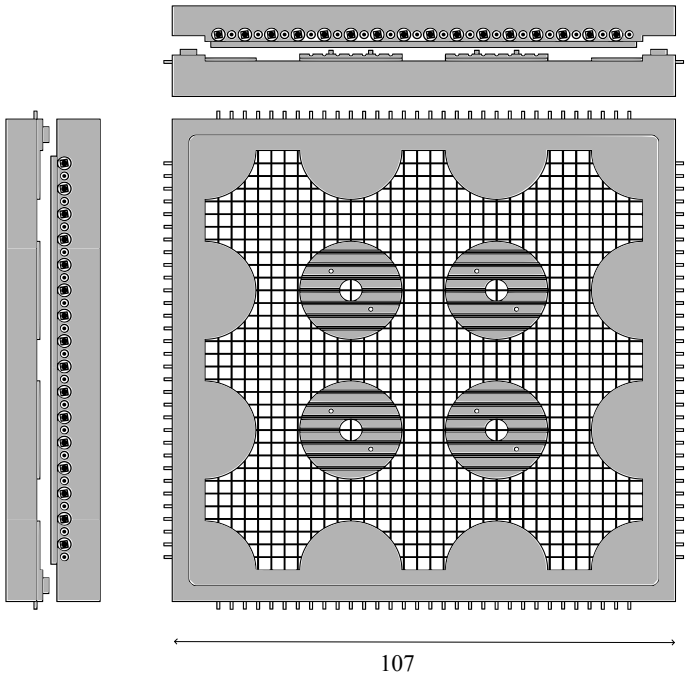

Figure 6.7: Schematic of one of the wire-meshes.

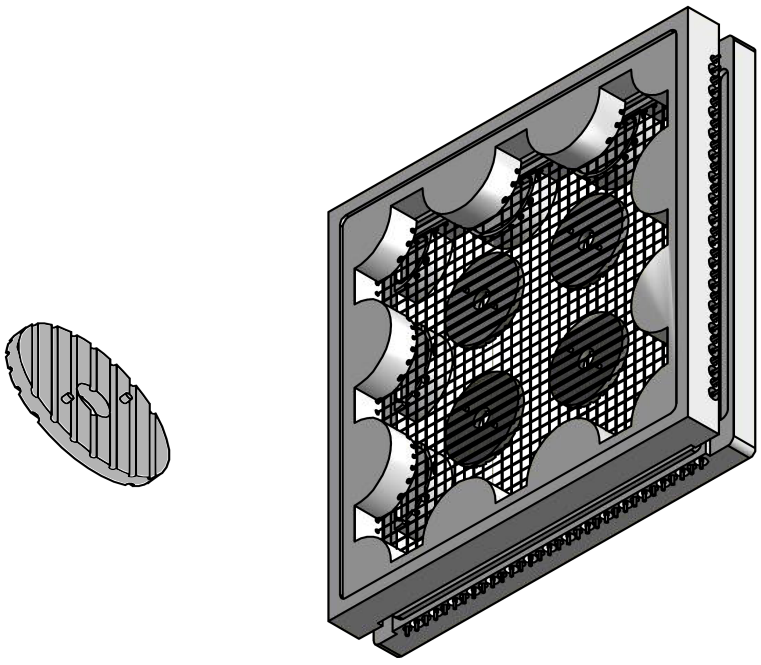

Figure 6.8: Small disks allowing the wires through the rods (left), and the total wire-mesh assembled (right).

The result of this can be seen in figure 6.9. In this figure, the top rod is fully assembled, with aluminum and PVC rod pieces between the two wire-mesh sensors, and the spacer that fits nicely into the rods. At the left and right of the figure, the spacer is clearly visible, as well as the two PVC disks hanging between the wires.

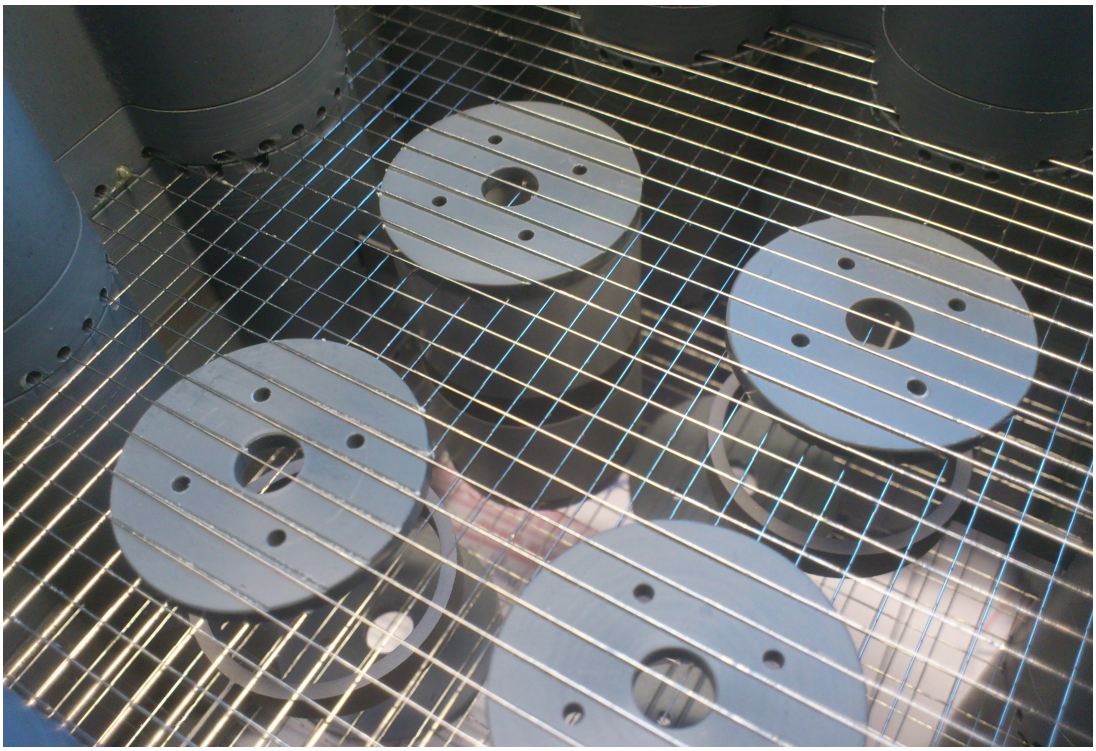

Figure 6.9: Both wire-mesh sensors assembled.

The 0.2 mm diameter wires are micro-welded onto very small screw-threads and can be tightened by screwing a small square screw-nut; the hole is closed with the help of a small rubber washer. In principle, this should make for a water-tight system. However, in reality a screw-thread of this dimension is so vulnerable 10 to 20 wire-holes in the wall of the duct kept leaking when the duct was filled with water. With the help of glue, the problem was reduced until the situation became workable. The wires are attached with small female connectors that are soldered on plugs, which transmit the signal to the electronic equipment (figure 6.10).

Figure 6.10: Wires sticking out of the outside of the wall of the duct, connected by small plugs with the equipment.

CHAPTER 7

Rod-Bundle Measurements

The equipment described in the last chapter was designed for acquiring localized mixing data for a scalar (salt) injected in the main flow. The two sensors designed for this purpose are positioned approximately 1 hydraulic diameter, or 40 millimeters, apart from each other in the streamwise direction. The idea about using two sensors is that it will allow to add experimental data about the streamwise length and velocity of the flow structures, to the measurements performed by Mahmood. A drawback to the current situation is that the available electronic equipment can only control 32 transmitter wires and 32 receiver wires. Because of this, it was decided to split the transmitter wires, effectively creating 62 transmitter wires, and only connecting the central 16 wires in the receiver layer of each sensor.

7.1 Wire-Mesh Output

As explained, the in-house designed and built sensors result in two measureable cross-sections in the rod-bundle flow. The tracer concentration is measured with a spatial resolution of 3 mm. The signal resulting from a measurement is shown in figure 7.1. In this figure, the tracer is injected in the center of the gap, 40 centimeters ($10D_h$) upstream of the top wire-mesh sensor.

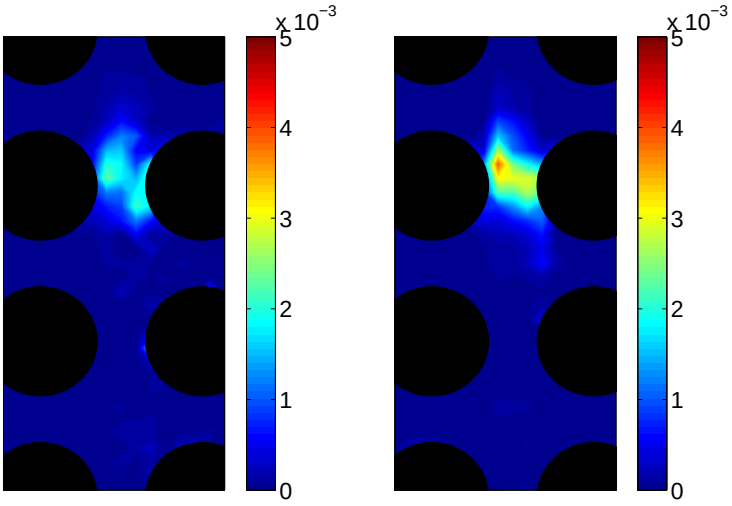

Figure 7.1: Snapshot of tracer concentration values at one moment, for the top (left) and bottom (right) sensor at the same instant. The concentration is normalized by its value at the injection point, in the center of the gap 40 cm upstream from the top sensor.

In figure 7.1 the output of both sensors is shown at the same time, since there is a distance of 4 cm between the two sensors, the measurements can be better compared when compensating for the extra traveling distance between both wire-meshes. In figure 7.2, the concentration values shown by the bottom sensor are measured 0.24 seconds later than in the top sensor. The correlation between the two sensor is clearly visible: two areas of higher concentration can be distinguished in both sensors. It is also visible that the values detected in the bottom sensor are generally higher than in the top sensor. In

the bottom sensor, where the tracer should have dispersed more, the signal is up to 20% higher than in the top sensor. A possible reason for this, is an error in the calibration data used. Between performing calibration for a highly-conductive homogeneous solution (which was done with the sensors outside of the entire rod-bundle set-up) and the measurements performed after installing the sensor in the flow-loop, the electronic equipment was damaged and needed to be repaired. It could be that in one half of the sensor the relation between conductivity and sensor-output changed, making the calibration data less accurate.

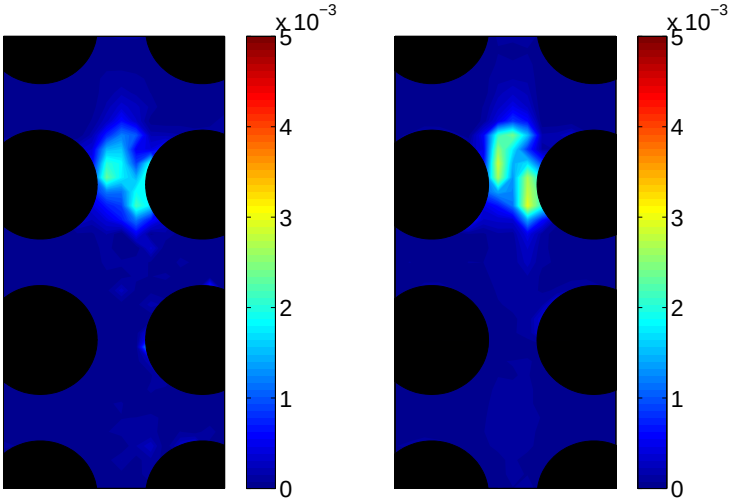

Figure 7.2: Tracer concentration values for the top (left) sensor at t=0s, and the bottom (right) sensor at t=0.24s. The concentration is normalized by its value at the injection point, in the center of the gap 40 cm upstream from the top sensor.

7.1.1 Time-Signal

Looking at the development of the tracer concentration in time, gives an even a better impression of the correlation between the two sensors. In figure 7.4, the tracer concentration in time is shown through line A (figure 7.3). In figure 7.4, the white lines are an indication of the sides of the tubes between which the tracer is injected.

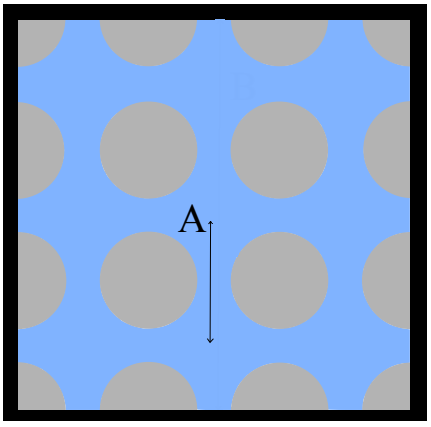

Figure 7.3: Measurement line A.

In figure 7.4, regions of higher tracer concentration can be observed on both sides of the gap. The correlation between tracer fluctuations in the top and bottom sensors is visible, but the time difference is better seen when looking at the signal over a shorter time (figure 7.5). Although the tracer concentration clearly evolves during the measurements, the correlation between the two sensors is clearly visible, as well as the time-lag between the two signals.

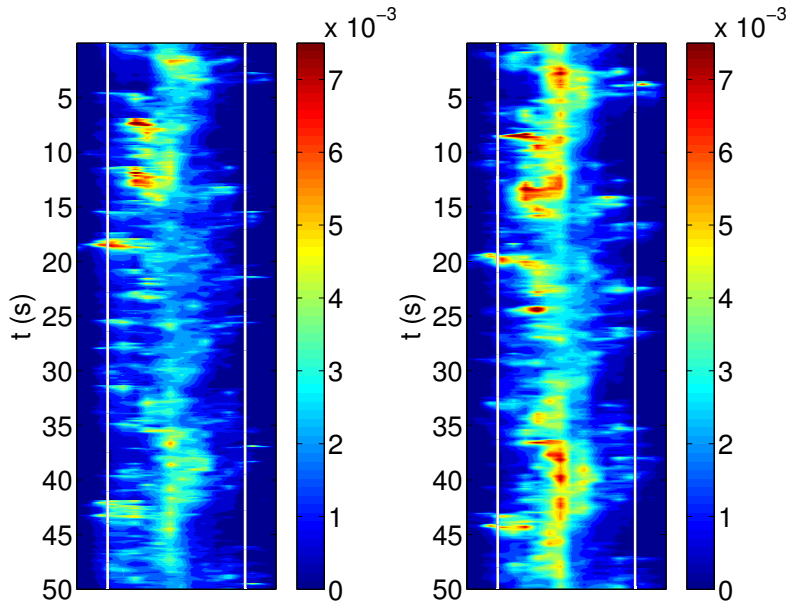

Figure 7.4: Tracer concentration over a line in a gap region, as it evolves over 50 seconds, in the top (left) and bottom (right) sensor. The concentration is normalized by its value at the injection point, in the center of the gap 40 cm upstream from the top sensor.

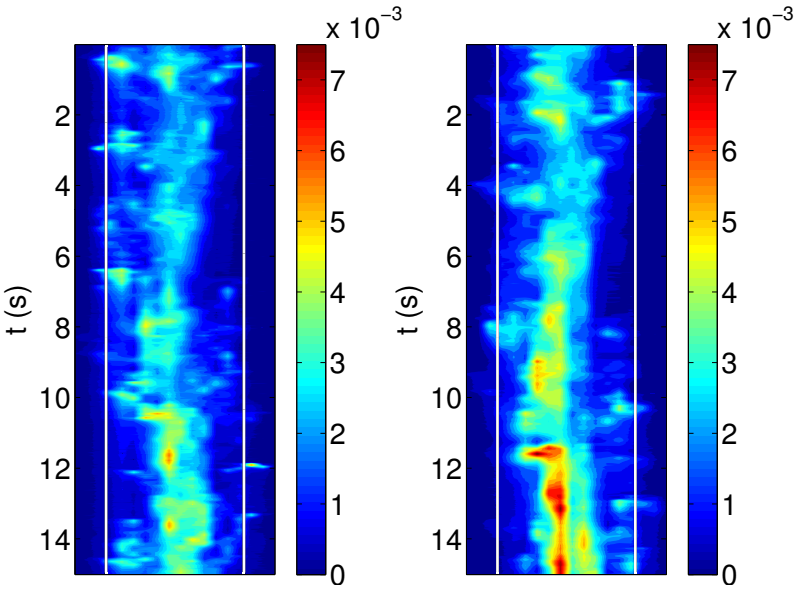

Figure 7.5: Tracer concentration over a line in a gap region, as it evolves over 15 seconds, in the top (left) and bottom (right) sensor. The concentration is normalized by its value at the injection point, in the center of the gap 40 cm upstream from the top sensor.

7.1.2 Mean Concentration

The average mixing of tracer injected in one sub-channel can be visualized by plotting the average tracer concentration over the cross-section of the rod-bundle. In figures 7.6 and 7.7, the mean concentration values are shown for two different injection points. The result is naturally a larger dispersion when the solution is injected further away from the sensor. The difference between the top and bottom sensors is as expected: the dispersion is larger in the bottom sensor which, of course, is further away from the injection point. No evidence can be found in these measurements for tracer dispersion to neighboring sub-channels. Also, no evidence is found in this figure that the injection device (which enters the tube from the top in figure 7.6 and 7.7) has any influence on the dispersion. It is clear that to measure dispersion from one sub-channel to another injection points further away from the sensors are necessary.

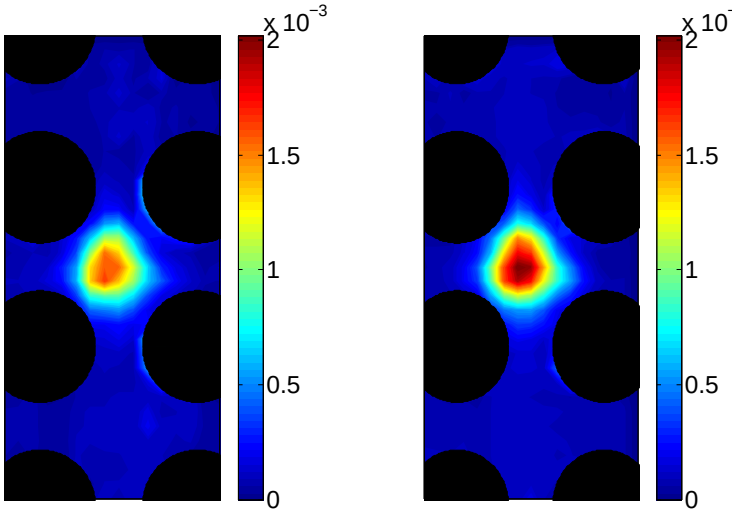

Figure 7.6: Mean tracer dispersion measured in the top (left) and bottom (right) sensors for Re=6000. The values are normalized with the tracer injected in the central sub-channel 40 cm upstream of the top sensor.

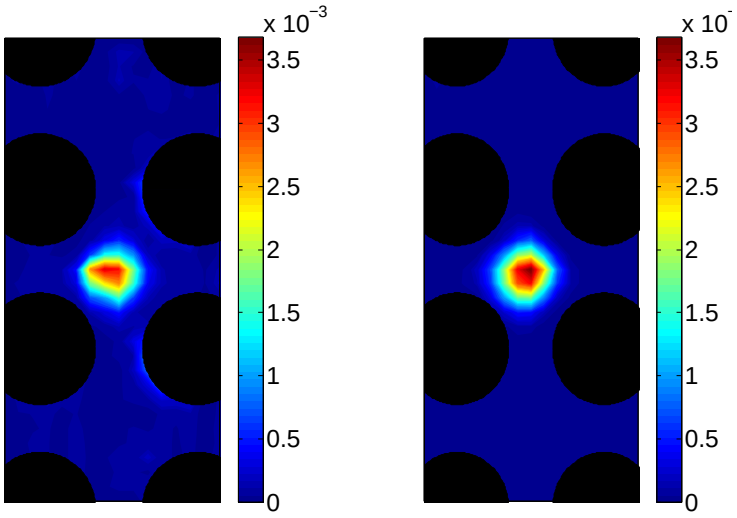

Figure 7.7: Mean tracer dispersion measured in the top (left) and bottom (right) sensors for Re=6000. The values are normalized with the tracer injected in the central sub-channel 16 cm upstream of the top sensor.

It is also interesting to note that, even though, as expected, there is a slightly larger dispersion in the mean concentration in the bottom sensor than in the top sensor, the magnitude in the values of the mean concentration is slightly larger in the the bottom sensor. The larger magnitude of the mean concentration in the bottom sensor is consistent with what was observed in figure 7.2 for the instantaneous concentrations; as mentioned in section 7.1, a possible reason for it is an error in the calibration, due to the damage that occurred in the electronic equipment between calibration and the measurements.

7.2 Time-Correlation

The wire-mesh equipment is not primarily meant to be a velocity measurement technique. One sensor, after all, can only give back localized conductivity data. However, in this research two separate sensors are installed at a distance of one hydraulic diameter (4 cm) apart. By cross-correlating the data from the top and bottom sensors, the time-lag between signals in the top and bottom sensors can be obtained. This time-lag can be used for acquiring the "concentration velocity".

7.2.1 Cross-Correlation

In section 7.1.1 it was shown that there exists a clear correlation between the concentration measured in the top and bottom sensors. By correlating the signals of the top and bottom sensors, the time-lag that maximizes the correlation of the two signals can be found. In figure 7.8 this cross-correlation as a function of the time-lag between the two signals is shown. The cross-correlation is performed between one measurement point in the gap-region of the top sensor and the corresponding measurement point in the bottom sensor, with tracer injected in the center of the gap, in a flow with Re=6000. The same figure can be seen zoomed in (figure 7.8b). The small time-lag that maximizes the cross-correlation between the signals is clearly visible in figure 7.8b

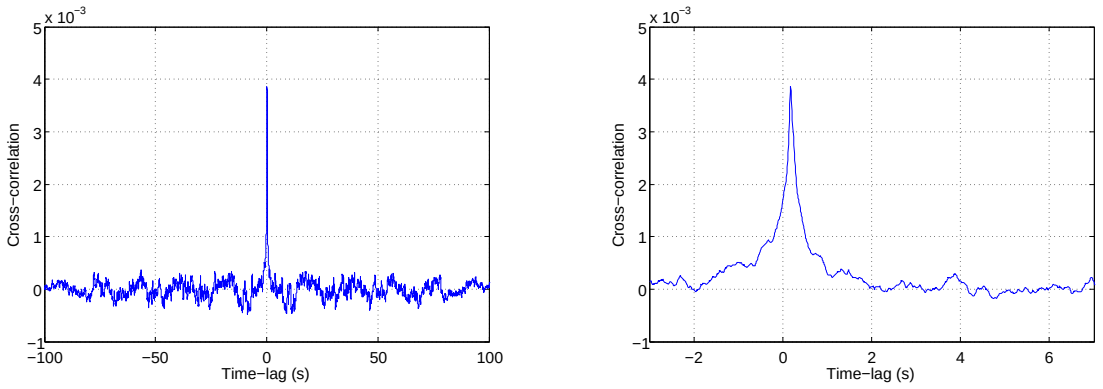

(a) Cross-correlation between the two sensors.

(b) Zoomed in cross-correlation between the two sensors.

Figure 7.8: Cross-correlation between the top and bottom wire-mesh, normal (left) and zoomed in around t=0 (right), with Re=6000.

For comparison, in figure 7.9, the cross-correlation is plotted in a flow with Re=500. The time-lag that maximizes the cross-correlation is larger and the correlation peak is less sharp, which is to be expected considering the slower velocity, but it is still easy to identify. The time-lag obtained from the cross-correlation gives information about the time it takes for fluctuations in the tracer concentration to travel from the top sensor to the bottom sensor.

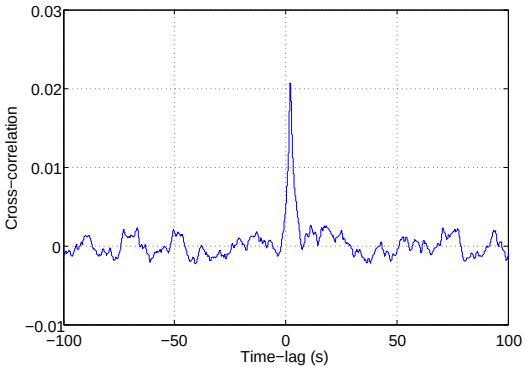

(a) Cross-correlation between the two sensors.

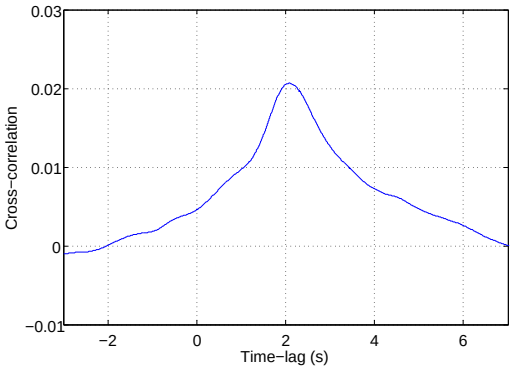

(b) Zoomed in cross-correlation between the two sensors.

Figure 7.9: Cross-correlation between the top and bottom wire-mesh, normal (left) and zoomed in around t=0 (right), with Re=500.

By using the distance between the two sensors, the concentration velocity of the structures can be obtained:

$$V_{con} = \frac{\Delta z_{sensors}}{\Delta t_{maxcorrelation}} \tag{7.1}$$

where in this case V_{con} is the streamwise "concentration velocity", Δz is the distance between the sensors and Δt the time-lag of the maximum correlation.

Note that Taylor's hypothesis is generally accepted when investigating small turbulence structures away from the walls. According to Taylor's hypothesis, if the salt would be a perfect tracer then $V_{con} = V_{fluid}$. However, Taylor's hypothesis is not necessarily correct when dealing with the large-scale structures in a rod-bundle geometry. The "concentration velocity" is the velocity of the pattern and, even if the salt is a perfect tracer, V_{con} is not necessarily equal to the (local) mean velocity of the fluid. On top of that, due to buoyancy effects and dispersion the salt does not necessarily behaves as a perfect tracer.

7.2.2 Profile of the Concentration Velocity

Using the time-lag of every measurement point found, following the method from section 7.2.1, the velocity with which the pattern of concentration fluctuations travel can be obtained for every measurement point. In figure 7.10, the concentration velocity profile over the cross-section is shown. In figure 7.10 the average concentration velocity, V_{con}, in every measurement point is normalized with the bulk velocity of the fluid which is obtained from the flow-rate and the total area of the cross-section of the duct. Since the tracer, injected $10D_h$ away from the top wire-mesh does not reach every point in the cross-section, not the entire cross-section is measured. The region where no relevant data was available is shown in dark red. The velocity, measured in the region where the tracer does reach, shows a relatively consistent behavior for the two Reynolds numbers shown in figure 7.10.

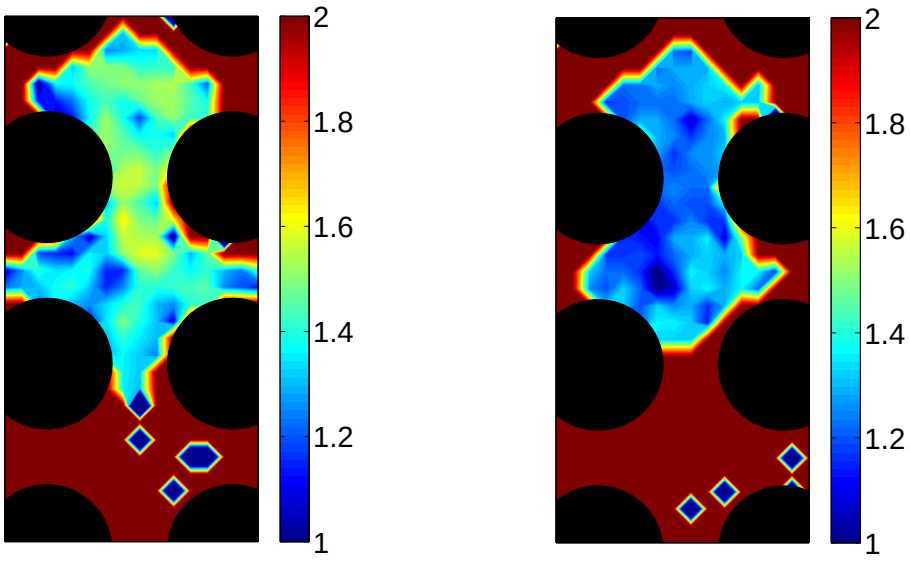

(a) Velocity in V_{con}/V_{bulk} for Reynolds=500.

(b) Velocity in V_{con}/V_{bulk} for Reynolds=3000

Figure 7.10: Concentration velocity normalized with the bulk velocity for two Reynolds numbers; dark red depicts the region where no tracer was measured, and therefore where no data is available. The tracer was injected in the center of the gap 40 cm upstream of the top sensor.

7.2.3 Comparison between the Concentration Velocity and Fluid Velocity

Measurements were performed in the exact same set-up by Mahmood (2011) with a Laser Doppler Anemometry. This measurement technique is used to acquire localized velocity data. The result of this is that Mahmood, besides looking at horizontal velocities, investigated mean velocities in different parts of the cross-section. His findings show that the velocity of the flow could vary greatly between the center of the gap and the center of a sub-channel. According to Mahmood, for laminar flows the velocity in the center of the sub-channel was approximately $1.6V_{bulk}$ while in the center of the gap the velocity was approximately equal to V_{bulk}. For turbulent flows, the differences between sub-channel and gap regions where a bit smaller, but still measurable: approximately $1.3V_{bulk}$ for the maximum velocity in the sub-channel and approximately $1.1U_{bulk}$ for the maximum velocity in the center of the gap region. Some results of his research are shown in figure 7.11. Note that the values at the central measurement points in the left and right figures should be the same. The small differences gives an indication about the uncertainty of the LDA measurements.

As explained in section 7.2.2, the concentration velocity and the fluid velocity are not necessarily equal. Indeed, comparing figures 7.10 and 7.11, it can be seen that even though, as expected, they are of the same order of magnitude, they are not equal. Mahmood (2011) found with PIV-measurements in more simple geometries that the velocity of the coherent structures was roughly the same as the fluid velocity in the center of the a sub-channel. Keeping this and the velocity from figure 7.11 in mind, a few interesting points regarding the results from figure 7.10 can be mentioned:

- At both Reynolds numbers, V_{con} is everywhere larger than V_{bulk}.
- For Re=500 in the gap and gap-channel layer regions V_{con} is roughly equal to the fluid velocity in the center of the sub channel for Re=631 (figure 7.11).
- For Re=500, V_{con} in the sub-channel is lower but still larger than V_{bulk}; here the large-scale structures might not be the dominant contribution to V_{con}.

- For Re=3000, V_{con} is roughly constant and a little higher then V_{bulk}. Again the value is approximately the same as the value of the velocity in the center of the sub-channel as measured by Mahmood (2011) for Re=3153.

So, both for Re=500 and Re=3000, V_{con} is roughly equal to the velocity in the center of the sub-channel measured by Mahmood (2011). This fits with the findings of Mahmood (2011) for more simple geometries using PIV.

Even though these results seem in good agreement, some sources of caution should be pointed out. It is not known how much influence the different density of the salt has on these results. It is assumed that the cross-correlation between both sensors gives the velocity of the fluid structures. However, it is not known how accurate this approximation is, or how the concentration velocity relates to the velocity of the fluid structures. They are equal only if the salt behaves as a perfect tracer, and due to buoyancy and dispersion it is not known to what extent the salt behaves as a perfect tracer.

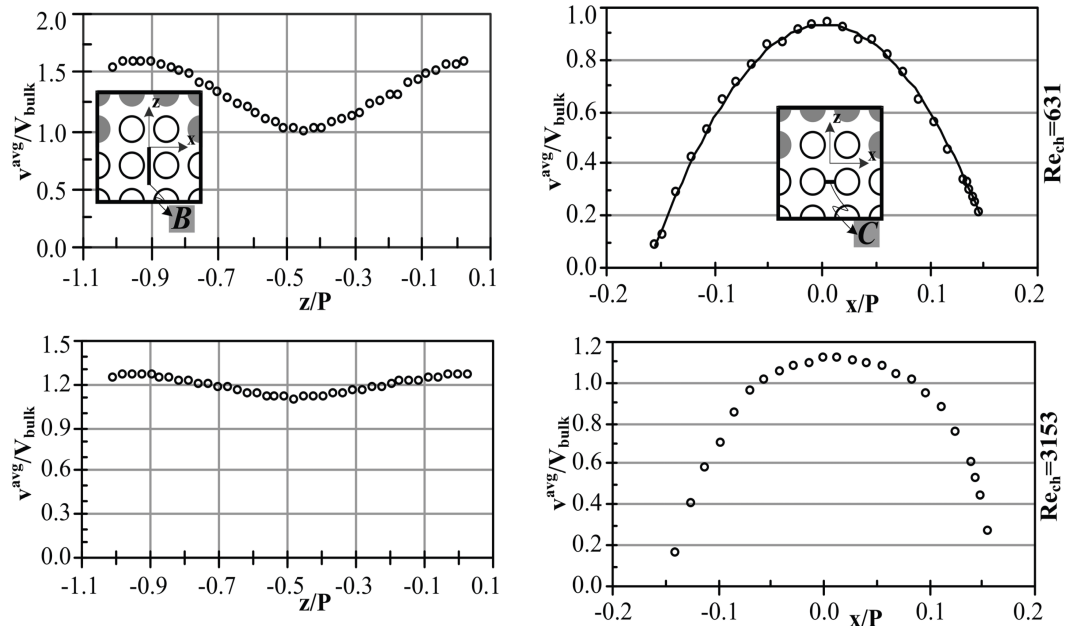

Figure 7.11: Streamwise velocity measurements by Mahmood (2011).

7.3 Coherent Structures

In section 4.5 ,one wire-mesh sensor was used for investigating structures in turbulent flow. Fluctuations in tracer concentration and regions in the flow with accumulated tracer were used to give an indication about the size of the larger turbulence structures, using Taylor's hypothesis. In this second part of this research, not these turbulent structures, but large-scale, coherent vortices are the structures of interest.

7.3.1 Previous Work

The same rod-bundle geometry was used in the past by van Campen (2009) and Mahmood (2011), for investigating the size of coherent structures on both sides of the gap regions. Results of their experiments can be found in figure 7.12. Their experiments show both the same trend: at lower Reynolds numbers the structures grow very large, while for larger Reynolds numbers their streamwise size tends to decrease to a smaller roughly constant value. Both used LDA, and the velocity data in one point as a function of the

time was auto-correlated. The distance between two peaks in the auto-correlation function was assumed to give the time-lag between two structures moving through that point. As mentioned above, based on PIV-measurements in simpler geometries, Mahmood (2011) used the fluid velocity in the center of the sub-channel to transform time-lag in the streamwise structure sizes shown in figure 7.12.

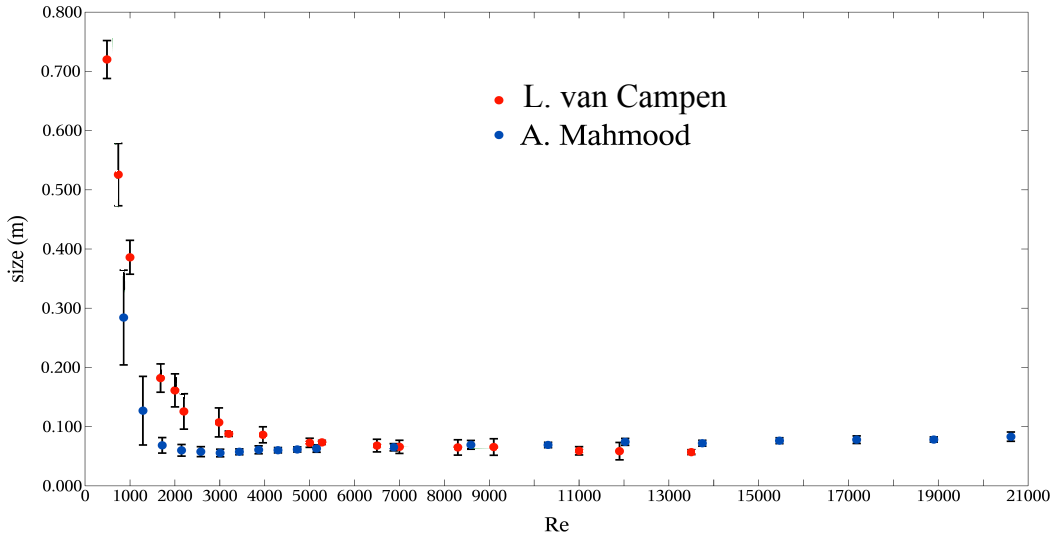

Figure 7.12: Structure streamwise-size in the rod-bundle geometry as a function of the bulk Reynolds number, found by Mahmood (2011) and van Campen (2009) using LDA measurements.

7.3.2 Fluctuations Auto-Correlation

As discussed in section 7.2.2, the advantage in this research is the availability of two sensors in the flow; because of this, cross-correlating can be used for acquiring localized velocity data. Therefore, the "concentration velocity" obtained from the time-lag in the cross-correlation between the two sensors was used to transform the time-lag into a streamwise distance. This should result in a more accurate estimation of the streamwise structure sizes. Note, however, that regardless of the velocity used to transform the time-lag into a streamwise distance, one of the key assumptions associated with Taylor's hypothesis is alway used: the structures are assumed "frozen" as they flow through the sensor.

In order to look at the possibilities of quantifying the sizes of the coherent structures, a few measurements where performed. In figure 7.13, the mean tracer concentration and the concentration velocity are shown for the individual measurement points in the top sensor. On the horizontal and vertical axis is shown the number of the receiver and transmitter wires. Each colored square portraits one measurement point. The coherent structures exist on the boundary between the gap and sub-channel regions, therefore, if fluctuations in the tracer concentration are primary caused by these structures, they should show up mostly in this layer and on the 'other' side of the gap. The injection is done with a capillary entering from the 'top' of each figure and the tracer is injected in the gap between the two central tubes at the top of the figures.

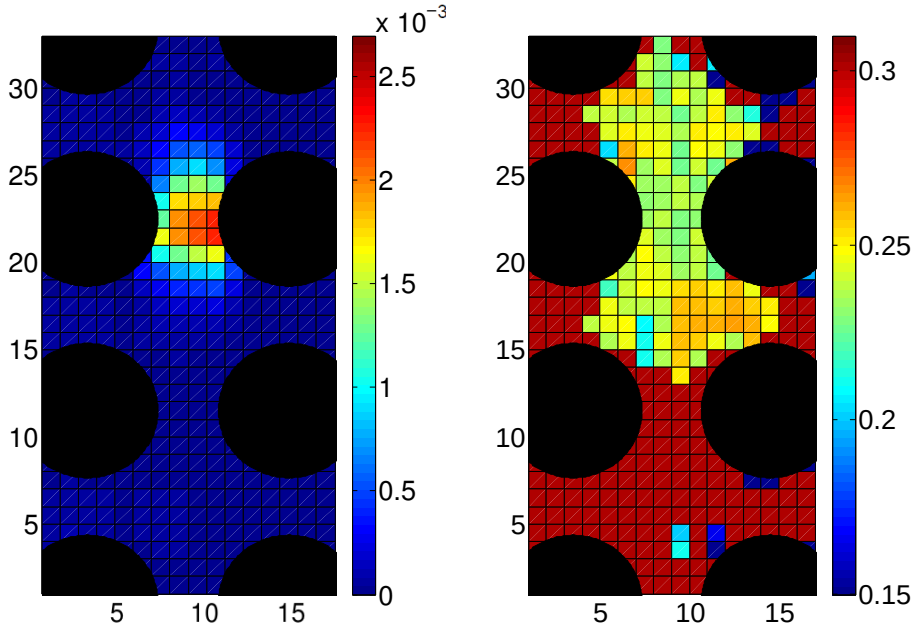

(a) Mean tracer concentration. **(b)** Velocity in m/s.

Figure 7.13: Mean concentration values and concentration velocity profile for the individual measurement points with Re=7000. Tracer is injected at the center of the gap 40cm upstream of the top sensor.

In figure 7.14a, is shown the auto-correlation of the measurement point made by the cross-point of receiver wire 9 with transmitter wire 19 (figure 7.13). In this figure, several peaks are clearly visible in the auto-correlation. It is assumed that the transport of tracer from the center of the gap region towards the sub-channel shows a peak for every structure passing through the sensor. This would indicate that the structures have a streamwise-size of 12 cm. When looking at 7.14b, which is the same measurement but then for a point closer to the sub-channel, similar behavior can be observed, allthough it is less pronounced.

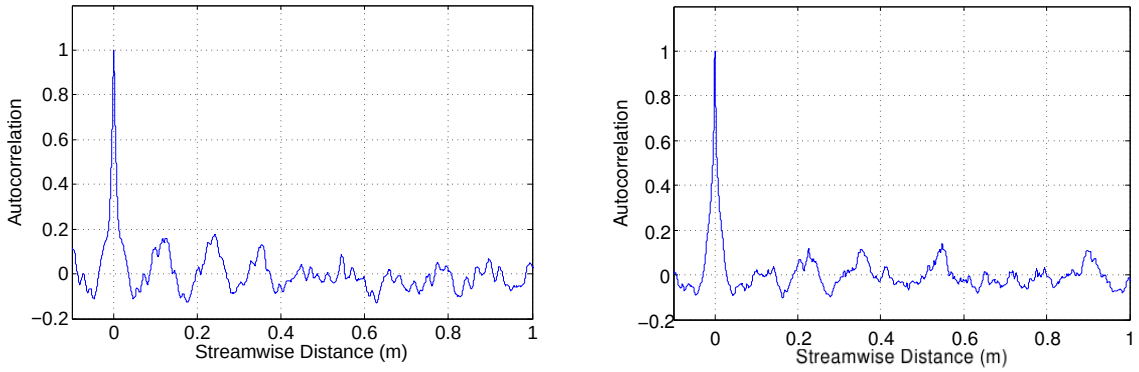

(a) Auto-correlation in point (9,19). **(b)** Auto-correlation in point (9,18).

Figure 7.14: Auto-correlation of the tracer concentration in time for two different measurement points with Re=7000. Tracer is injected at the center of the gap 40cm upstream of the top sensor.

In figure 7.15, the results for measurements done with Re=3000 and Re=750 are shown. According to Mahmood and van Campen, the structures streamwise-size starts to increase sharply somewhere below Re=3000. In figure 7.15, this should become especially visible in the measurements at Re=750. At Re=3000 there are still clearly identifyable peaks and the distance between them seems to grow towards approximately 18 cm, compared to the 12 cm at Re=7000. At Re=750, the peaks are less clear, but it is possible to identify peaks; the distance between them is approximately 30 cm, indicating coherent structures with this streamwise-size. The results of these early sets of measurements show the same qualitative behavior, with values in the same range, as the findings from Mahmood (2011) and van Campen (2009), indicating that using two wire-meshes for quantifying different characteristics of coherent structures is possible.

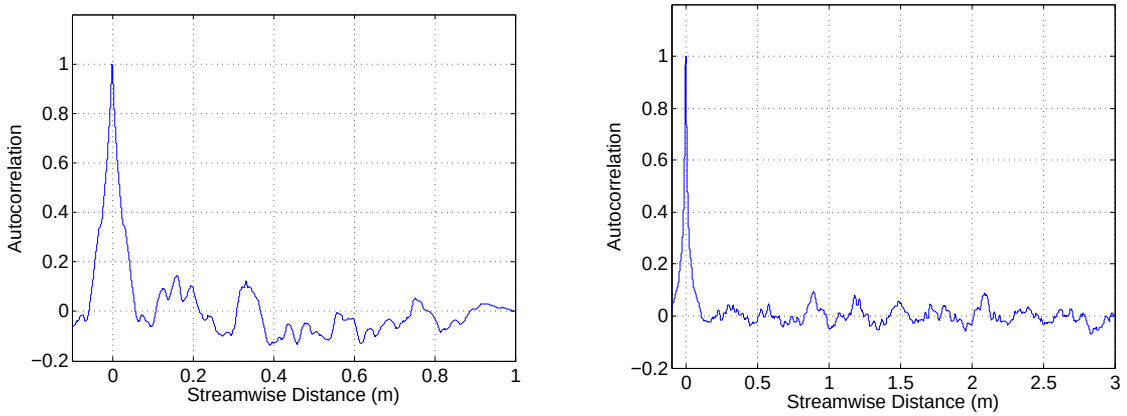

(a) Auto correlation in point (9,19) for Re=3000.

(b) Auto correlation in point (9,19) for Re=750.

Figure 7.15: Auto-correlation of the tracer concentration in time for two different Reynolds numbers. Tracer is injected at the center of the gap 40cm upstream of the top sensor.

CHAPTER 8

Conclusions and Recommendations

8.1 Conclusions

Central in this project was the application of a wire-mesh measurement equipment in a duct with rod-bundle geometry mimicking the geometry, of a nuclear reactor core. In part I of this research, the capabilities of a wire-mesh equipment in a horizontal pipe-flow where investigated. In part II, the designing, construction and application of a custom wire-mesh, specifically made for an existing rod-bundle geometry is treated. The reasons for the construction of this wire-mesh were mostly the acquisition of localized mixing data, and the identification of large-scale coherent structures.

8.1.1 Part I

An existing horizontal pipe set-up with wire-mesh was adjusted for use in single-phase measurements. The injection of tracer material by using a small L-shaped capillary was looked at and no influence of it was detectable by the wire-mesh sensor. With this set-up, various characteristics of the the wire-mesh and possible adjustments for using the equipment in single-phase flow were investigated .

The method of calibration was adjusted for a highly conductive tracer and checked for reliability. It showed that measurements in homogeneous solutions benefited greatly from calibrating. The inaccuracy decreased from deviations of up to 40% from the average value to less than 10%. The attempt that was made to increase the measureable range of the equipment by adding additional resistance to the receiver wires was unsuccessful, as the reliability of the signals started to suffer noticeably from the resistors.

The dispersion of a tracer injected as a point source in the turbulent flow was measured. The results are clear and are sufficiently reliable. A good agreement was found with results from the literature for the dispersion as a function of the injection distance and the turbulence intensity in the flow, as well as for the concentration values in the center of the tube.

Getting quantitative information about turbulence structures with the help of a two-dimensional scalar measurement equipment is not a trivial enterprise. By using Taylor's hypothesis with the mean velocity of the flow, it was possible to start looking at the size of the structures in the streamwise direction. Power spectra of the fluctuating concentration where made, and from them the most influential structure sizes in the dispersion of the tracer were determined. The results found were limited by their theoretical maximum at the large side of the spectrum size, and by the equipment on the small side, leading to the conclusion that for large structures the measurement technique is usable. The structure size in the cross-section was obtained by looking at the cross-correlation between different measurement points. The cross-sectional size of the largest structures was found to be roughly D/10, which fits with the results from the literature. Close to the wall it was found that the structures tended to be slightly larger in the the circumferential direction than in the radial direction, which also fits with the results from the literature.

In conclusion, it was found that using a scalar measurement equipment for investigating turbulence structures is possible. The very high time-resolution , together with a reasonable spatial-resolution allows for good measurements when measuring in the central regions of a turbulent pipe-flow.

8.1.2 Part II

The wire-mesh that was custom-made for the rod-bundle geometry was installed and used in some early experiments. As with the wire-mesh in the horizontal pipe, the high time-resolution and reasonable spatial-resolution allows for an accurate, and for all purposes instantaneous, representation of the tracer concentration in a plane. The (mean) spread of the tracer throughout a sub-channel, or throughout a gap-region was acquired for several situations.

The cross-correlation between the two sensors in the set-up, separated by 4 cm, allows for an estimation of the speed of the structures along the flow direction. The results that were obtained for the concentration velocities match with the findings from Mahmood (2011) for the velocity of the flow structures. The velocity of the large-scale structures appears to be roughly equal to the mean velocity of the fluid in the center of the sub-channel. Mahmood (2011) found a similar result using PIV-measurements in a simpler geometry and used it to estimate the streamwise size of the large-scale structures in the rod-bundle geometry where he performed LDA measurements. Here, we verify that, indeed, the hypothesis of Mahmood for the velocity of the large-scale structures in the rod bundle geometry appears to be correct.

The streamwise structure-sizes, which were found by auto-correlating the concentration spectra and applying Taylor's hypothesis with the velocities found by cross-correlating the two sensors, match the results from literature fairly well. Qualitatively the same behavior is found: the structures grow when the Reynolds number gets smaller. Also, quantitatively the results are close to the results from literature.

It is clear that installing a wire-mesh sensor in a rod-bundle geometry results in some interesting measurement possibilities. Both the velocities and sizes of large-scale coherent vortices seem possible to find. Besides that, the cross-sectional tracer dispersion can also be measured. Since the technique is virtually non-intrusive and it allows virtually instantaneous measurements with a reasonable spatial-resolution, it is a powerfull technique for global measurements in complex geometries, where optical technique might be very difficult or impossible to use.

8.2 Future Work

Several additions to the current experiments should be considered when continuing this research:

- In order to acquire more information about the sizes of the structures, more, and, most important, longer measurements should be done. Especially at low Reynolds numbers, the amount of structures passing through the sensor in one measurement should be increased, in order for the auto-correlation to result in clearer peaks, and thus more reliable structure sizes.

- The injection position should be varied in the cross-sectional direction in order to further investigate the influence of the salt injection on the results. Besides that, this will also yield more insight in the way a scalar is transported through the gap towards another sub-channel.

- Aside from continuous salt injection, pulsed tracer injection should be performed, this will yield information about the streamwise dispersion of the salt and any influence that the buoyancy might have on the results.

- More information about the influence of the salt solution characteristics and buoyancy effects could be found by (pulsed) injection of salt in a zero or very small velocity flow.

- Further research could be combined with numerical work into the same geometry, this would give a good insight in the reliability of the experiments, and could later be expanded to geometries with different characteristics.

8.3 Recommendations

For possible improvements to the set-up, sensor and other experimental procedures, the following recommendations can be made.

8.3.1 Set-Up

Several improvements could be made to the set-up to get more extensive, and more accurate measurements.

- More accurate flow regulators should be installed in the set-up. This will make estimating the (bulk) flow characteristics more accurate.
- Either the pressure drop over the set-up should be lowered, or the water reservoir responsible for the flow should be heightend. This will make a larger range of velocities, and thus Reynolds number, accessible for measurements.
- More injection points can be installed, so that the tracer dispersion over larger distances can be measured. This is needed especially with respect to dispersion between sub-channels.
- A temperature control mechanism could be installed for keeping the temperature, and thus a variety of fluid characteristics, more constant while measuring. At this moment, both the pumping system and the natural temperature difference between the top of the experimental hall and the floor introduce an inaccuracy in the measurements that is undesirable.
- Some adjustments to the set-up should be made for maintenance purposes. The output of the wire-mesh equipment is sensitive to possible tarnish to the wires, therefore, regular maintenance and calibration measurements should be performed. Also, making sure the flow-loop is kept clean by, for example, installing a sieve should make this a lot easier.

8.3.2 Wire-Mesh

The electronic equipment used in this research is clearly an older specimen that has been used for a variety of experiments over the past years. This results in a signal that is not as homogeneous as possible and some electronic noise. Newer equipment should also have more possibilities with respect to fine-tuning the driving voltages, the length of transmitted pulses, and the surpression of cross-talk between wires.

Newer electronic equipment would also allow for more wires to be controlled, this would give the ability to measure the entire cross section of the tube with two meshes instead of half of the tube. This could give a more complete indication of scalar dispersion, especially when a scalar is injected further away.

8.3.3 Tracer

As discussed the use of salt-water as a tracer has many advantages. It is cheap, safe, easy to use, and has many characteristics that are similar to the normal tap water used as bulk liquid. A disadvantage is the density difference between the salt-water tracer and the tap water. It is recommended that the importance of the buoyancy on the experimental results is investigated by additional measurements and that, if necessary, a solution should be found for improving the similarities between the characteristics of the tracer and of the bulk fluid. One measure that could be taken is using demi-water as bulk liquid. This would reduce the background signal enormously, and would allow for a much lower concentration of salt to be used as tracer. An added benefit would be that the measurement range between the background signal and the maximum conductivity the equipment can handle would increase, resulting in easier and more accurate measurements.

Bibliography

L. Aanen. *Measurement of Turbulent Scalar Mixing by means of a combination of PIV and LIF*. PhD thesis, Delft University of Technology, 2002.

N. Altinsoy and A.B. Tuğrul. A radiotracer application for the turbulent dispersion of fluids. *Applied Radiation and Isotopes*, 51:367 – 375, 1999.

R.J. Belt. *On the liquid film in inclined annular flow*. PhD thesis, Delft University of Technology, 2007.

R. Byron Bird, Warren E. Steward, and Edwin N. Lightfoot. *Transport Phenomena*. John Wiley & Sons, 1 edition, 1962.

G. Brethouwer. *Mixing of Passive and Reactive Scalars in Turbulent Flows*. PhD thesis, Delft University of Technology, 2001.

M.N. Descamps. *Experimental Study of Three-Phase Gass-Lift*. PhD thesis, Delft University of Technology, 2007.

T. Ikeno and T. Kajishima. Analysis of dynamical flow structure in a square arrayed rod bundle. *Nuclear Engineering and Design*, 240:305 – 312, 2010.

J. Jiménez. The largest scales of turbulent wall flows. *Center for Turbulence Research Annual Research Briefs*, 1998.

I.D. Johnson. Method and apparatus for measuring water in crude oil, us patent. (4644263), 1987.

Pijush K. Kundu and Ira M. Cohen. *Fluid Mechanics*. Elsevier Academic Press, 3 edition, 2000.

A. Mahmood. *Single-Phase Crossflow Mixing in a Vertical Tube Bundle Geometry*. PhD thesis, Delft University of Technology, 2011.

A. Manera. *Experimental and analytical investigations on flashing-induced instabilities in natural circulation two-phase systems*. PhD thesis, Delft University of Technology, 2003.

H. Pietruske and H.-M. Prasser. Wire-mesh sensors for high-resolving two-phase flow studies at high pressures and temperatures. *Flow Measurement and Instrumentation*, 18, 2005.

Stephan B. Pope. *Turbulent Flows*. Campbridge University Press, 1 edition, 2000.

H.-M. Prasser, A. Böttger, and J. Zschau. A new electrode-mesh tomograph for gas-liquid flows. *Flow Measurement and Instrumentation*, 9:111–119, 1998.

H.-M. Prasser, M. Misawa, and I. Tiseanu. Comparison between wire-mesh sensor and ultra-fast x-ray tomograph for an air-water flow in a vertical pipe. *Flow Measurement and Instrumentation*, 16, 2005.

O. Reynolds. An experimental investigation of the circumstances which determine wether the motion of water shall be direct or sinuous, and of the law of resistance in parallel channels. *Proceedings of the Royal Society of London*, 35(224-226):84–99, Januari 1883.

S. Richter, M. Aritomi, H.-M. Prasser, and R. Hampel. Approach towards spatial phase reconstruction in transient bubbly flow using a wire-mesh sensor. *International Journal of Heat and Mass Transfer*, 45: 1063 – 1075, 2002.

J.T. Rogers and N.E. Todreas. Coolant interchannel mixing in reactor fuel rod bundles single-phase coolants. In *ASME Annual Winter Meeting, New York, U.S.A.*, 1968.

D.S. Rowe, B.M. Johnson, and J.G. Knudsen. Implications concerning rod bundle crossflow mixing based on measurements of turbulent flow structure. *Internation Journal of Heat and Mass Transfer*, 17: 407 – 419, 1974.

M.J. Da Silva, E. Schleicher, and U. Hampel. Capacitance wire-mesh sensor for fast measurement of phase fraction distributions. *Measurement Science and Technology*, 18, 2007.

P.T.M. Smeets. Spatially resolved phase distributions in a vertical ga. Master's thesis, Delft University of Technology, Delft, 2009.

A.S. Taylor and S. Middleman. Turbulent dispersion in drag-reducing fluids. *American Institute for Chemical Engineers Journal*, 20:454 – 461, 1974.

G. Taylor. The dispersion of matter in turbulent flow through a pipe. *Proceedings of the Royal Society of London*, 223:446–468, 1954.

L.J.A.M. van Campen. An experimental investigation on the use of fep as refractive index matching material for lda in a rod bundle flow. Master's thesis, Delft University of Technology, Delft, 2009.

A.T. van Nimwegen. Direct numerical simulation of turbulent flow in rough pipes. Master's thesis, Delft University of Technology, Delft, 2010.

E. Van Vliet. *Turbulent Reactive Mixing in Process Equipment*. PhD thesis, Delft University of Technology, 2003.

E. Van Vliet, S.M. Van Bergen, J.J. Derksen, L.M. Portela, and H.E.A. Van den Akker. Time-resolved, 3d, laser-induced fluorescence measurements of fine-structure passive scalar mixing in a tubular reactor. *Experiments in Fluids*, 37:1 – 21, 2004.

C. Walker, M. Simiano, R. Zboray, and H.-M. Prasser. Investigations on mixing phenomena in single-phase flow in a t-junction geometry. *Nuclear Engineering and Design*, 239, 2009.

C.D. Winant and F.K. Browand. Vortex pairing: the mechanism of turbulent mixinglayer growth at moderate reynolds number. *Journal of Fluid Mechanics*, 63:237–255, 1973.

A. Ylönen, W.-M. Bissels, and H.-M. Prasser. Single-phase cross-mixing measurements in a 4 x 4 rod bundle. *Nuclear Engineering and Design*, 241:2484 – 2493, 2011.

Acknowledgments

Considering the large amount of help I received during this project and the support I got while doing it, I would like to take the time to thank those giving me this help and support in this section.

First of all I would like to thank Luis Portela for supervising my project. Luis availability throughout the project was fantastic and after a discussion with him I always new in which direction to take my research. Also his confidence in my abilities and in the designed equipment was of great support. His great knowledge about fluid dynamics, a field in which, prior to this project, I had little knowledge of was great to have at my disposition.

Second I would like to thank Martin Rohde for giving me the chance to do this project. Even though I should have dropped by his desk more often I could always expect a helpfull reply or discussion after an email or whenever we had a meeting.

I received lots of help from Dick de Haas who was of invaluable worth as a contact between me and the technicians at the RID. Also his own, vast experience and knowledge as an experimental researcher himself, providing me with lots of usefull feedback and ideas.

An important part of this project was the construction and installation of a custom designed wire-mesh, this was an even more complicated enterprise then originally estimated and would not have been brought to a satisfying conclusion without the various staff members in the DEMO department at the RID. I specifically would like to thank Rene Gommers for his work on designing the wire-mesh and Raymon, Rien, and René for taking care of the construction of the equipment. I also would like to thank the supporting staff at the Kramer's lab. Jan, Jaap, Jaap, Evert and Wouter were of great support to my project. Both in helping me completing my experimental setup as well as giving their frank opinions about everything they came across, related and unrelated to my project.

Of my (PhD-)student companions at multi-scale physics I specifically want to thank Laurens van Campen and Dries van Nimwegen. Their knowledge, experience and feedback with respect to the wire-mesh equipment, the rod-bundle set-up and data post-processing helped me through the project. Also their presence as experimental researchers supplied me with a healthy amount of close colleagues, even at my experimental facility. Besides them I would like to thank Sinta, Romboud, Rudi and Alexander and all the other students and PhD-students that made working at mutli-scale physics something enjoyable. Wether it was someone to complain with or someone to laugh with, there always was someone available for some distraction and for providing necessary assistance or feedback.

Most importantly I would like to thank Brigitte, mom, dad, Paula and Ellis for All the support I received from them. Not only during this project but throughout my entire study, they where there to help me move along, motivate me and helped me get through the rough spots. I'm very lucky to have them.

And finally there are the friends I picked up during various stages of my life and study. Tram 17, de Uithofslaan, Ångström, and my 'world-problem-solvers-during-lunch' study buddies. I owe all of them my thanks, I could not have done it without them.

'Make haste slowly'

Imperator Caesar Divi filius Augustus